

# **Dynamics and Control Analysis of In-Flight Wing Damage Recovery Using Morphing Wing**

a project presented to  
The Faculty of the Department of Aerospace Engineering  
San Jose State University

in partial fulfillment of the requirements for the degree  
*Master of Science in Aerospace Engineering*

by

**Zongnan Chen**

May 2023



approved by

Dr. Long Lu  
Faculty Advisor

© 2023  
Zongnan Chen  
ALL RIGHTS RESERVED

## **Abstract**

# **Dynamics and Control Analysis of In-Flight Wing Damage Recovery Using Morphing Wing**

**by Zongnan Chen**

This project investigates the stability of a wing-damaged general transport aircraft. Damage to aircraft wing in flight results in the loss of lateral/directional stability; such failure is likely to result in a complete fatal crash. In this project, the damaged-wing aircraft model is derived, and the stability of the aircraft is analyzed. A wing-level PID controller design was implemented to stabilize the damaged aircraft. The end goal is to employ in-wing morphing technology to reshape the aircraft's lifting surfaces to regain stability in the long run. The morphing wing dynamics and the wing-damaged aircraft system are derived and analyzed. Lastly, modern control design techniques help improve recovery from the damaged-wing fatal mode.

## Contents

<b>List of Figures</b> .....	6
<b>List of Tables</b> .....	8
<b>Symbols</b> .....	9
<b>1. Introduction</b> .....	12
1.1 Motivation .....	12
1.2 Literature Review .....	12
1.3 Project Proposal.....	17
1.4 Methodology .....	18
<b>2. Asymmetrical Aircraft Modeling</b> .....	20
2.1 Setup.....	20
2.2 Translational Equations of Motion.....	20
2.3 Rotational Equations of Motion .....	21
2.4 Linearization.....	22
2.5 Stability and Control Derivatives .....	23
2.6 Fully Decoupled Equations of Motion .....	24
<b>3. Asymmetrical Aircraft Analysis and Simulation</b> .....	26
3.1 Aerodynamic and Mass Properties.....	26
3.2 Open-Loop Simulation .....	28
3.3 Open Loop Analysis.....	30
3.4 Closed Loop Controller Design.....	31
3.4.1 Setup.....	31
3.4.2 Results .....	32
<b>4. Morph Wing Design</b> .....	37
<b>5. Morph Wing Analysis</b> .....	40
5.1 Morph Design Flow Diagrams .....	40
5.2 Lift vs. Drag Analysis .....	42
5.3 Instantaneous morph simulation model.....	45
<b>6. Morph Wing Actuation Design</b> .....	49
6.1 Actuation Requirement .....	49
6.2 Hydraulic Actuator Modeling .....	50

6.3 Actuation simulation .....	51
<b>7. Morph Wing Controller Design and Full Simulation .....</b>	<b>53</b>
7.1 Setup.....	53
7.2 Simulation Result and Analysis .....	54
<b>8. Conclusion and Future Work.....</b>	<b>60</b>
8.1 Conclusion.....	60
8.2 Future work .....	60
<b>References .....</b>	<b>62</b>
<b>Appendices.....</b>	<b>65</b>
Appendix A – Damaged-Wing Dynamic Derivation.....	65
Appendix B – Damage Wing Simulation Code .....	78
Appendix C – Wing-level Controller Design for Damaged Wing.....	86
Appendix D – Aerodynamic Data for Airfoil .....	91
Appendix E – Instantaneous Morph Simulation Code.....	93
Appendix F – Actuation Code.....	95
Appendix G – Full Simulation Code.....	96

## List of Figures

Figure 1.1 General multi-body dynamic [1] .....	13
Figure 1.2 Bell X-5 aircraft [5] .....	14
Figure 1.3 Chord morphing example [9] .....	14
Figure 1.4 Variation of CG due to wing Loss [14] .....	16
Figure 1.5 a) independent control design, b) integrated control design [4] .....	17
Figure 1.6 Open-loop block diagram concept.....	18
Figure 1.7 Closed-loop controller design concept diagram .....	19
Figure 2.1 Damage wing setup diagram .....	20
Figure 3.1 Input signal for simulation.....	28
Figure 3.2 Wing damage rotational angle output.....	29
Figure 3.3 Wing damage angular rate output.....	29
Figure 3.4 Velocity for damaged and undamaged aircraft .....	30
Figure 3.5 Block diagram for wing level controller design .....	32
Figure 3.6 Block diagram for wing level controller design .....	33
Figure 3.7 Deflection under 5-degree input .....	33
Figure 3.8 Roll angle response under 5-degree input signal.....	34
Figure 3.9 10-degree input signal .....	35
Figure 3.10 Control surfaces response under 10-degree input .....	35
Figure 3.11 Control surfaces response under 10-degree input .....	36
Figure 4.1 Different types of morphing wings [28].....	37
Figure 4.2 Morph wing design preview .....	38
Figure 4.3 Morph section concept [28].....	38
Figure 5.1 Morph wing damage aircraft flow chart.....	40
Figure 5.2 Morph dynamic model flow chart (morph implementation block 1) .....	41
Figure 5.3 Actuation implementation flow chart.....	42
Figure 5.4 Boeing 747 root airfoil shape, generated from XFLR5.....	42
Figure 5.5 Lift at various span and chord lengths.....	43
Figure 5.6 Drag curve with variation in span and chord.....	44
Figure 5.7 Lift comparison between no-damage, damaged, and variable morph.....	45
Figure 5.8 Drag comparison between no-damage, damaged, and variable morph.....	45
Figure 5.9 Input disturbance signal.....	46
Figure 5.10 Morphed roll angle response .....	47
Figure 5.11 Unmorphed roll response .....	47
Figure 5.12 Morphed aileron response .....	48
Figure 6.1 Side view of a sliding 5-cell extension solution, retracted(top) and extended(bottom) [28].....	49
Figure 6.2 Relationship between stress and morph .....	50
Figure 6.3 Linear hydraulic actuator control diagram [30].....	50
Figure 6.4 Actuation diagram flow chart.....	51
Figure 6.5 Hydraulic Actuation from zero percent morph to thirty percent morph .....	52

Figure 7.1 Full system morph design with damaged wing block diagram .....	54
Figure 7.2 Disturbance signal .....	55
Figure 7.3 Roll response with no morph.....	55
Figure 7.4 Roll response with morph.....	56
Figure 7.5 Actuation response commanded vs actual.....	57
Figure 7.6 Aileron and rudder response with no morph .....	57
Figure 7.7 Aileron and rudder response with morph .....	58
Figure 7.8 Roll angle response with morph and PID controller .....	59

## List of Tables

<b>Table 3.1</b> - Aerodynamic coefficient for 33% damaged wing aircraft [22] .....	26
<b>Table 3.2</b> - Mass and geometry properties for 33% of damaged wing aircraft [22] .....	27
<b>Table 3.3</b> - Aerodynamic coefficients for undamaged wing aircraft [22].....	27
<b>Table 3.4</b> - Mass and geometry properties for 33% of damaged wing aircraft [22] .....	27
<b>Table 3.5</b> - Longitudinal pole locations for damaged and undamaged aircraft.....	30
<b>Table 3.6</b> - Lateral/directional pole locations for damaged and undamaged aircraft.....	31
<b>Table 3.7</b> - Controllability and observability matrices ranks .....	31
<b>Table 3.8</b> - PID controller gain values .....	32
<b>Table 4.1</b> - Material comparison of strain and max force [29] .....	39
<b>Table 6.1</b> - Hydraulic actuator parameters used in simulation [30] .....	51
<b>Table 7.1</b> - PID controller parameters for aileron and rudder .....	58

## Symbols

Symbol	Definition	Units
$m_a$	Mass of the aircraft	lbs
$I_{xx}$	Moment of inertia along x axis	lbf*s*ft*s
$I_{yy}$	Moment of inertia along y axis	lbf*s*ft*s
$I_{zz}$	Moment of inertia along z axis	lbf*s*ft*s
$I_{xz}$	Products of inertial along x and z axis	lbf*s*ft*s
b	Span of wing	ft
$\bar{c}$	Chord of wing	ft
S	Area of wing	ft
$F_{x,y,z}$ & $f_{x,y,z}$	Force in the x y z direction	lbf
$M_{x,y,z}$	Rotational moments about x, y, z axis	lbf*ft
$({}^E H^{B/B_0})$	Angular moment of the body with respect to Earth ref. frame	lbf*ft*s
$V^{E/B}$	Velocity of body with respect to Earth ref. frame	ft/s
$\omega^{E/B}$	Angular velocity of body with respect to Earth ref. frame	rad/s
U, u	Aircraft's velocity along x direction	ft/s
V, v	Aircraft's velocity along y direction	ft/s
W, w	Aircraft's velocity along z direction	ft/s
P, p	Aircraft's rotational velocity about x axis	rad/s
Q, q	Aircraft's rotational velocity about y axis	rad/s
R, r	Aircraft's rotational velocity about z axis	rad/s
L, l	Aircraft's roll moment	lbf*ft
M, m	Aircraft's pitch moment	lbf*ft
N, n	Aircraft's yaw moment	lbf*ft
$\Phi, \phi$	Euler's roll angle	rad
$\Theta, \theta$	Euler's pitch angle	rad
$\Psi, \psi$	Euler's yaw angle	rad
$\alpha$	Angle of attack	rad
$\beta$	Side-slip angle	rad
<b>Aerodynamic parameters</b>		
$X_u$	X force with respect to x velocity	1/s
$X_\alpha$	X force with respect to angle of attack	ft/s <sup>2</sup>
$X_{\delta_e}$	X force with respect to elevator deflection	ft/s <sup>2</sup>
$Z_u$	Z force with respect to x velocity	1/s
$Z_\alpha$	Z force with respect to angle of attack	ft/s <sup>2</sup>
$Z_{\dot{\alpha}}$	Z force with respect to rate of change of angle of attack	1/s

$Z_q$	Z force with respect to pitch rate	ft/s <sup>2</sup>
$Z_{\delta_e}$	Z force with respect to elevator deflection	ft/s <sup>2</sup>
$Y_p$	Y force with respect to roll rate	1/s
$Y_r$	Y force with respect to yaw rate	1/s
$Y_\beta$	Y force with respect to side-slip angle	ft/s <sup>2</sup>
$Y_{\delta_a}$	Y force with respect to aileron deflection	ft/s <sup>2</sup>
$Y_{\delta_r}$	Y force with respect to rudder deflection	ft/s <sup>2</sup>
$N_p$	N moment with respect to roll rate	1/s
$N_r$	N moment with respect to yaw rate	1/s
$N_\beta$	N moment with respect to side-slip angle	1/s <sup>2</sup>
$N_{\delta_a}$	N moment with respect to aileron deflection	1/s <sup>2</sup>
$N_{\delta_r}$	N moment with respect to rudder deflection	1/s <sup>2</sup>
$L_p$	L moment with respect to roll rate	1/s
$L_r$	L moment with respect to yaw rate	1/s
$L_\beta$	L moment with respect to side-slip angle	1/s <sup>2</sup>
$L_{\delta_a}$	L moment with respect to aileron deflection	1/s <sup>2</sup>
$L_{\delta_r}$	L moment with respect to rudder deflection	1/s <sup>2</sup>
$M_u$	M moment with respect to x velocity	1/ft*s
$M_\alpha$	M moment with respect to angle of attack	1/s <sup>2</sup>
$M_{\dot{\alpha}}$	M moment with respect to rate of angle of attack	1/s
$M_q$	M moment with respect to pitch rate	1/s <sup>2</sup>
$M_{\delta_e}$	M moment with respect to elevator deflection	1/s <sup>2</sup>
$C_{L0}$	Coefficient of lift	-----
$C_{D0}$	Coefficient of drag	-----
$C_{m\alpha}$	Coefficient of pitch moment with respect to AoA	-----
$C_{D\alpha}$	Coefficient of drag with respect to AoA	-----
$C_{mq}$	Coefficient of pitch moment with respect to pitch rate	-----
$C_{L\alpha}$	Coefficient of lift with respect to AoA	-----
$C_{X\delta_e}$	Coefficient of X force with respect to elevator deflection	-----
$C_{Z\delta_e}$	Coefficient of Z force with respect to elevator deflection	-----
$C_{m\delta_e}$	Coefficient of moment with respect to elevator deflection	-----
$C_{yp}$	Coefficient of Y force with respect to roll rate	-----
$C_{y\beta}$	Coefficient of Y force with respect to side-slip angle	-----
$C_{l\beta}$	Coefficient of roll moment with respect to side-slip angle	-----
$C_{n\beta}$	Coefficient of yaw moment with respect to side-slip angle	-----
$C_{lp}$	Coefficient of roll moment with respect to roll rate	-----
$C_{np}$	Coefficient of yaw moment with respect to roll rate	-----
$C_{lr}$	Coefficient of roll moment with respect to yaw rate	-----
$C_{nr}$	Coefficient of yaw moment with respect to yaw rate	-----

$C_{L\delta\alpha}$	Coefficient of roll moment with respect to aileron deflection	-----
$C_{n\delta\alpha}$	Coefficient of yaw moment with respect to aileron deflection	-----
$C_{y\delta r}$	Coefficient of Y force with respect to rudder deflection	-----
$C_{l\delta r}$	Coefficient of roll moment with respect to rudder deflection	-----
<b>Acronym</b>		
AoA	Angle of attack	-----
GTM	General transport model	-----
CO	Controllability matrix	-----
OB	Observability matrix	-----
CG	Center of gravity	
<b>Subscripts/Hyphens</b>		
$()_1$	Subscript “1” indicates the steady-state flight condition	-----
$(\dot{\quad})$	“Dot”, indicates time derivative of the variable	-----

# 1. Introduction

## 1.1 Motivation

In-flight wing damage often results in catastrophic scenarios where the aircraft becomes too challenging to maneuver and land safely. However, the rise of morph wing technology extends from large-scale morphing to reshape the platform entirely. Therefore, introducing such a capability to compensate for loss of control in flight due to damages can reshape the outcome of these incidents. Furthermore, the application of this research not only extends to commercial aircraft usage but also extends to combat aerial vehicles.

Morphable wing technology dates back to the early 30s, when the initial inspiration stems from observing natural flyers in the sky. Even today, nature has much more to teach us and continuously inspires great minds in fields far beyond aerospace. Wild flyers can continually morph their wings and bodies like birds and flies to better adapt to flight conditions. However, in most modern aircraft designs, the main frame of the body, fuselage, wings, and other lifting surfaces are primarily static. While morph wing technology continues to improve over the years, recent breakthroughs in small-scale morphing extend the possibility of morphable aircraft. Over the century, much attention was paid to morphing the wing into different flight modes and optimizing the performance during respective flight segments. However, very little attention was given to using morphable wing technology in critical flight conditions, like a damaged wing. Even though most aircraft were designed considering potential damage, any damage done to the aircraft can make it extremely difficult to maneuver. The motivation for this project stems from the fact that significant damage to the main wing of any aircraft is nearly impossible to recover from. However, with the help of morphable technology, the gap between catastrophic and still flyable can be widened.

## 1.2 Literature Review

Much research has been done on morphable wings, and examples of attempts at morphable wings can date back to the World War II era [1]. However, the focus of morphable wings in recent times has been adapting to various flight modes (cruise, dash, loiter, etc.) for performance optimization. The dynamics and control of morphing aircraft have been given much attention in literature [1]. This literature review will focus on the following key points:

- Rigid body modeling
- Morphable Wings
- Translational Equations of Motion
- Rotational Equations of Motion
- Damage Wing Analysis
- Control System Design

The main challenge of morphable wings comes from the non-static dynamic models of the aircraft's rigid body. A typical transition can be categorized as pre-morph, morphing, and post-morph shapes, each of which has its rigid body modeling. Due to the moving parts and their effect on the inertia of the body, one rigid body model for the aircraft is insufficient. Two rigid model body modeling methods were presented in "Modeling of Flight Dynamics of Morphing-Wing Aircraft" [1]. Obradovic and Subbarao [1], propose modeling the entire aircraft as a single body but treating the inertia tensor as a function of time, displacement, and rotations. While this

method is more complex and computationally taxing, it allows the configuration to exclude the actuator dynamics [1]. One key assumption for the inertia tensor rigid body model is that the morphing rate must be slow, meaning quasi-static morphing.[2] For a higher morph rate, the inertia tensor might include a time-varying correction term to account for the angular momentum, Equation (1.1). Another rigid body modeling method was proposed in [3,4], where each moving part of the morphable wing was considered a single rigid body. This method raises complexity as the number of moving parts increases, which happens in morphable wings since each actuator consists of multiple parts. But this method is computationally less expensive than modeling as a single body. For any general multibody system, the configuration can be expressed as each member of the system's coordinates multiplied by the velocity of each component, which can be described as a system of differential equations, Equation (1.2). Multibody rigid body modeling must account for actuation coming from morphable components. The actuation equation of motion can be modeled as a system of string and dampeners [1]. One approach is to model the elastic potential energy of each component as a function of the position vector of each part and natural stiffness [1].

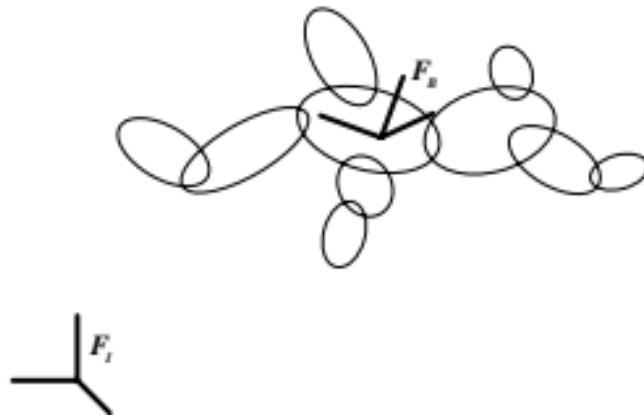


Figure 1.1 General multi-body dynamic [1]

$$[J]\dot{\omega} + [j]\omega = \tau \quad (1.1)$$

$$\dot{q} = C(q, t)y + D(q, t) \quad (1.2)$$

Morphable wings include a variety of morphing techniques, including large-scale and small-scale morphing. The variable-sweep wing achieved the first iteration of morph wings [4]. Such design is ideal for aircraft rated to fly at different speeds; a more swept wing is suitable for transonic and supersonic flight, while a less swept wing is suitable for low-speed applications [4]. Another type of large-scale morphing, variable wing tip, enables the change in dihedral angle for wingtips. Smith et al. [5] found that when the wing planform undergoes wingtip morphing, the aircraft tends to lose lift along the main wing and dramatically increase drag. The key benefit of wingtip morphing is its ability to reduce the overall wing bending moment at the root [5]. Min et al. [6] categorize morphing wings into three distinct types, rotational, telescopic, and inflation. Rotational is a large-scale morphing method that involves rotating the entire wing or parts of the wing. One prime example of rotational morphing is variable-sweep wing designs, like the Bell X-5 aircraft, Figure 1.2. Telescopic morphing can change the span, camber, and

wing area of the wing; such changes are usually happening progressively over smaller cross-sections of the wing, equivalent to changing the aerodynamic performance [6]. The first successful iteration of telescopic morphing aircraft was the MAK-10, which was capable of a 62% span and 57% area increase [7]. Variation in aspect ratio enables aircraft to be suitable for both high-speed, maneuverable, and low-speed, long-range missions. Inflation morphing is typically associated with foldable wing design, where parts of the wing get inflated during flight and change the overall shape, mostly seen in applications for deployable UAVs [6]. The key benefits of inflation wings are low-cost, long storage life, dampens vibration, and recoverable [8]. At the same time, the drawbacks of the inflation system are obvious, and easily subject to external damage and consideration for gas.



Figure 1.2 Bell X-5 aircraft [5]

Another type of small-scale morphing technique is chord change, Figure 1.3. Most modern aircraft achieve some form of chord morphing using high-lift devices like leading/trailing edge flaps [9]. However, research has shown that increasing chords can increase overall lift from the wing due to a large wing area [10].

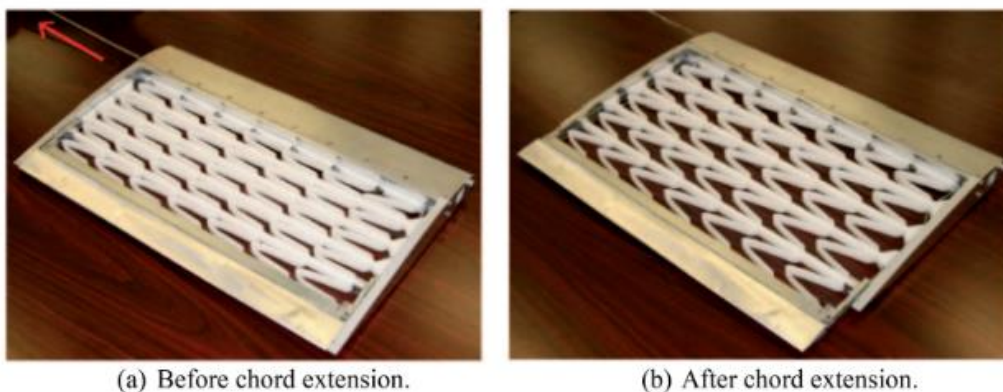


Figure 1.3 Chord morphing example [9]

The translational equation of motions for morphable aircraft must consider the morphable wing. As wing planform changes shape in flight, the sum of the forces and center of mass of the system varies. Using the Newtonian approach, for large-scale morphing, the motion of each part can be modeled by the aerodynamic forces, internal forces, gravity, and thrust [11]. Account for the geometrical changes, the full equation of motion can be modeled as a function of the position vector of each movable component and its respective forces, Equation (1.3).

$$F_{aero} + G + T - \sum_{i=1}^2 m_i \frac{dV_{S_i}}{dt} = (m_0 + \sum_{i=1}^2 m_i) \frac{dV_0}{dt} \quad (1.3)$$

Equation (1.3) only accounts for the morphing wing equation of motion, combined with a generic longitudinal model for a conventional design, which gives Equation (1.4) [9].

$$\begin{bmatrix} \Delta \dot{V} \\ \Delta \dot{q} \\ \Delta \dot{\alpha} \\ \Delta \dot{\theta} \end{bmatrix} = \begin{bmatrix} (T^V - X^V)/m_t & 0 & -(T_\alpha + D^\alpha)/m_t + g \cos \theta & -g \cos \theta \\ C_M^V/I_{y_t} & C_M^q/I_{y_t} & C_M^\alpha/I_{y_t} & 0 \\ -(T^V \alpha + L^\alpha)/m_t V & 1 & -(T + L^\alpha)/m_t V + g \sin \theta / V & -g \sin \theta / V \\ 0 & 1 & 0 & 0 \end{bmatrix} \begin{bmatrix} \Delta V \\ \Delta q \\ \Delta \alpha \\ \Delta \theta \end{bmatrix} + \begin{bmatrix} 0 \\ C_M^{\delta_e}/I_{y_t} \\ -L^{\delta_e}/mV \\ 0 \end{bmatrix} \delta_e + \begin{bmatrix} F_{xd} \\ C_{md} \\ F_{zd} \\ 0 \end{bmatrix} \quad (1.4)$$

Where force terms differ between the traditional longitudinal and morph wing dynamic models, force terms are a function of the position of each movable component in a morphable wing design. Gravity and variation of center of mass (CG) must also be modeled. The change in gravitational force can be modeled as a function of the original mass location plus the change in mass location, Equation (1.5) [12]. Assuming all morphing is instantaneous, Equation (1.5) combined with a flat-earth model for rigid-body aircraft can turn into Equation (1.6) [12].

$$m = m^* + \Delta m \quad (1.5)$$

$$F_B = m \frac{dV}{dt} + m \frac{d\omega}{dt} \times \Delta r + m \omega \times \frac{d\Delta r}{dt} - W \quad (1.6)$$

Where  $\omega$  is the gravitational force vector, and  $\Delta r$  is the change in position of the CG

Rotational equations of motion follow the same scheme as translational equation motion. The rotation equation considers the open-frame angular momentum of the aircraft combined with the change in mass, position vector, and each sub-components respective velocity, Eq. (1.7).

$$H_B = I\omega + m\Delta r \times V \quad (1.7)$$

Where  $m\Delta r \times V$  is the corrective term that accounts for the morphing actions in-flight [12], taking the derivative of Equation (1.7) and combining it with a generic twin-engine aircraft later-directional model gives Equation (1.8 – 1.10).

$$L = I_{xx}\dot{p} - I_{xy}\dot{q} - I_{xz}\dot{r} + I_{xy}pr - I_{xz}pq + (I_{zz} - I_{yy})qr + I_{yz}(r^2 - q^2) + m(qv + r\omega)\Delta x + m(\dot{\omega} - qu)\Delta y - m(\dot{v} + ru)\Delta z \quad (1.8)$$

$$M = -I_{xy}\dot{p} + I_{yy}\dot{q} - I_{yz}\dot{r} + I_{yz}pq - I_{xy}qr + (I_{xx} - I_{zz})pr + I_{xz}(p^2 - r^2) - m(\dot{\omega} + pv)\Delta x + m(pu + r\omega)\Delta y + m(\dot{u} - rv)\Delta z \quad (1.9)$$

$$N = -I_{xz}\dot{p} - I_{yz}\dot{q} + I_{zz}\dot{r} + I_{xz}qr - I_{yz}pr + (I_{yy} - I_{xx})pq + I_{xy}(q^2 - p^2) + m(\dot{v} - p\omega)\Delta x - m(\dot{u} + q\omega)\Delta y + m(pu + qv)\Delta z \quad (1.10)$$

The additional terms with  $\Delta x$ ,  $\Delta y$ ,  $\Delta z$  are the corrective morphing terms, which account for the additional moments introduced by movable components [12].

In-flight damage analysis determines the aircraft's stability and control post-damage and defines the design parameter for this project. Although it would take about 16000 flights for a 6mm crack to cause a stringer failure, internal damage due to fatigue or material wear down can also contribute to wing damage [13]. In a damage transport analysis, researchers found that damage/area loss to one of the main wings can result in lift and lateral control complications [14]. The biggest concern with wing damage is the loss of controllability and recoverability for roll moment introduced from the asymmetrical wing. While it is possible to use the undamaged wing's aileron to compensate for the rolling moment, this limits the controllability of the aircraft [13]. The coefficient of lift has been shown to decrease dramatically as a function of the fraction of wing loss, reaching lift generation by 25% at 50% wing loss [12]. Due to changes in lift and differences in drag, the longitudinal and lateral motions of the aircraft become coupled and introduce changes in angular rates [12]. Another aspect of wing damage is the shift in the center of mass of the aircraft. The CG of the aircraft will shift towards the undamaged side as the percentage of damage increases; Figure 1.4 showcases the variation in CG as a function of wing loss.

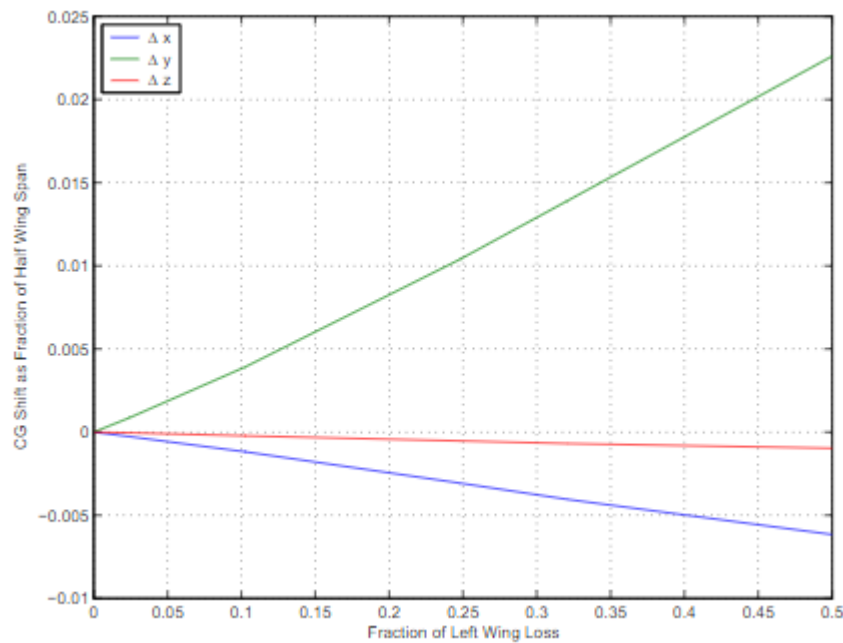


Figure 1.4 Variation of CG due to wing Loss [14]

Control system design for morphable wings creates a certain level of uncertainty due to model-based aircraft control [4]. Each mode/configuration of the aircraft has its control for a multi-rigid body system. Seigler and Neal [4] proposed two modeling techniques for control system designs, independent and integrated control, Figure 1.5. Aside from the flight and morphing control design, the type of design also affects the outcome, open-loop or close-loop morphing designs. Close-loop morphing introduces a feedback error state, which tracks the

difference between the desired and current states, which presents another degree of controllability in the system. In addition, the control model needs to account for the actuation of movable components. In the case of simple servo change, the dynamics and control of the servo will also be modeled along with the flight dynamics of the aircraft [15]. Various other control techniques can be used to optimize the design. Proportional-integral-derivative controller, PID, is one of the most used controller designs. The stability and rapidity of the morphing wing can be controlled and stabilized using PID controllers [3].

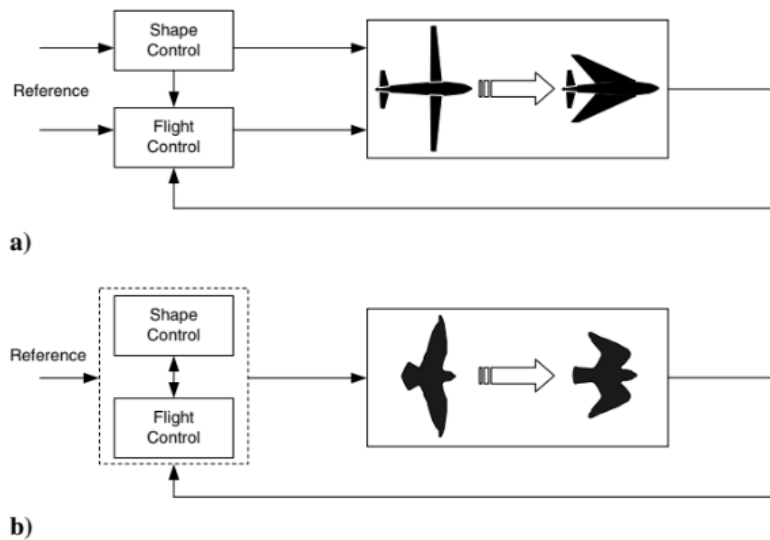


Figure 1.5 a) independent control design, b) integrated control design [4]

Morphing actuation poses another challenge in the study of morphable wing designs. Much of the literature has been paying attention to morphing design with a quasi-static condition, only considering before and after morphing. However, the morphing actuation is often not modeled. Ajaj and Friswell [16] modeled the elasticity of a span morphing wing using the Rayleigh-Ritz method of using shape functions. It considers the wing's uncoupled bending and torsional modes as shape functions [16]. In another project, Ajaj et al. [17] again modeled a span morphing wing using shape functions, Equation (1.11) and Equation (1.12).

$$h_i(y) = \{h_{1i} = 0 \leq y \leq l_i, h_{2i} = l_1 < y \leq l_1 + l_2, h_{3i} =; l_1 + l_2 < y \leq l_1 + l_2 + l_3\} \quad (1.11)$$

$$\phi_i(y) = \{\phi_{1i} = 0 \leq y \leq l_i, \phi_{2i} = l_1 < y \leq l_1 + l_2, \phi_{3i} =; l_1 + l_2 < y \leq l_1 + l_2 + l_3\} \quad (1.12)$$

The aeroelastic model can also be introduced using a modal analytic technique, where the bending and torsional deformations are expressed as a truncated series [18].

### 1.3 Project Proposal

This project aims to derive, design, and simulate how morphable wings can contribute to helping damaged aircraft regain control in flight. The focus will be on providing a working mathematical model, in-depth analysis, open-loop analysis, closed-loop analysis and simulation,

and wing-damaged aircraft flight dynamics and control. In addition, this project aims to determine how morphing technology can contribute to in-flight damaged wing scenarios. What kind of benefits can morphable wings bring? How significant is the change, if any?

## 1.4 Methodology

To fully understand and design viable solutions for the in-flight damage problem, the first step is to derive the equation of motion for a regular commercial airliner. The complete translational and rotational equation of motion is a foundation for analysis and design mentioned in Section 1.3. This project intends to derive the entire equation of motion using Newton's method and compute the aerodynamic derivatives using CFD tools like XFLR5. With the entirely derived equation of motion, the next consideration would be the rigid body modeling for asymmetrical aircraft and its dynamic model. The asymmetrical modeling will include various wing loss percentages to simulate a more realistic scenario. This contributes to the analysis of wing-damaged aircraft and enables the design limitation of morphable wing aircraft.

Secondly, the design of morphable wings will be broken down into two parts. Part one is the derivation of morphing wing dynamics and control. This part will consider the morphable as a function of the remaining wing. Part two will combine the fully derived model with the damaged wing model. The open-loop analysis will be done as a baseline comparison with the complete model of the morphing wing, airframe, and damaged wing. The fully derived model should follow the scheme shown in Figure 1.6,



Figure 1.6 Open-loop block diagram concept

The next steps are closed-loop analysis alongside controller design to regain static and dynamic stability for wing-damaged aircraft. A closed-loop analysis following the scheme of Figure 1.7 will be shown for this project. This will include various design techniques like PID, LQR, dynamic inversion, etc. Each of the design techniques will be compared, and determine the best solution for wing-damaged scenarios. Lastly, the simulation of the derived model provides insight into the feasibility of the design.

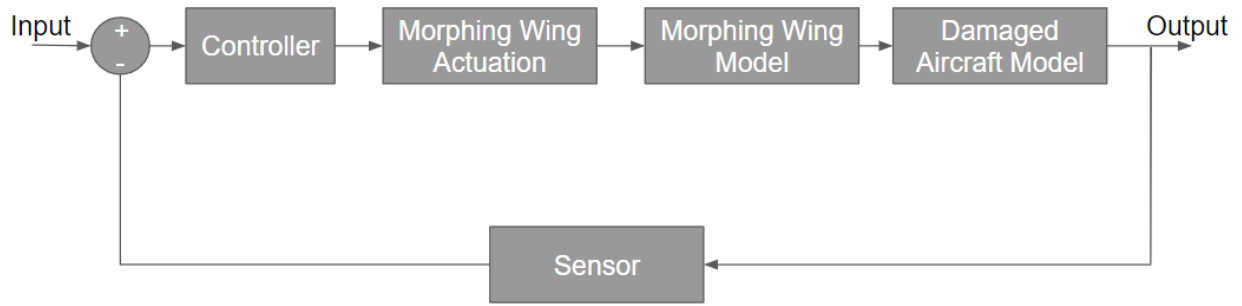


Figure 1.7 Closed-loop controller design concept diagram

## 2. Asymmetrical Aircraft Modeling

### 2.1 Setup

The damaged wing proposed in this project only applies to one side of the aircraft, which will introduce asymmetry into the rigid body model of the aircraft. As shown in Figure 2.1, the constraint for this project is to analyze the damage to wing control and dynamics up to 50% loss on only one side of the wing. As damage happens in flight, the center of gravity will be shifted to a new position post-damaged. The new location of the CG can be represented by position vector  $\Delta r$ , where  $\Delta r$  is equal to the change in displacement from the original CG,  $[\Delta b, \Delta h, \Delta d]$ .

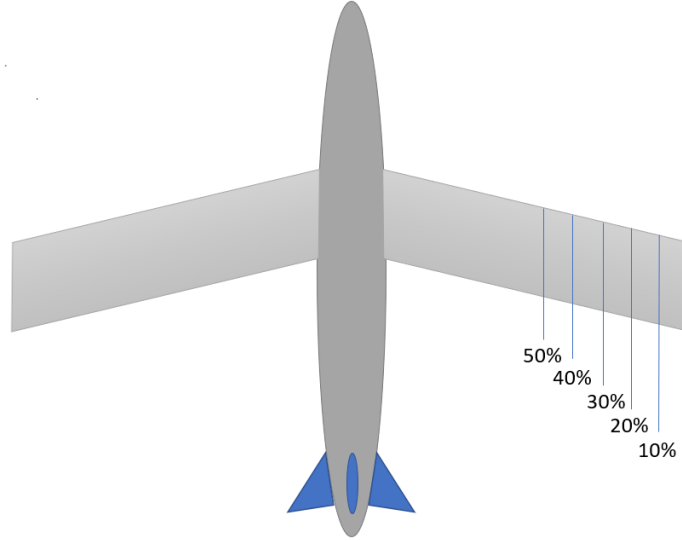


Figure 2.1 Damage wing setup diagram

### 2.2 Translational Equations of Motion

The translational equations of motion can be broken down into two distinct parts, the symmetrical wing-body and the extra component from the undamaged wing. Then, using Newton's method, the sum of the forces in the system can be modeled as:

$$\sum F = m * \frac{Edv^{E/B}}{dt} + \frac{d}{dt} (\omega^{E/B} \times r * dm) \quad (2.1)$$

Where  $({}^B \omega^E \times r * dm)$  is the additional term that accounts for the undamaged wing side, the cross product of angular velocity, and the product of position vector and instantaneous change of mass. The velocity  $V^{E/B}$  and angular velocity  $\omega^{E/B}$  vectors can be expressed as:

$$V^{E/B} = Ub_x + Vb_y + Wb_z \quad (2.2)$$

$$\omega^{E/B} = Pb_x + Qb_y + Rb_z \quad (2.3)$$

Substitute Equation (2.2) and Equation (2.3) into Equation (2.1), we can obtain the sum of the forces for an asymmetrical aircraft:

$$\sum F = m \begin{bmatrix} \dot{U} + QW - RV - (Q^2 + R^2)\Delta b + (QP - \dot{R})\Delta h + (RP + \dot{Q})\Delta d + g\sin(\Theta) \\ \dot{V} + RU - PW + (PQ + \dot{R})\Delta b - (P^2 + R^2)\Delta h + (QR - \dot{P})\Delta d - g\cos(\Theta)\sin(\Phi) \\ \dot{W} + PV - QU + (PR - \dot{Q})\Delta b + (QR + \dot{p})\Delta h - (P^2 + Q^2)\Delta d - g\cos(\Theta)\cos(\Phi) \end{bmatrix} \quad (2.4)$$

Where  $\Delta b$ ,  $\Delta h$ ,  $\Delta d$  are variations in CG location due to the loss of some portions of the wing. Comparing Equation (2.4) with the symmetrical generic equation of motion [19]:

$$\sum F = \begin{bmatrix} X \\ Y \\ Z \end{bmatrix} = \begin{bmatrix} \dot{U} + QW - RV \\ \dot{V} + RU - PW \\ \dot{W} + PV - QU \end{bmatrix} \quad (2.5)$$

Equation (2.4) and Equation (2.5) shared similar parameters like  $\dot{U}$ ,  $\dot{V}$ ,  $\dot{W}$  with Equation (2.4) with extra terms for the extra mass on the undamaged wing. Which are functions of change in CG location along x, y, z, and respective angular velocity rates. From Equation (2.4) is clear that now the translational equations of motion are coupled with angular velocities rates. This is due to loss in portions of the wing creating differential drag and lift, introducing yaw and roll motions.

### 2.3 Rotational Equations of Motion

The rotation equation of motion follows the same scheme as the translation equation of motion; starting from Newton's method, the sum of the moments in the system can be defined as:

$$\sum M = \frac{Ed}{dt} ({}^E \mathbf{H}^{B/B_0}) + m\Delta \mathbf{r} \times \mathbf{V}^{E/B} \quad (2.6)$$

Similar to Section 1.2,  $\Delta \mathbf{r}$  is the position vector from undamaged aircraft CG to the damaged aircraft CG and can be expressed as  $[\Delta b, \Delta h, \Delta d]$ . The extra term  $m\Delta \mathbf{r} \times {}^E \mathbf{V}^B$  accounts for the extra mass from the undamaged wing. The angular momentum term ( ${}^E \mathbf{H}^{B/B_0}$ ), can be expressed as:

$$({}^E \mathbf{H}^{B/B_0} = I \times \boldsymbol{\omega}^{E/B}) \quad (2.7)$$

The I term in Equation (2.7) is the symmetrical mass properties of the aircraft. Expanding and solving for the sum of moments in the system.

$$\frac{Ed}{dt} ({}^E \mathbf{H}^{B/B_0}) = \begin{bmatrix} I_{xx}\dot{P} - I_{xy}\dot{Q} - I_{xz}\dot{R} - I_{xz}PQ + I_{xy}PR + (I_{zz} - I_{yy})QR + (R^2 - Q^2)I_{yz} \\ I_{yy}\dot{Q} - I_{xy}\dot{P} - I_{yz}\dot{R} + I_{yz}PQ - I_{xz}PQ + (I_{xx} - I_{zz})PR + (P^2 - R^2)I_{xz} \\ I_{zz}\dot{R} - I_{xz}\dot{P} - I_{yz}\dot{Q} + I_{xz}QR - I_{yz}PR + (I_{yy} - I_{xx})PQ + (Q^2 - P^2)I_{xy} \end{bmatrix} \quad (2.8)$$

$$m\Delta\mathbf{r} \times^E \mathbf{V}^B = m \begin{bmatrix} (PV - QU + \dot{W} - g\cos(\Theta)\cos(\Phi))\Delta h + (PW - RU - \dot{V} + g\cos(\Theta)\sin(\Phi))\Delta d \\ (QU - PV - \dot{W} + g\cos(\Theta)\cos(\Phi))\Delta b + (QW - RV + \dot{U} + g\sin(\Theta))\Delta d \\ (RU - PW + \dot{V} - g\cos(\Theta)\sin(\Phi))\Delta b + (RV - QW - \dot{U} - g\sin(\Theta))\Delta h \end{bmatrix} \quad (2.9)$$

Equation (2.7) is the same as a generic airliner rotational equation of motion. The additional terms account for the asymmetry as a function of P, Q, R, U, V, W, and angular velocities rates. Due to the asymmetry now, the pitching moment is also coupled with the yaw and roll modes of the aircraft, as observed in Equation (2.10).

$\Phi$ ,  $\Theta$ , and  $\Psi$  are NASA standard (3-2-1) Euler's rotational angles, corresponding to roll, pitch, and yaw. Equation (2.10) maps the relationship between the previously defined angular rate and Euler's angle.

$$\begin{bmatrix} P \\ Q \\ R \end{bmatrix} = \begin{bmatrix} 1 & 0 & -\sin(\theta) \\ 0 & \cos(\phi) & \sin(\phi)\cos(\theta) \\ 0 & -\sin(\phi) & \cos(\phi)\cos(\theta) \end{bmatrix} \begin{bmatrix} \dot{\phi} \\ \dot{\theta} \\ \dot{\psi} \end{bmatrix} \quad (2.10)$$

## 2.4 Linearization

With the fully defined equation of motion for both translational and rotational, the next step is to linearize the equations of motion. A perturbation model is applied for this project since wing damage will most likely happen during steady-level flight conditions. The steady-level flight conditions assume that:

- Constant thrust
- Constant altitude/flight level, lift = weight
- Constant velocity, thrust = drag

The perturbation model introduces steady-level equilibrium terms and short-period perturbed terms [20]. Perturbed terms are defined as lowercase variables, and steady-level flight terms are described with one subscript. The velocity, force, velocity rates, angular velocity, and angular velocity rates can be expressed as the sum of equilibrium terms and perturbed terms.

- $U = U_1 + u, V = V_1 + v, W = W_1 + w$
- $\dot{U} = \dot{U}_1 + \dot{u}, \dot{V} = \dot{V}_1 + \dot{v}, \dot{W} = \dot{W}_1 + \dot{w}$
- $P = P_1 + p, Q = Q_1 + q, R = R_1 + r$
- $\Psi = \Psi_1 + \psi, \Theta = \Theta_1 + \theta, \Phi = \Phi_1 + \phi$
- $X = X_1 + f_x, Y = Y_1 + f_y, Z = Z_1 + f_z$
- $X_T = X_{T_1} + f_{T_x}, Y_T = Y_{T_1} + f_{T_y}, Z_T = Z_{T_1} + f_{T_z}$
- $L = L_1 + l, M = M_1 + m, N = N_1 + n$
- $L_T = L_{T_1} + l_T, M_T = M_{T_1} + m_T, N_T = N_{T_1} + n_T$

Combining the equilibrium and perturbed terms with equations of motion derived from Sections 1.2 and 1.3. Applying steady-level flight conditions and neglecting high order terms,  $uv, uw, wv$ , etc. Along with small angle approximation, the entire state equation of motion for damaged wing aircraft simplifies to:

$$-g\theta \cos(\Theta) + \frac{f_x}{m_a} + \frac{f_{tx}}{m_a} = \dot{u} - \dot{r}\Delta h + \dot{q}\Delta d \quad (2.11)$$

$$\phi g * \cos(\Theta_1) + \frac{f_y}{m_a} + \frac{f_{ty}}{m_a} = \dot{v} + U_1 r - \dot{p}\Delta d + \dot{r}\Delta b \quad (2.12)$$

$$-g\theta * \sin(\Theta_1) + \frac{f_z}{m_a} + \frac{f_{tz}}{m_a} = \dot{w} + U_1 q + \dot{p}\Delta h - \dot{q}\Delta b \quad (2.13)$$

$$l = I_{xx}\dot{p} - I_{xz}\dot{r} - I_{xy}\dot{q} \\ + m_a \left( (\dot{w} - U_1 q + g\theta \sin(\Theta_1))\Delta h + (U_1 r - \dot{v} + g\phi \cos(\Theta_1))\Delta d \right) \quad (2.14)$$

$$m = I_{yy}\dot{q} - I_{xy}\dot{p} - I_{yz}\dot{r} \\ + m_a \left( (U_1 q - \dot{w} - g\theta \sin(\Theta_1))\Delta h + (\dot{u} + g\theta \cos(\Theta_1))\Delta d \right) \quad (2.15)$$

$$n = -I_{xz}\dot{p} + I_{zz}\dot{r} - I_{yz}\dot{q} \\ + m_a \left( (U_1 r + \dot{v} - g\phi \cos(\Theta_1))\Delta b + (\dot{u} - g\theta \cos(\Theta_1))\Delta h \right) \quad (2.16)$$

Equations (2.11-2.16) are linearized equations of motion using the perturbation modeling method. Terms involving  $[\Delta b, \Delta h, \Delta d]$  multiplying with itself is negligible and assumed to be zero since even with up to 50% loss in wing area, the shift in change is relatively small, in the order of thousandths [14].

## 2.5 Stability and Control Derivatives

From Section 2.4, equations of motion derived from Newton's method still contain unknown terms like  $f_x, f_y, l, m, n$ , etc. These terms can be expressed as function so aerodynamic and control contributions from both aircraft body frame and aerodynamic forces.

$$\frac{f_x}{m_a} = X_u u + X_\alpha \alpha + X_{\delta_e} \delta_e \quad (2.17)$$

Where  $X_u, X_\alpha, X_{\delta_e}, X_T$ , are x-force contributions with respect to aircraft velocity, angle of attack, elevator deflection, and thrust, respectively. Similarly, the  $\frac{f_y}{m_a}, \frac{f_{ty}}{m_a}, \frac{f_z}{m_a}, \frac{f_{tz}}{m_a}$  can be expressed as:

$$\frac{f_z}{m_a} = Z_u u + Z_\alpha \alpha + Z_{\dot{\alpha}} \dot{\alpha} + Z_q q + Z_{\delta_e} \delta_e \quad (2.18)$$

$$\frac{f_y}{m_a} = Y_p p + Y_{\delta_a} \delta_a + Y_r r + Y_{\delta_r} \delta_r + Y_\beta \beta \quad (2.19)$$

$\beta$  is the sideslip angle of the aircraft, the angle between the heading and incoming airflow. In addition, the moment terms can be expressed from their respective coefficient terms and rates:

$$\frac{n}{I_{zz}} = N_{\delta_a} \delta_a + N_{\delta_r} \delta_r + N_{\beta} \beta + N_r r + N_p p \quad (2.20)$$

$$\frac{l}{I_{xx}} = L_{\delta_a} \delta_a + L_{\delta_r} \delta_r + L_{\beta} \beta + L_r r + L_p p \quad (2.21)$$

$$\frac{m}{I_{yy}} = M_u u + M_{\alpha} \alpha + M_{\dot{\alpha}} \dot{\alpha} + M_q q + M_{\delta_e} \delta_e \quad (2.22)$$

## 2.6 Fully Decoupled Equations of Motion

Substituting Equations (2.17- 2.22) into Equations (2.11- 2.16) and uncoupling the system equations solving for  $\dot{u}, \dot{\alpha}, \dot{\beta}, \dot{p}, \dot{q}, \dot{r}$ . Under steady-level flight conditions,  $Z_{\dot{\alpha}}$ , and  $Z_q$  contributions are small and therefore neglected. On the other hand,  $\dot{\beta} = \frac{\dot{w}}{U_1}$  and  $\dot{\alpha} = \frac{\dot{w}}{U_1}$  due to the geometric shape of the aircraft. Applying these assumptions and uncoupling the equations of motion, Equations (2.1- 2.16) can be expressed as:

$$\begin{aligned} \dot{u} = & \left[ X_u - \Delta dM_u - \frac{\Delta dM_{\dot{\alpha}} Z_u}{K} \right] * u + \left[ X_{\alpha} - \Delta dM_{\alpha} - \frac{\Delta dM_{\dot{\alpha}} Z_{\alpha}}{U_1 K} \right] * \alpha + \left[ -\frac{\Delta dU_{1M_{\dot{\alpha}}}}{K} - \Delta dM_q \right] * q + \\ & \left[ \frac{g \sin(\Theta_1) \Delta dM_{\dot{\alpha}}}{K} - g \cos(\Theta_1) \right] * \theta + [\Delta h N_p] * p + [\Delta h N_{\beta}] * \beta + [\Delta h N_r] * r + [\Delta h * N_{\delta_a}] * \delta_a + \\ & [\Delta h N_{\delta_r}] * \delta_r + [X_{\delta_e} - \Delta h M_{\dot{\alpha}} Z_{\delta_e} - \Delta dM_{\delta_e}] * \delta_e \end{aligned} \quad (2.23)$$

$$\begin{aligned} \dot{\alpha} = & \left[ \frac{Z_u}{K} + \frac{\Delta b M_u}{K} \right] * u + \left[ \frac{Z_{\alpha}}{K} + \frac{\Delta b M_{\alpha}}{K} \right] * \alpha + \left[ \frac{U_1}{K} + \frac{\Delta b M_q}{K} + \frac{Z_q}{K} \right] * q + [-g \sin(\Theta_1)] * \theta + \left[ -\frac{\Delta h L_p}{K} \right] * \\ & p + \left[ -\frac{\Delta h L_{\beta}}{K} \right] * \beta + \left[ -\frac{\Delta h L_r}{K} \right] * r + \left[ -\frac{\Delta h L_{\delta_a}}{K} \right] * \delta_a + \left[ -\frac{\Delta h L_{\delta_r}}{K} \right] * \delta_r + \left[ \frac{Z_{\delta_e}}{K} + \frac{\Delta b M_{\delta_e}}{K} \right] * \delta_e \end{aligned} \quad (2.24)$$

$$\begin{aligned} \dot{\beta} = & \left[ \frac{Y_p}{U_1} + \frac{\Delta d L_p}{U_1} - \frac{\Delta b N_p}{U_1} \right] * p + \left[ \frac{Y_{\beta}}{U_1} + \frac{\Delta d L_{\beta}}{U_1} - \frac{\Delta b N_{\beta}}{U_1} \right] * \beta + \left[ \frac{Y_r}{U_1} + \frac{\Delta d L_r}{U_1} - \frac{\Delta b N_r}{U_1} - 1 \right] * r + \\ & \left[ \frac{g * \cos(\Theta_1)}{U_1} \right] * \phi + \left[ \frac{Y_{\delta_a}}{U_1} + \frac{\Delta d L_{\delta_a}}{U_1} - \frac{\Delta b N_{\delta_a}}{U_1} \right] * \delta_a + \left[ \frac{Y_{\delta_r}}{U_1} + \frac{\Delta d L_{\delta_r}}{U_1} - \frac{\Delta b N_{\delta_r}}{U_1} \right] * \delta_r \end{aligned} \quad (2.25)$$

$$\begin{aligned} \dot{p} = & \left[ \frac{m_a \Delta h Z_u}{I_{xx}} \right] * u + \left[ -\frac{m_a \Delta h Z_{\alpha}}{I_{xx}} \right] * \alpha + \left[ -\frac{m_a \Delta h h q}{I_{xx}} \right] * q + \left[ L_p + \frac{m_a \Delta d Y_p}{I_{xx}} \right] * p + \left[ L_{\beta} + \frac{m_a \Delta d Y_{\beta}}{I_{xx}} \right] * \\ & \beta + \left[ L_r + \frac{m_a \Delta d Y_r}{I_{xx}} \right] * r + \left[ L_{\delta_a} + \frac{m_a \Delta d Y_{\delta_a}}{I_{xx}} \right] * \delta_a + \left[ L_{\delta_r} + \frac{m_a \Delta d Y_{\delta_r}}{I_{xx}} \right] * \delta_r + \left[ -\frac{m_a \Delta h Z_{\delta_e}}{I_{xx}} \right] * \delta_e \end{aligned} \quad (2.26)$$

$$\dot{q} = \left[ M_u + \frac{Z_u M_{\dot{\alpha}}}{K} + \frac{m_a \Delta b Z_u}{I_{yy}} - \frac{m_a \Delta d X_u}{I_{yy}} + \frac{\Delta b M_u M_{\dot{\alpha}}}{K} \right] * u + \left[ M_{\alpha} + \frac{Z_{\alpha} M_{\dot{\alpha}}}{K} + \frac{m_a \Delta b Z_{\alpha}}{I_{yy}} - \frac{m_a \Delta d X_{\alpha}}{I_{yy}} + \frac{M_{\dot{\alpha}} \Delta b M_{\alpha}}{K} \right] * \alpha + \left[ M_q + \frac{M_{\dot{\alpha}} U_1}{K} + \frac{M_{\dot{\alpha}} Z_{\alpha}}{K} + \frac{M_{\dot{\alpha}} \Delta b M_{\alpha}}{K} \right] * q + \left[ -\frac{M_{\dot{\alpha}} g \sin(\Theta_1)}{K} \right] * \theta + \left[ \frac{-M_{\alpha} \Delta h L_p}{K} \right] * p + \left[ \frac{-M_{\alpha} \Delta h L_{\beta}}{K} \right] * \beta + \left[ \frac{-M_{\alpha} \Delta h L_r}{K} \right] * r + \left[ \frac{-M_{\alpha} \Delta h L_{\delta a}}{K} \right] * \delta_a + \left[ \frac{-M_{\alpha} \Delta h L_{\delta r}}{K} \right] * \delta_r + \left[ M_{\delta_e} + \frac{M_{\dot{\alpha}} * Z_{\delta_e}}{K} + \frac{m_a \Delta b Z_{\delta_e}}{I_{yy}} - \frac{m_a \Delta b X_{\delta_e}}{I_{yy}} + \frac{-M_{\dot{\alpha}} M_{\delta_e} \Delta b}{K} \right] \delta_e \quad (2.27)$$

$$\dot{r} = \left[ \frac{m_a \Delta h X_u}{I_{zz}} \right] * u + \left[ \frac{m_a \Delta h X_{\alpha}}{I_{zz}} \right] * \alpha + [0] * q + \left[ N_p - \frac{m_a * \Delta b * Y_p}{I_{zz}} \right] * p + \left[ N_{\beta} - \frac{m_a * \Delta b * Y_{\beta}}{I_{zz}} \right] * \beta + \left[ N_r - \frac{m_a * \Delta b * Y_r}{I_{zz}} \right] * r + \left[ N_{\delta_a} - \frac{m_a * \Delta b * Y_{\delta_a}}{I_{zz}} \right] * \delta_a + \left[ N_{\delta_r} - \frac{m_a * \Delta b * Y_{\delta_r}}{I_{zz}} \right] * \delta_r + \left[ \frac{m_a \Delta h X_{\delta_e}}{I_{zz}} \right] * \delta_e \quad (2.28)$$

Where K represent  $(U_1 - \Delta b M_{\dot{\alpha}})$ . Equations (2.23-2.28) fully model the open airframe of the asymmetrical aircraft for a conventional design. Comparing Equation (2.23) to Equation (2.28) to symmetrical undamaged aircraft equations of motion, Equation (2.29), and Equation (2.30), if the shift in CG terms  $[\Delta b, \Delta h, \Delta d]$  is zero, then the equations of motion would be identical to the undamaged equations of motion. For the full derivation, readers can reference Appendix A.

$$\begin{bmatrix} \dot{u} \\ \dot{\alpha} \\ \dot{q} \\ \dot{\theta} \end{bmatrix} = \begin{bmatrix} X_u & X_{\alpha} & 0 & -g \\ \frac{Z_u}{U_1} & \frac{Z_{\alpha}}{U_1} & 1 & 0 \\ M_u + \frac{M_{\dot{\alpha}} Z_{\alpha}}{U_1} & M_{\alpha} + \frac{M_{\dot{\alpha}} Z_{\alpha}}{U_1} & M_q + M_{\dot{\alpha}} & 0 \\ 0 & 0 & 1 & 0 \end{bmatrix} \begin{bmatrix} u \\ \alpha \\ q \\ \theta \end{bmatrix} + \begin{bmatrix} X_{\delta_e} \\ \frac{Z_{\delta_e}}{U_1} \\ M_{\delta_e} + \frac{M_{\dot{\alpha}} Z_{\delta_e}}{U_1} \\ 0 \end{bmatrix} \delta_e \quad (2.29)$$

$$\begin{bmatrix} \dot{\phi} \\ \dot{p} \\ \dot{\beta} \\ \dot{r} \\ \dot{\psi} \end{bmatrix} = \begin{bmatrix} 0 & 1 & 0 & 0 & 0 \\ 0 & L_p & L_{\beta} & L_r & 0 \\ \frac{g * \cos(\Theta_1)}{U_1} & \frac{Y_p}{U_1} & \frac{Y_{\beta}}{U_1} & \frac{Y_r}{U_1} - 1 & 0 \\ 0 & N_p & N_{\beta} & N_r & 0 \\ 0 & 0 & 0 & 1 & 0 \end{bmatrix} \begin{bmatrix} \phi \\ p \\ \beta \\ r \\ \psi \end{bmatrix} + \begin{bmatrix} 0 & 0 \\ L_{\delta_r} & L_{\delta_a} \\ \frac{Y_{\delta_r}}{U_1} & \frac{Y_{\delta_a}}{U_1} \\ N_{\delta_r} & N_{\delta_a} \\ 0 & 0 \end{bmatrix} \begin{bmatrix} \delta_r \\ \delta_a \end{bmatrix} \quad (2.30)$$

### 3. Asymmetrical Aircraft Analysis and Simulation

This chapter focuses on the simulation and analysis of the model defined in Chapter 2, Equations (2.23- 2.28), to provide a clear view of the damaged wing open loop dynamics and a closed-loop controller design. To simulate Equation (2.23-2.28), unknown terms  $X_w, X_\alpha, X_{\delta e}$ , etc., needs to be redefined following the damaged wing aerodynamic properties. In addition, unlike undamaged/nominal aircraft, damaged wing airplanes have complicated stability behavior due to aerodynamic and inertia coupling between longitudinal and lateral/directional modes. Therefore, the entire system must be reassessed and reevaluated.

#### 3.1 Aerodynamic and Mass Properties

Control and Stability derivatives for Boeing 747 are well defined in literature; however, little attention is given to wing damage scenarios. But based on the physical change, damaged aerodynamic properties will significantly differ from its undamaged/nominal state. When only one side of the wing sustains damage, portions of it are missing, the most noticeable effect is the roll instability introduced to the system. Due to differential lift, the aircraft should have a new tendency to roll into the damaged wing side. In addition, as mentioned in [21], due to the shift in CG location affecting the moment arm of each mode, some of the control surfaces are now less or more effective compared to the nominal case. For example, in the case of CG shift along the x direction, it has a mitigating effect on the elevator of the aircraft, weakening its effectiveness due to the decrease in distance between the elevator aerodynamic center to the CG location. Due to the changes mentioned in this section, aerodynamic properties for the damaged wing scenario must be calculated. However, this would require running extensive computational fluid dynamics, CFD, and analysis for the damaged wing body frame, which is not the focus of this project. Therefore, damaged wing aerodynamics and mass properties were obtained through similar literature, on a Boeing 747 with 33% damage to the left-wing [22]. This section only reviews the 33% wing-damaged case to validate the equations of motion defined in Chapter 2. However, most damage cases will be reviewed in later sections.

**Table 3.1** - Aerodynamic coefficient for 33% damaged wing aircraft [22]

<b>Aerodynamic coefficient</b>	<b>Value</b>	<b>Aerodynamic coefficient</b>	<b>Value</b>
$C_{L0}$	0.29588	$C_{y\beta}$	-0.89
$C_{D0}$	0.0443	$C_{l\beta}$	-0.141
$C_{m\alpha}$	-1.1952	$C_{n\beta}$	0.1605
$C_{D\alpha}$	0.5	$C_{lp}$	-0.229
$C_{mq}$	-25.194	$C_{np}$	-0.02284
$C_{L\alpha}$	4.75	$C_{lr}$	0.12
$C_{x\delta e}$	0	$C_{nr}$	-0.329
$C_{z\delta e}$	0.29	$C_{L\delta\alpha}$	0.007056
$C_{m\delta e}$	-1.19	$C_{n\delta\alpha}$	0.0018
$C_{yp}$	0	$C_{y\delta r}$	0.117
$C_{n\delta r}$	-0.094	$C_{l\delta r}$	0.008024

**Table 3.2** - Mass and geometry properties for 33% of damaged wing aircraft [22]

Parameter	Value	Parameter	Value
Weight	623903.08 lbf	$I_{yy}$	33090070 <i>slugs.ft<sup>2</sup></i>
b	161.06 ft	$I_{zz}$	46598720 <i>slugs.ft<sup>2</sup></i>
$\bar{c}$	28.54 ft	$I_{xx}$	15097500 <i>slugs.ft<sup>2</sup></i>

For comparison, Tables 3.3 and 3.4 showcase the aerodynamic, mass, and geometry properties of undamaged/nominal cases.

**Table 3.3** - Aerodynamic coefficients for undamaged wing aircraft [22]

Aerodynamic coefficient	Value	Aerodynamic coefficient	Value
$C_{L0}$	0.29	$C_{y\beta}$	-0.9
$C_{D0}$	0.0305	$C_{l\beta}$	-0.16
$C_{m\alpha}$	-1.6	$C_{n\beta}$	0.16
$C_{D\alpha}$	0.5	$C_{lp}$	-0.34
$C_{mq}$	-25.5	$C_{np}$	0.020
$C_{L\alpha}$	5.5	$C_{lr}$	0.13
$C_{x\delta e}$	0	$C_{nr}$	-0.033
$C_{z\delta e}$	0.29	$C_{L\delta\alpha}$	0.014
$C_{m\delta e}$	-1.2	$C_{n\delta\alpha}$	0.0018
$C_{yp}$	-0.0272	$C_{y\delta r}$	0.118
$C_{n\delta r}$	-0.095	$C_{l\delta r}$	0.008

**Table 3.4** - Mass and geometry properties for 33% of damaged wing aircraft [22]

Parameter	Value	Parameter	Value
Weight	636636 lbf	$I_{yy}$	33100000 <i>slugs.ft<sup>2</sup></i>
b	195.68 ft	$I_{zz}$	49700000 <i>slugs.ft<sup>2</sup></i>
$\bar{c}$	27.31 ft	$I_{xx}$	18200000 <i>slugs.ft<sup>2</sup></i>

Comparing Tables 3.1 and 3.2 to Tables 3.3 and 3.4, losing portions of the wing dramatically affects the aerodynamic and mass properties of the aircraft. For longitudinal stability,  $C_{m\alpha}$  decreased significantly and made the mode less stable. While it is still stable, it does show that due to the shift in CG, the damping effects from horizontal stabilizers are less effective. In addition, similar behavior is observed for parameters like  $C_{m\delta e}$  and  $C_{mq}$ . On the other hand, for lateral/direction stability,  $C_{np}$  increased because of a less effective roll rate due to loss in the wing area. In addition,  $C_{lp}$  becomes less effective due to less force and shorter moment arm.

Control and Stability terms were calculated using equations listed in Nelson [23, Sec. 3] and [24]. Equations (3.1, 3.2) showcase the A and B matrix of the damaged wing state-space model.

$$A_d = \begin{bmatrix} -0.0182 & 1.0196 & -0.0002 & -32.1458 & 0 & 0.0003 & 0.0331 & -0.0048 & 0 \\ -0.0001 & -0.3253 & 1.0000 & -0.0015 & 0 & 0 & 0.0001 & 0 & 0 \\ -0.0001 & -1.2859 & -0.4990 & 0.1754 & 0 & 0 & 0 & 0 & 0 \\ 0 & 0 & 1 & 0 & 0 & 0 & 0 & 0 & 0 \\ 0 & 0 & 0 & 0 & 0 & 1 & 0 & 0 & 0 \\ 0.0001 & 0.5568 & 0 & 0 & 0 & -0.2685 & -1.0938 & 0.1678 & 0 \\ 0 & 0 & 0 & 0 & 0.0369 & 0 & -0.0535 & -1.0000 & 0 \\ 0 & 0.007 & 0 & 0 & 0 & 0.0062 & 0.6868 & -0.1012 & 0 \\ 0 & 0 & 0 & 0 & 0 & 0 & 0 & 1 & 0 \end{bmatrix} \quad (3.1)$$

$$B_d = \begin{bmatrix} 0 & -0.015 & -0.0005 \\ -0.0176 & 0 & 0 \\ -1.0525 & 0 & 0 \\ 0 & 0 & 0 \\ 0 & 0 & 0 \\ 0.0301 & 0.2040 & 0.1271 \\ 0 & 0.0036 & 0 \\ 0 & -0.3145 & -0.0113 \\ 0 & 0 & 0 \end{bmatrix} \quad (3.2)$$

### 3.2 Open-Loop Simulation

This section covers the open-loop simulation for the nominal/undamaged wing body and the 33% damaged model discussed in Section 3.1. For this project, only the roll and yaw state are presented in this section, but the full state open-loop output can be found in Appendix B.

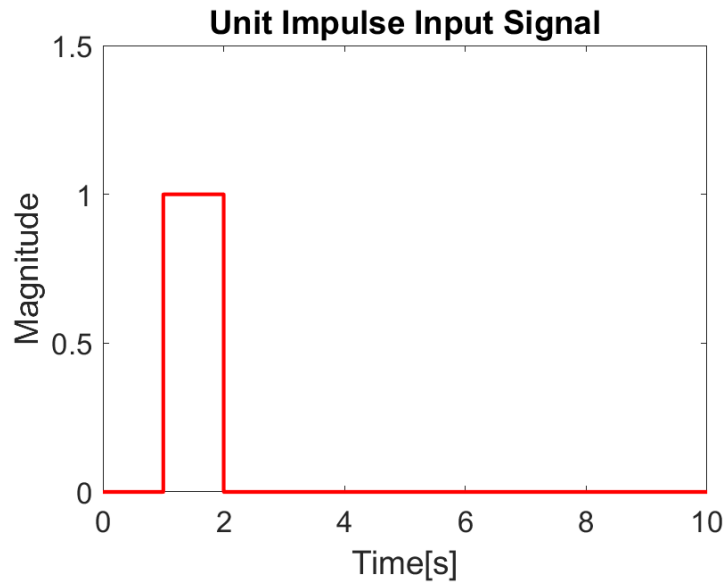


Figure 3.1 Input signal for simulation

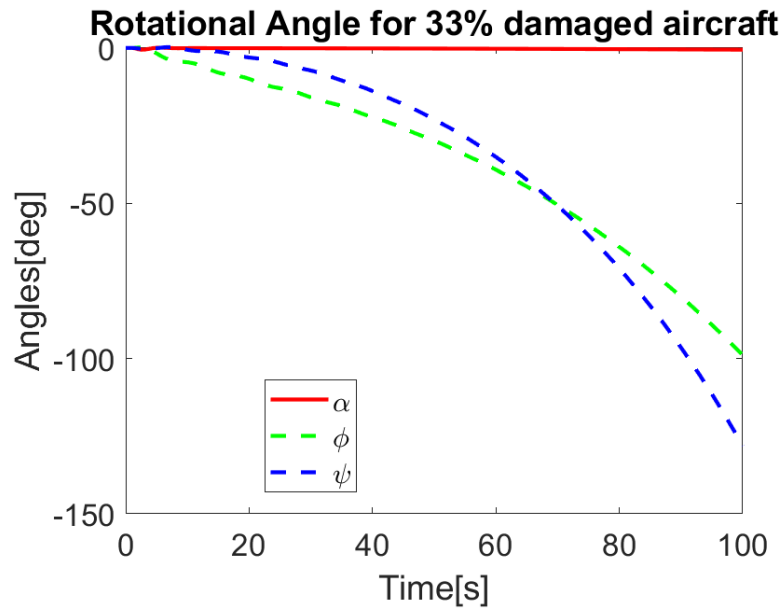


Figure 3.2 Wing damage rotational angle output

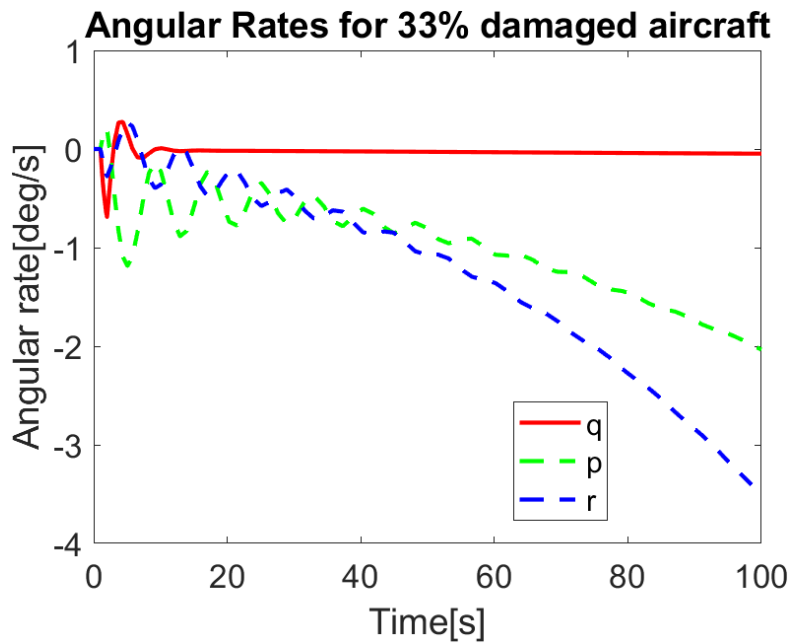


Figure 3.3 Wing damage angular rate output

The open loop response is simulated using a unit-impulse input signal, as shown in Figure 3.1. This input signal is meant to simulate how the system responds under sudden changes in its states; in this scenario, sudden changes in yaw, pitch, and roll angle. Firstly, the damage wing scenario causes complex coupling between longitudinal and lateral-directional modes. Despite showing very subtle differences in pitch angle and rate, the pitch angle diverges as time goes to infinity, which is the expected behavior from the damage case scenario. The nose-down motion can be explained by the overall lift reduction produced by both wings. As a result of the

loss of lift, the aircraft's speed also increases dramatically due to a nosedive, Figure 3.4. On the side of lateral-directional behavior, very oscillatory roll and yaw rates are observed. This is due to the inverse coupling effect of the damaged wing system. With the damage sustained on the left wing, the aircraft will now tend to roll to the left, a negative roll. Similarly, due to the damage, a differential drag was also introduced to the system, introducing a yaw moment away from the damaging side, positive yaw. The system exhibits very oscillatory behavior due to the constant tug-of-war behavior of yaw and roll motion. Since the rolling motion is more dominant than yaw, mainly because of the lifting surface differences, eventually, roll motion wins the battle and drives both states to negative infinity.

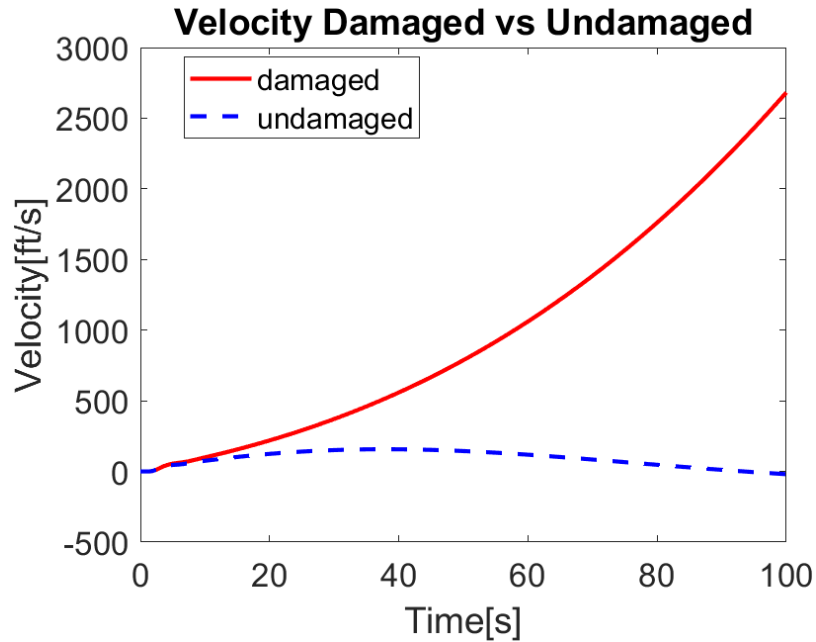


Figure 3.4 Velocity for damaged and undamaged aircraft

Looking at the open loop comparison between damaged and undamaged cases, Figure 3.4, after sustaining 33% damage to its left wing, the aircraft quickly becomes unstable and unrecoverable. In Section 3.5, a wing-level controller design will aim to restore the system post-damage.

### 3.3 Open Loop Analysis

This section reviews the pole locations of the damaged wing aircraft and comparison with the undamaged/nominal case.

**Table 3.5** - Longitudinal pole locations for damaged and undamaged aircraft

Mode	Damaged pole location	Undamaged pole location
Short-Period	$-0.4121 \pm 1.1306i$	$-0.4678 \pm 1.2469i$
Phugoid	$-0.0182, 0$	$-0.218, 0$

**Table 3.6** - Lateral/directional pole locations for damaged and undamaged aircraft

Mode	Damaged pole location	Undamaged pole location
Roll	0.0093	-0.5099
Spiral	0.0049	-0.4758
Dutch	$0.0146 \pm 0.0118i$	$-0.1073 \pm 1.0106i$

The pole location comparison between undamaged and damaged are listed in Table 3.5 and Table 3.6. The longitudinal pole locations indicate that the short-period mode became less stable post-damage, -0.4121 and -0.4678. This aligns with the observation seen with the open-loop simulation in Section 3.2, with a high imagine part and a stable real part. Since the short-period approximation is only suitable for the initial few seconds, it is reasonable that it cannot predict the divergent behavior seen in Figure 3.3. On the other hand, the phugoid mode also became less stable, which aligns with Figure 3.4.

The lateral-directional modes for the damaged aircraft share a similar story. The spiral mode is slightly unstable compared to the undamaged case, and the Dutch roll mode is unstable and oscillatory. Roll mode pole location is also expected, 0.0093 compared to -0.4758. As discussed before, all three of the previously stable later-directional modes are now unstable and coupled due to the damaged wing.

### 3.4 Closed Loop Controller Design

As seen in Section 3.2, the damaged wing model exhibit very unstable and oscillatory roll and yaw coupling. This chapter will aim to design a wing-level controller using modern control techniques to regain stability for the aircraft post-damage.

#### 3.4.1 Setup

Figure 3.3 shows that the roll and yaw angle has a very high coupling effect and is unstable in the damage case. While the pitch angle is somewhat unaffected by the damaged wing scenario. Therefore, for the wing level controller design, the elevator deflection will remain zero, fix-stick condition, aileron, and rudder will be the main source of control surfaces to level the aircraft. The very first step is to check the controllability and observability of the full system; the observability and controllability matrices are outlined as follows [25]:

$$CO = [B, AB, A^2B, \dots, A^{n-1}B] \quad (3.3)$$

$$OB = [C; CA; CA^2; \dots; CA^{n-1}] \quad (3.4)$$

Using *obsv* and *ctrb* from MATLAB built-in mathematical tools, the controllability and observability matrices are calculated, and the rank of each matrix is computed. For more detail, review Appendix C. As seen in table 4.1, the full-state 9x9 matrix is fully controllable and observable.

**Table 3.7** - Controllability and observability matrices ranks

Controllability rank	9
Observability rank	9

### 3.4.2 Results

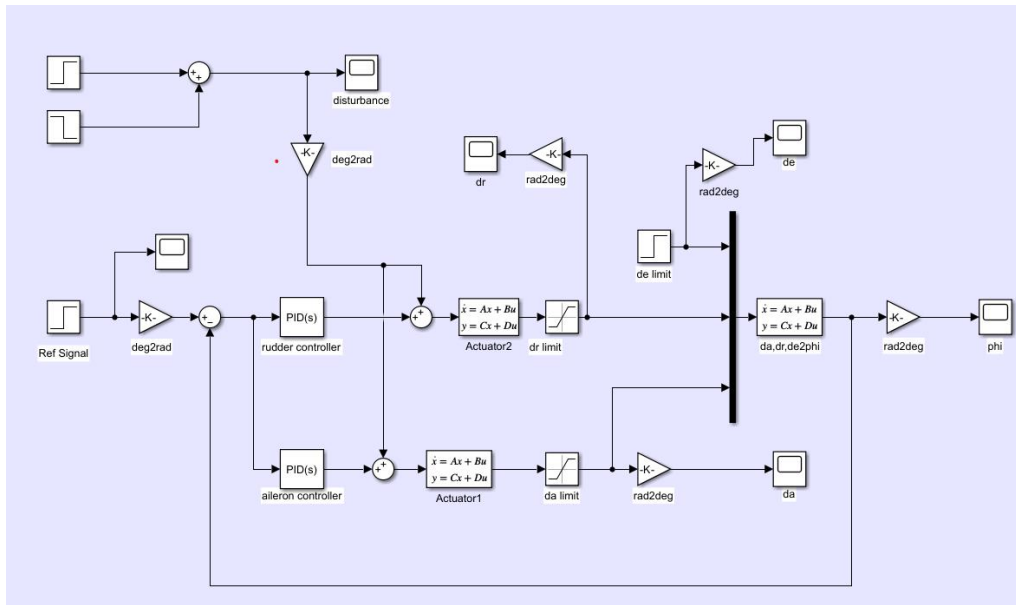


Figure 3.5 Block diagram for wing level controller design

The controller design uses the modern PID control method, which features three new gain variables to place the pole locations of the system, proportional gain ( $K_p$ ), integral gain ( $K_i$ ) and derivative gain ( $K_d$ ). Each control surface has its own PID controller and actuator matrix, Table 3.8 and Equation (3.5), respectively. For general commercial transport like the Boeing 747, the control surfaces limitation is listed in Equation (3.6) [26]. Lastly, the system is simulated using an impulse signal on the rudder and aileron control surfaces, Figure 3.6.

$$\text{Control Surface Actuator} = \frac{10}{s+10} \quad (3.5)$$

$$-30^\circ \leq \delta_e \leq 20^\circ, -20^\circ \leq \delta_a \leq 20, -30^\circ \leq \delta_r \leq 30 \quad (3.6)$$

**Table 3.8** - PID controller gain values

	$K_p$	$K_i$	$K_d$
Aileron	15	6	10
Rudder	1	1	1

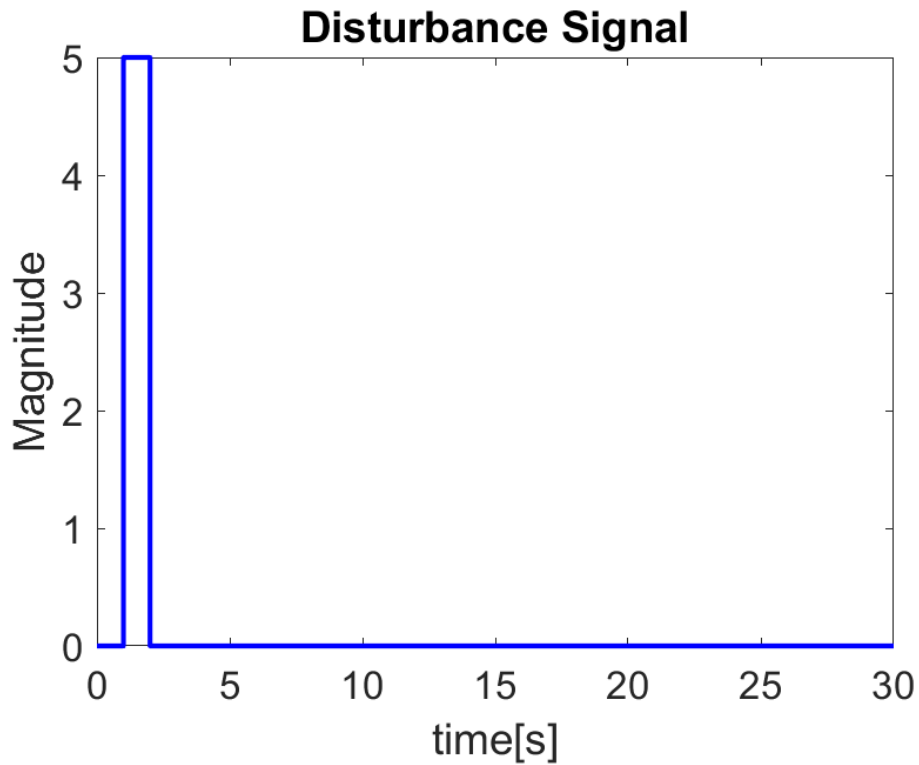


Figure 3.6 Block diagram for wing level controller design

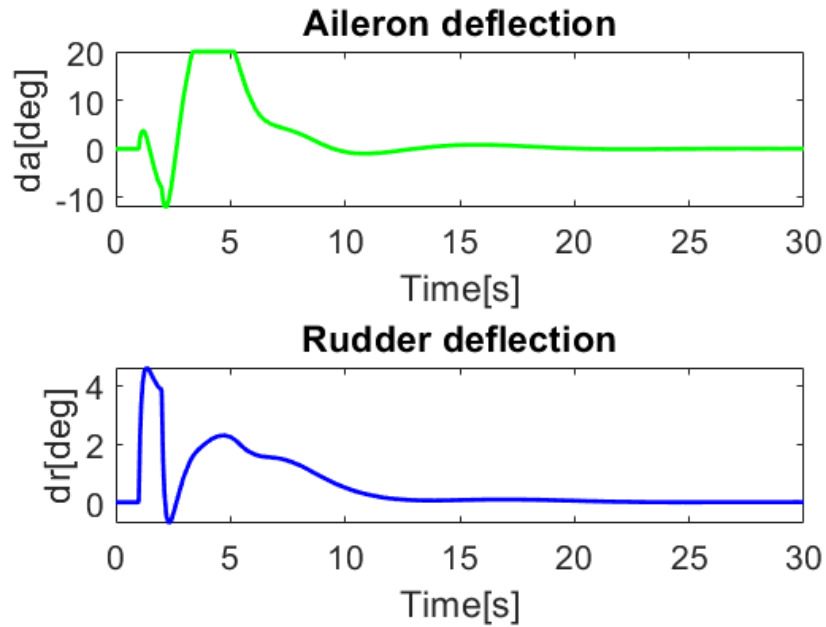


Figure 3.7 Deflection under 5-degree input

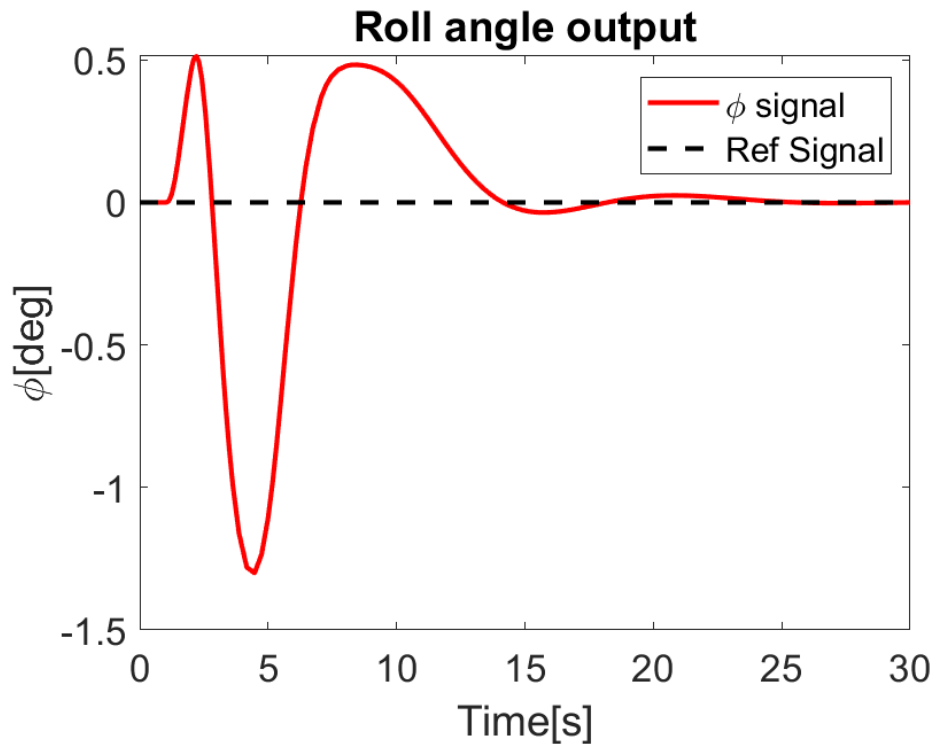


Figure 3.8 Roll angle response under 5-degree input signal

As seen in Figure 3.8, the system can achieve an equilibrium state after a 5-degree impulse input signal within 1 sec, with both rudder and aileron deflection angle within the control surfaces limitation. One key thing to note is that during recovery, the aileron deflection did max out at 20 degrees for 2-3 seconds. This indicates that while the system can track the reference signal, a higher input signal should result in a divergent state. If the maximum deflection of the aileron cannot overcome the disturbance moment, combined with the differential lift moment, the aircraft roll motion will result in an unstable state. Therefore, although a simple PID controller can level the wing, it is insufficient from a long-term stability standpoint. Figures 3.9-3.10 showcase the roll angle response down a 10-degree input signal. This calls for a more advanced and powerful control method to stabilize the damaged aircraft, which will be the research focus of the later part of this project.

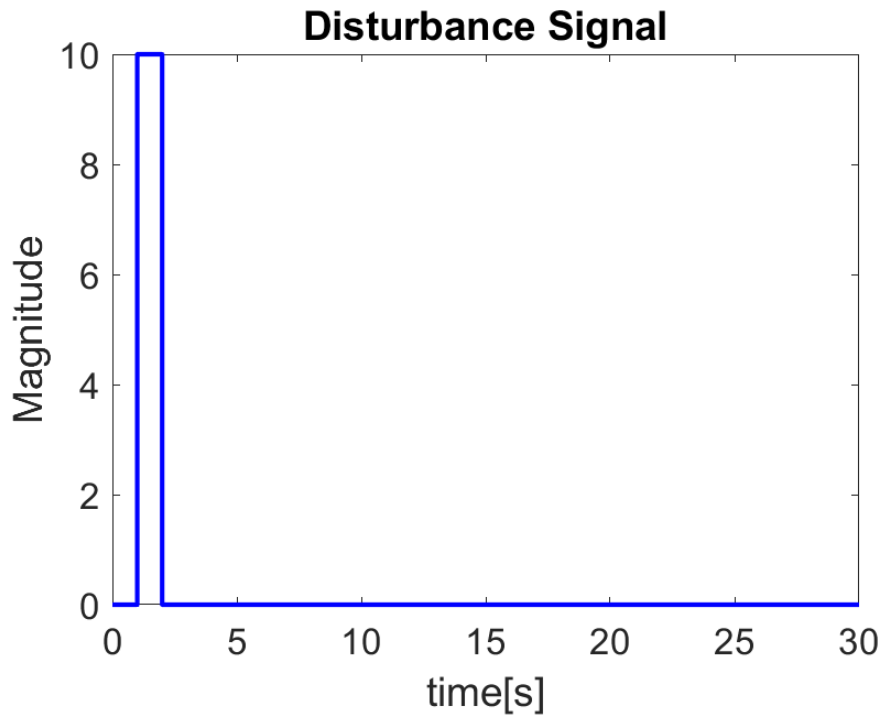


Figure 3.9 10-degree input signal

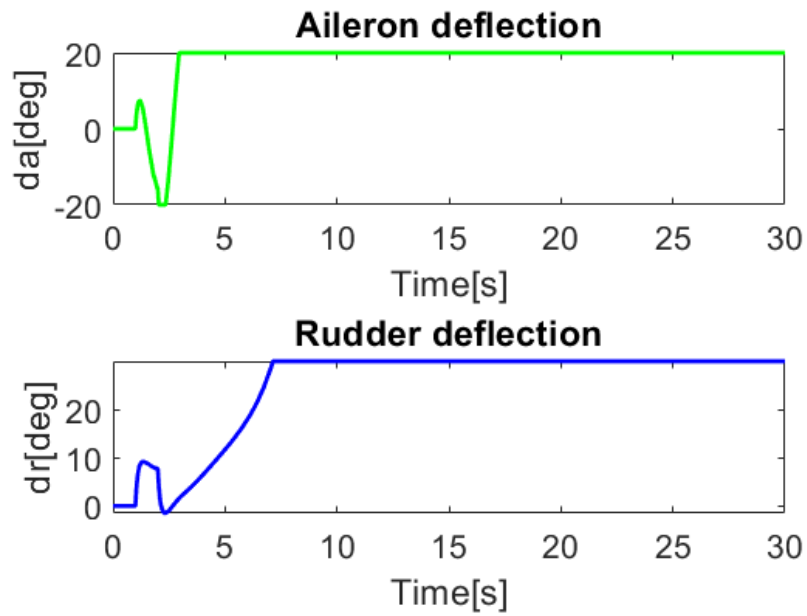


Figure 3.10 Control surfaces response under 10-degree input

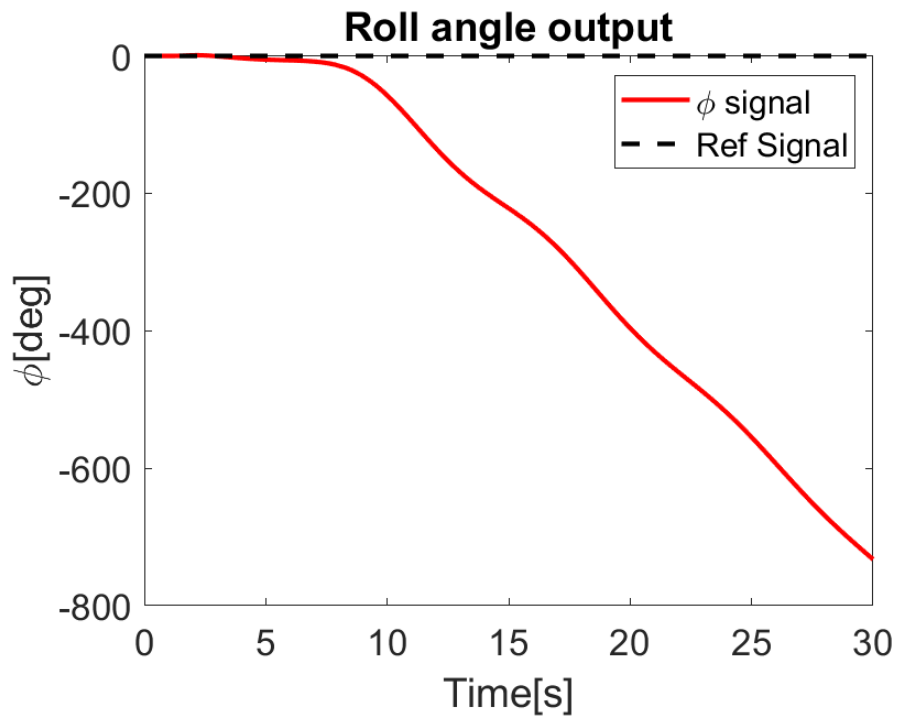


Figure 3.11 Control surfaces response under 10-degree input

## 4. Morph Wing Design

As seen in previous sections, the damaged wing model introduces the nominally stable system to an unstable disaster state. Even with a good enough control design, the existing control surfaces do not provide sufficient headroom to land the plane safely. The most significant issues with losing a portion of the wing are the differential lift and drag introduced to the system. While it is possible to deploy other control surfaces as contingencies like flaps and differential thrust to counter the instability, those control surfaces should not be considered emergency solutions due to airplanes' reliance on said surfaces to land safely. Therefore, an out-of-the-box solution is desired. This chapter discusses the assumption, concept, and feasibility of the morph wing implementation in traditional commercial airplanes.

Modern technological advancement introduced the wonders of morph wing technologies; the biggest challenge in current morph wing design is material and structural problems. The material selected for morphing must be flexible enough to sustain the transformation process while retaining its properties. On the other hand, the transformed structure must sustain the new aerodynamic forces and structural loads introduced to the system. However, morph wing design offers many benefits, ranging from low flow separation to minimal weight penalties [27]. While most literature on morph implementation focuses on making the aircraft more energy and aerodynamically efficient, morph wing design can be utilized as an emergency solution to damaged wing scenarios. Despite many morphing methods, this project focuses on in-plane chord-wise morphing along the entire wing, Figure 4.1.

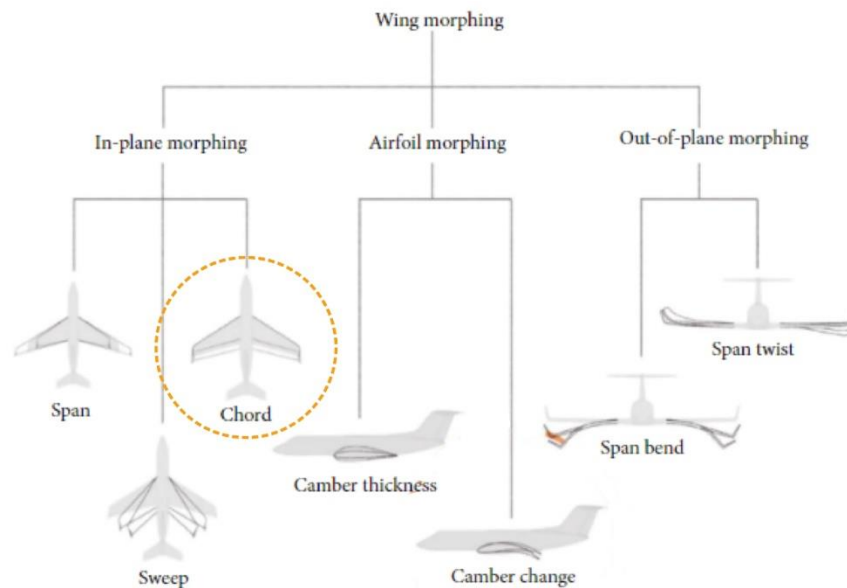


Figure 4.1 Different types of morphing wings [28]

In-plane chord-wise morphing is a type of morphing technique that extends the chord of the aircraft in flight. As a result, the wing area is drastically increased. This morphing design is selected due to the damaged aircraft's behavior. As discussed in previous chapters, damaged-

wing aircraft tend to roll violently and yaw into the damaged side from the missing lift and drag forces. On the other hand, an in-plane chord-wise morphed wing increases the lift and drag forces. If said design is deployed on the damaged wing side, this can help the aircraft to recover the missing lift and drag forces and reintroduce stability to the system. Figure 4.2 showcases the simplified model for the proposed design, with one side of the wing morphed while the opposite remains the same.

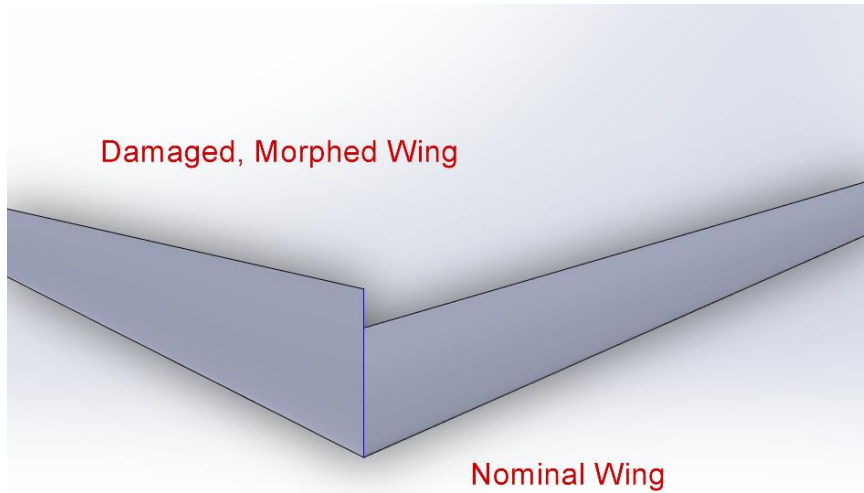


Figure 4.2 Morph wing design preview

The internal structure of the morphing wing also plays an important role as well. The design of the morphing mechanism was inspired by Barbarino, Gandhi, and Webster's application of morphing design in helicopter blades [27]. Barbarino et al. [27] proposed an internal cellular structure design for an airfoil that can undergo one-dimensional morphing along the chord direction. The main morphing mechanism span from the quarter-chord point (25%) to 15% from the trailing edge, leaving a 60% morphable region in the wing, Figure 4.2. The main source of concern for a morphable wing is strain and stress [27]. First, the material selection must be able to sustain a 50% displacement without any form of permanent deformation. Therefore, the combined strain from aerodynamic forces and stretching forces must be well within its elastic region. Second, due to the increase in lifting surfaces, the internal load distribution must be able to withhold the new wing flight conditions.

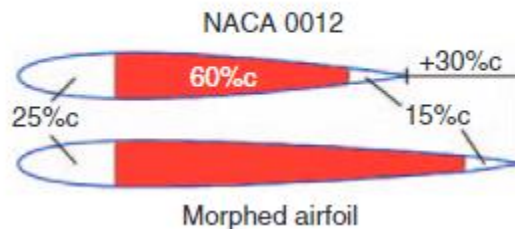


Figure 4.3 Morph section concept [28]

To qualify for suitable material, the material must have a “low in-plane stiffness and low out-of-plane deformations of the unsupported section under aerodynamic loads” [27]. Elastomeric materials are suitable candidates for morph wing application due to their high maximum strain with low activation forces [28]. The material itself must have a high sustain pressure value while remaining flexible. Tecoflex 93A is an ideal candidate for material selection due to its high-pressure load with over 100% deformation tolerance [29]; refer to Table 4.1 below. Tecoflex is a medical-grade aliphatic polyether polyurethane that offers good mechanical and thermal properties.

**Table 4.1** - Material comparison of strain and max force [29]

<b>Material</b>	<b>Strain</b>	<b>Max force (lbs)</b>
Tecoflex 80A	2	7.98
Tecoflex 100A	0.581	20.62
Tecoflex 93A	1.12	139.88
Riteflex 640A	1	11.57
Riteflex 663A	0.613	16.63
Arnitel	1.24	81.64
Shape memory polymer	1.04	9.68
Spandura	0.78	235.96
Tru-stretch (stiffly woven)	0.2	231.22
Tru-stretch (lightly woven)	0.7	179.47

The morph mechanism proposed in this project will operate under the following assumptions and conditions. First, due to the unpredictability of damage locations, the damaged side control surfaces are assumed to malfunction, leaving only one aileron for control. Second, the morphing structure should not affect the overall internal structure of the wing. Fuselage, flaps, and slats are assumed to maintain their function under morphed conditions. Third, since the morph motion is along the x-direction of the airframe, shift in the center of lift and mass along the y-direction is assumed to be negligible. Last, the morphing motion should be automatically deployed upon a sensor built-into the wing. All assumptions are listed as:

- The base/root of the wing cannot be morphed due to physical constraints. The morphable section is 95% of the full span.
- The morphing mechanism is built on top of the existing supporting structure.
- The morph motion does not affect the internal static components like fuel cells.
- The morphing structure does not affect the deployment of flaps and slats.
- The morphing mechanism should automatically deploy upon the high rolling moment and angle.

## 5. Morph Wing Analysis

This chapter covers the morph wing design concept proposed in Chapter 4, from basic design ideas to baseline design simulations. One of the biggest challenges is to design a closed-loop feedback system that takes in the current state of the aircraft and modifies the morphing ratio respectively. This chapter will discuss the morphing ratio based on the morphed section's lift and drag contribution, along with the damaged-wing lift and drag forces.

### 5.1 Morph Design Flow Diagrams

First, it is important to discuss the general design idea of the morph wing implementation with a full system overview. Figure 5.1 showcases the basic flow diagram for the morph wing implementation on top of the typical aircraft control design. The morph implementation block would take the system state as input and calculate the required morphing ratio to counter the differential lift and drag needed to restabilize the aircraft.

### Morph Wing Damage Aircraft Design Flow Chart

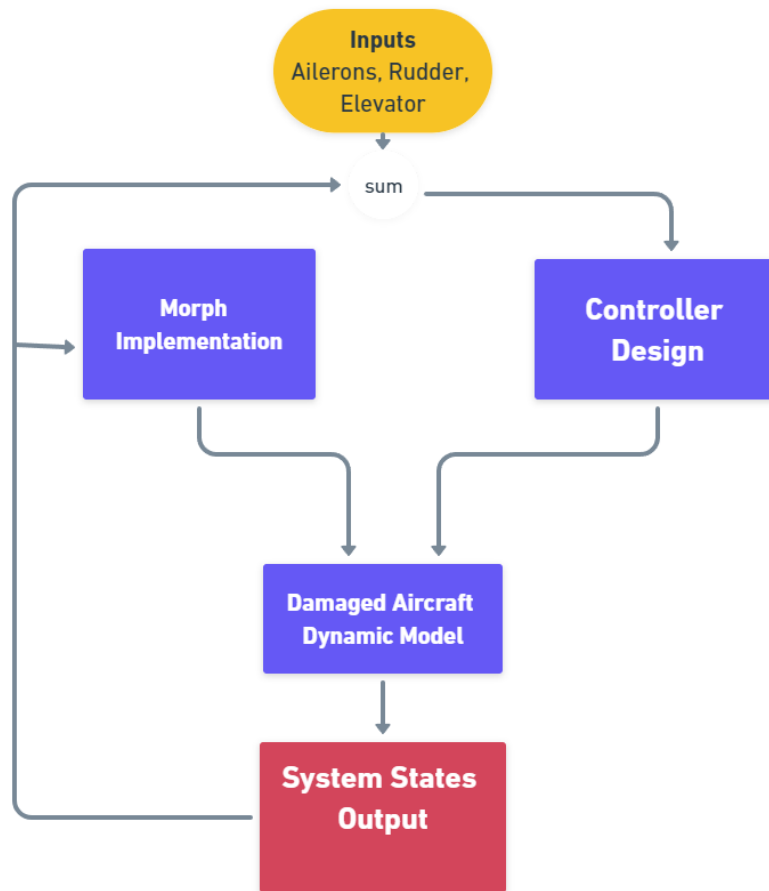


Figure 5.1 Morph wing damage aircraft flow chart

The Morph implementation block can be broken down into two distinct, consecutive sub-sections, Figure 5.2 and Figure 5.3. The morph dynamic block measures rolling angle and damage sensor input along with pre-calculated aerodynamic and mass properties data. The block

essentially uses the damage percentage to determine the differential lift and drag and correlate the change in area with the change in lift/drag. Therefore, calculating the exact yawing and rolling moment is required to re-stabilize the aircraft. Then the morph dynamic block outputs morph percentage to actuation control. Figure 5.3 displays the actuation design for the morph wing model. The actuation method considers percentage morph to physical actuation, actuation to the airframe change, and the aerodynamic/control derivatives changes due to airframe changes. Combining these two designs completes the morph implementation proposed in this project.

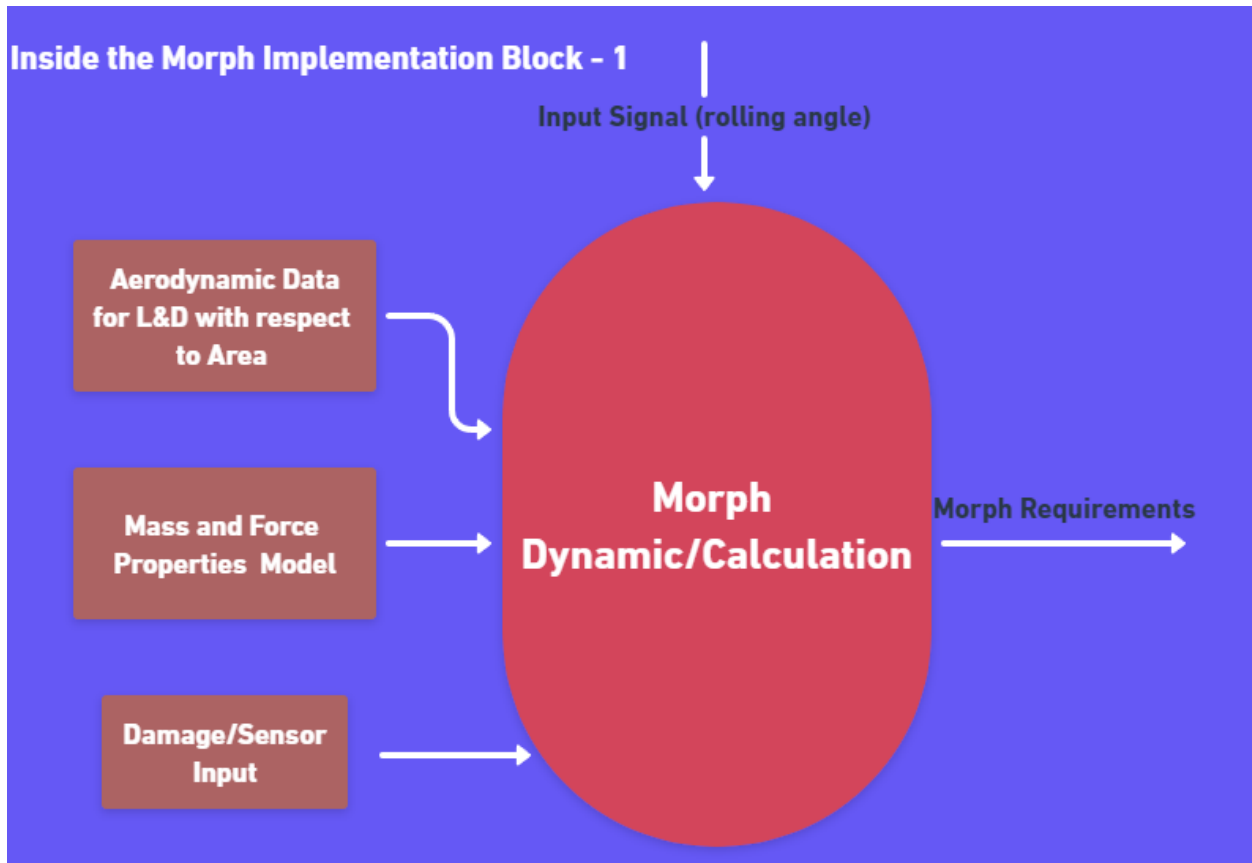


Figure 5.2 Morph dynamic model flow chart (morph implementation block 1)

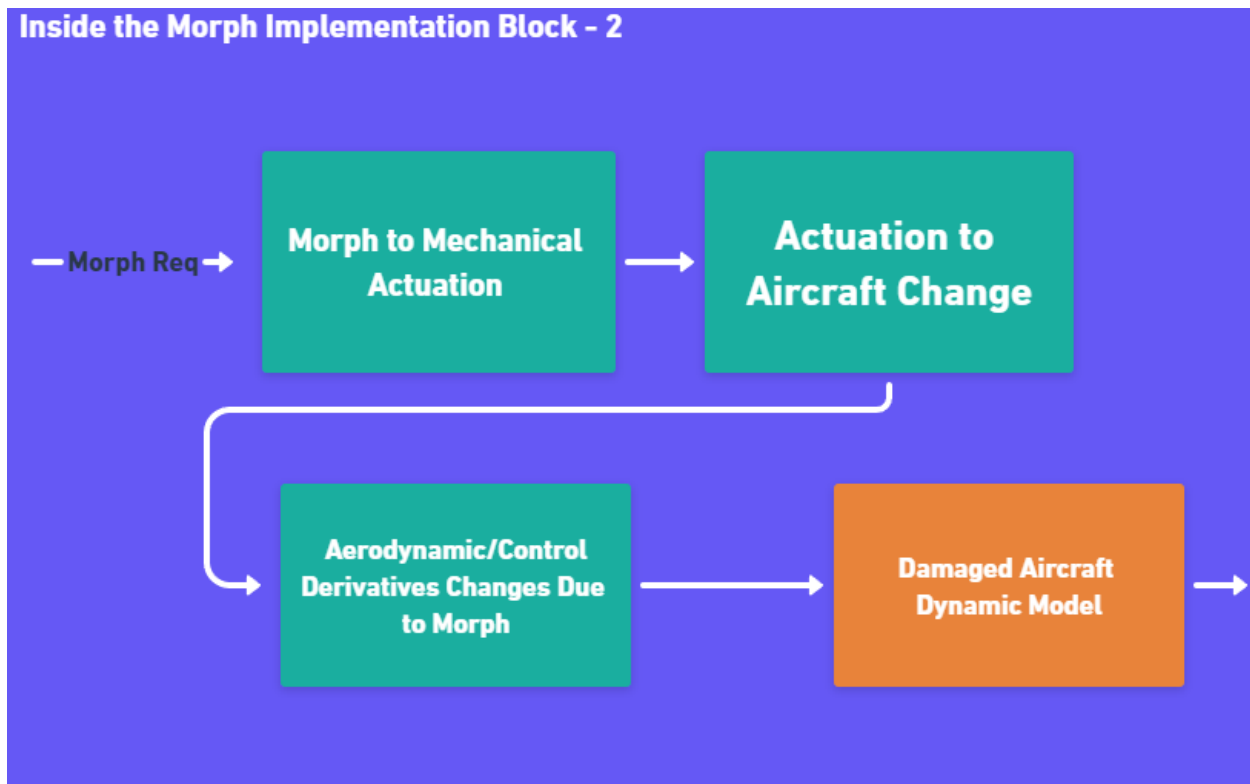


Figure 5.3 Actuation implementation flow chart

## 5.2 Lift vs. Drag Analysis

From Chapter 4, the maximum morphed length will be 30% of the original chord. This section analyzed a variety of chord lengths from a 0%-10% increase. Variation of chord and span length determines the efficiency of the morphing wing, based on the lift and drag calculation given by Equation (5.1) and Equation (5.2). Equation (5.2) considers the induced drag generated from Equation (5.1) and the skin friction drag caused from different surfaces. This is used to determine the lift and drag gained from morphing at various span and chord lengths. As shown in Figure 5.4, since both lift and drag are directly proportional to span and chord, the maximum lift and drag gained with both terms are maximized. Therefore, to maximize the efficiency of the morph wing design, the morphing mechanism is said to be across the entire wing span. Not only does this increase the overall efficiency of the morphing wing, but it also allows all sections of the wing to morph regardless of the damage location. All data used to generate Figure 5.5 to Figure 5.8 originates from XFLR5 and can be found in Appendix C.



Figure 5.4 Boeing 747 root airfoil shape, generated from XFLR5

$$L = \frac{Cl * \rho * V^2 * A}{2} \quad (4.1)$$

$$D_i = \frac{C_d * \rho * V^2 * A}{2} \quad (4.2)$$

Lift curve with variation in span and chord

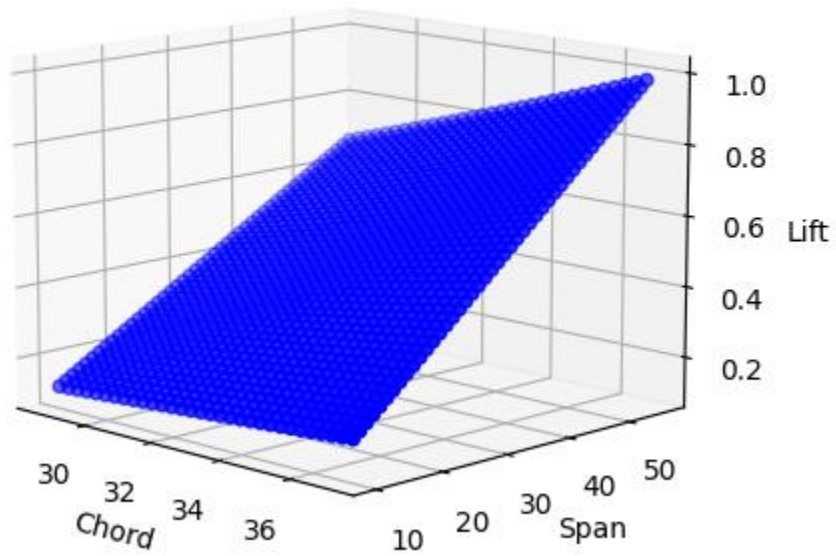


Figure 5.5 Lift at various span and chord lengths

## Drag curve with variation in span and chord

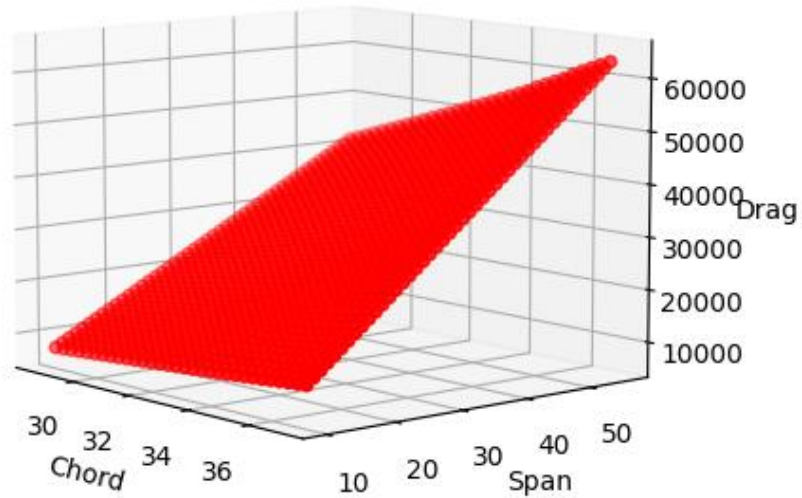


Figure 5.6 Drag curve with variation in span and chord

As observed in the lift and drag comparison plots, Figure 5.7 and Figure 5.8, the damaged wing scenario lacks a significant amount of lift and drag forces. However, by using the morph wing design, the missing lift and drag forces can be regained by only using 27% morphed wing. Although it might seem ideal, the lift and drag plots below do not represent that the aircraft at 30% morph can fully regain stability and control. This is due to the lack of consideration in terms of the moment arm and center of forces. The data presented below are only an indication that the morph wing design is feasible and offers real benefits to the damage wing recovery scenario. The stability and dynamics of the vehicle before, during, and after morphing will be covered in a later chapter.

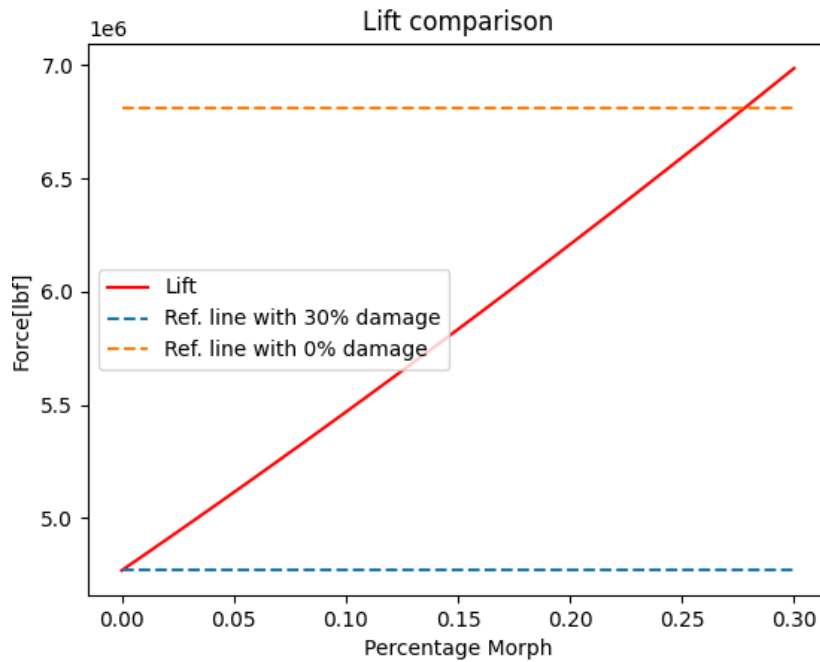


Figure 5.7 Lift comparison between no-damage, damaged, and variable morph

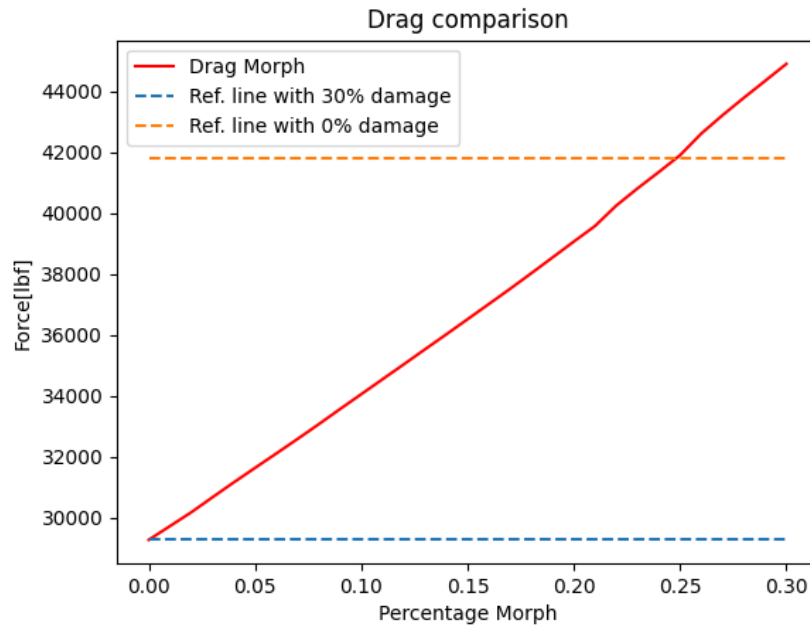


Figure 5.8 Drag comparison between no-damage, damaged, and variable morph

### 5.3 Instantaneous morph simulation model

The instantaneous simulation model is a simplified control design that considers a generic commercial airliner and assumes the rolling moment ratio as the dominant force in the aircraft's roll. With the damaged wing on the right side, the coefficient of the rolling moment concerning

the rolling rate can be expressed as Equation (4.3) [23]. The coefficient of the rolling moment can be defined as the sum of the lifting forces on the rolling wing. As the aircraft rolls towards one side, the wing provides a negative rolling moment based on the wing shape and area. In the right-side damaged wing scenario, the rolling behavior can be modeled as aircraft naturally rolling toward the damaged side. And the natural recovering tendency can be expressed as a function of the morph wing area. As part of the assumption, the aircraft is said to be stable if the lifting and drag forces are equal between the left and right sides. Therefore, the morphing wing implemented equation of motion for the damaged wing can be modeled as the differential lifting forces between the two wings, Equation (4.4).

$$C_{l_p} = -\frac{4 \cdot C_{L\alpha_w}}{S \cdot b^2} * \int_0^{b/2} c * y^2 dy \quad (4.3)$$

$$\sum L = -|L_{right} * y_{right}| + |L_{left} * y_{left}| \quad (4.4)$$

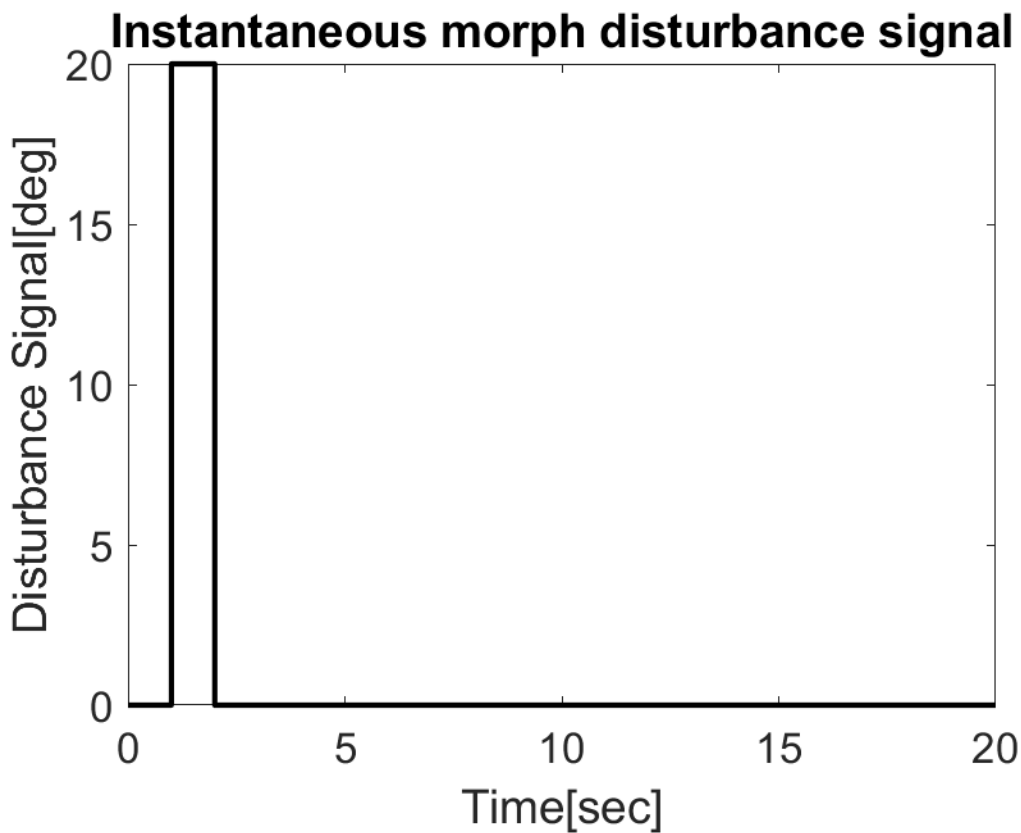


Figure 5.9 Input disturbance signal

Figure 5.9 showcases the input signal for the disturbance of the damaged wing aircraft to simulate the system's initial violent rolling behavior. Under the extreme initial rolling angle, the morph wing model initially struggles to balance the aircraft using the existing maximum aileron deflection, Figure 5.10 and Figure 5.12. On the other hand, Figure 5.11 showcases the system response unmorphed, as the state quickly becomes unstable and grows exponentially. Note that in the simulation showcased here, the aileron efficiency halves the nominal value due to only

considering one effective aileron surface. However, as the morph wing mechanism is deployed, the aircraft can recover to its initial state without needing additional aileron input signals.

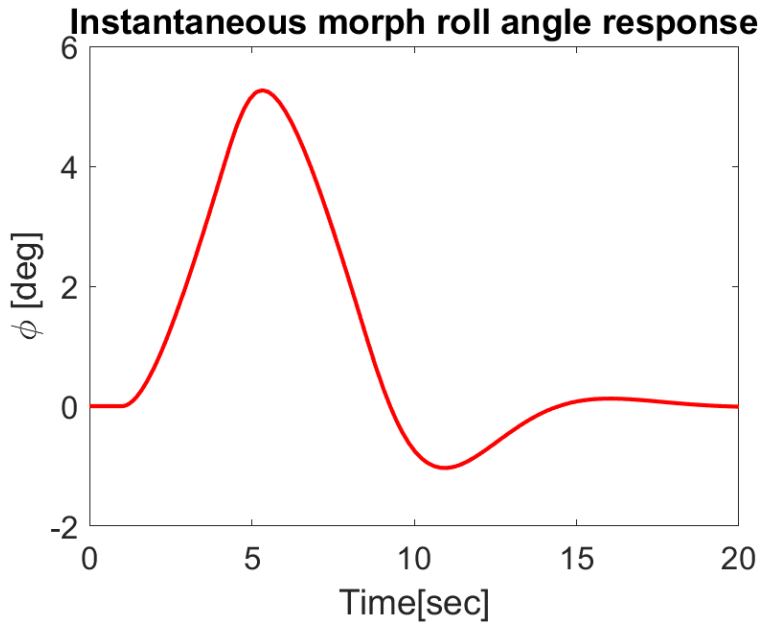


Figure 5.10 Morphed roll angle response

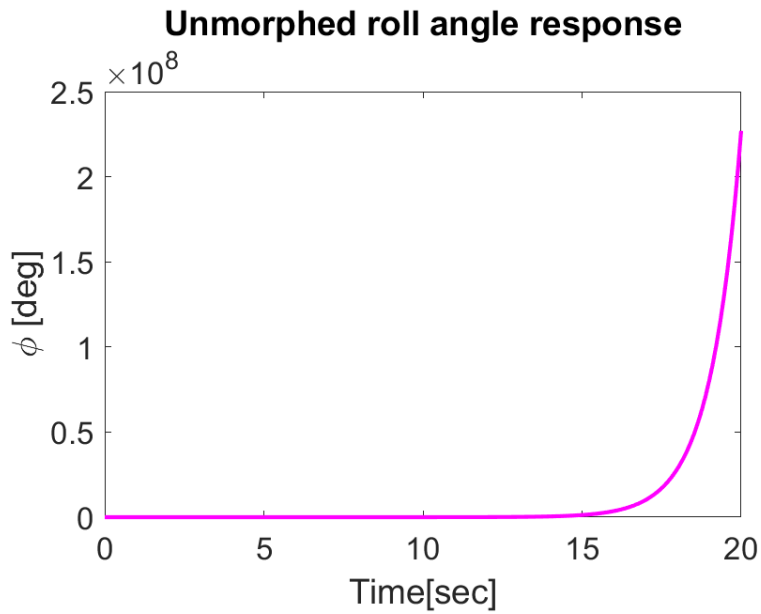


Figure 5.11 Unmorphed roll response

Figure 5.12 displays the morphed aircraft aileron response while initially maxing the available controller deflection angle. The aileron response quickly converts to 0 since the aircraft regain stability.

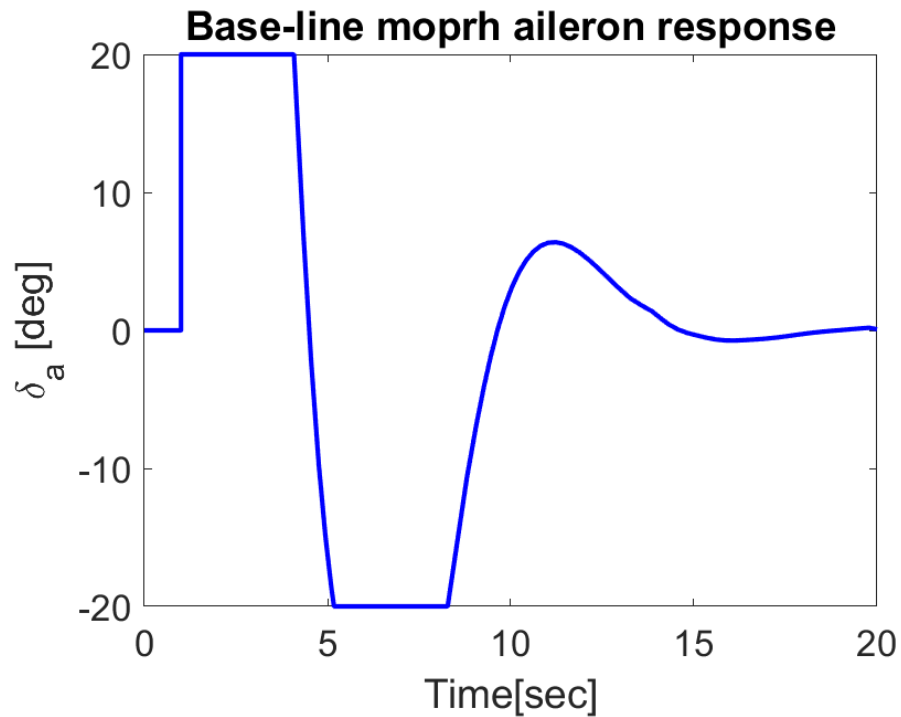


Figure 5.12 Morphed aileron response

This chapter discussed the feasibility and capability of the morph wing implementation and how it can affect the aircraft's stability parameter with the simple baseline simulation. It is shown that the aircraft can recover from its imbalance lift and drag conditions with sufficient morph wing area. However, the baseline model method considers an instantaneous deployment of the morphed section. The following chapters will discuss the nuances of the morph wing mechanical implementation from the actuation method and control design perspective. And developed a more realistic control design.

## 6. Morph Wing Actuation Design

This chapter discusses the actuation method, design, and modeling of the physical system. First, it is crucial to determine the actuation method of the morph wing design. Most chord-wise morphing design adapts an approach of ribs extension along with supporting structures stretching out the wing surfaces. Presented in Figure 6.1 is an extension design that employs a central extendable spar with a 5-cell design [28]. The 5-cell design isolates each section and localizes each stretchable surface. The benefit of this design is its ability to provide overall more structural support. In this project, the chord-wise morphing actuation method will adapt to the design presented in Figure 6.1.

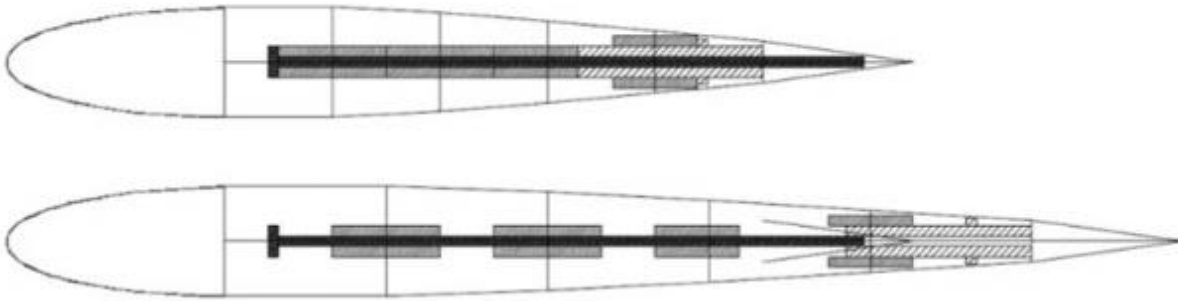


Figure 6.1 Side view of a sliding 5-cell extension solution, retracted(top) and extended(bottom) [28]

### 6.1 Actuation Requirement

As discussed in Chapter 4, this project's maximum stretch requirement is 30 percent of its original shape. Therefore, the required pressure to maintain and actuate the morphing motion must be calculated to satisfy that requirement. Using Hooke's Law in one dimension (uniaxial loading), the relationship between pressure, area, and displacement can be expressed by Equation (6.1). The  $P$  term in Eq. (6.1) is the pressure applied along the stretching surface,  $A$  is the original surface area,  $L$  is the actual length,  $\delta$  is the displacement, and  $E$  is Young's modulus of the material.

$$\frac{P}{A} = \sigma = E \frac{\delta}{L} \quad (6.1)$$

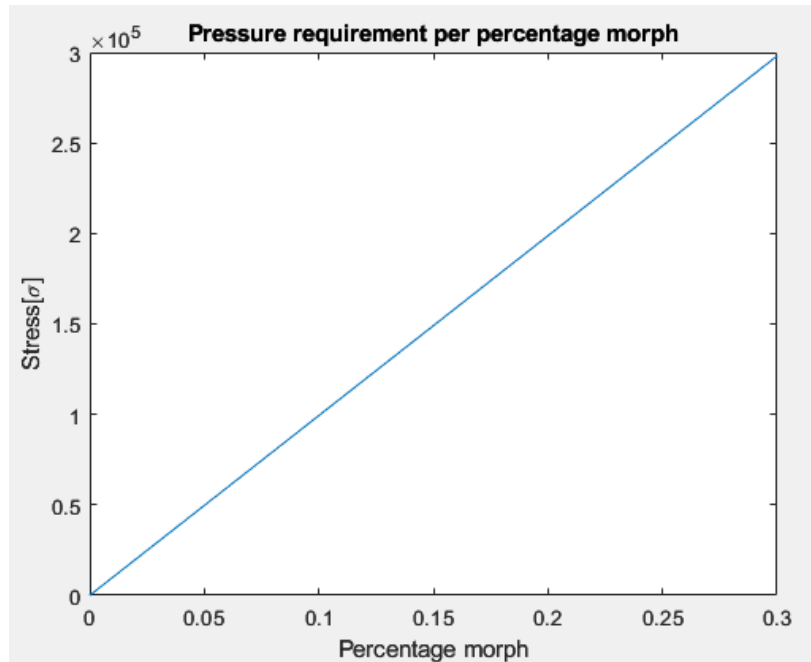


Figure 6.2 Relationship between stress and morph

## 6.2 Hydraulic Actuator Modeling

Similar to other control surfaces like the flaps and slats, the proposed morphing mechanism would adapt to a linear hydraulic actuator that spans the entire wing. The hydraulic actuator will use a closed-loop linear hydraulic actuator from MATLAB's hydraulic toolbox. The closed-loop linear hydraulic actuator is presented in Figure 6.2. This actuator control system takes in the input of forces and command position. Using the provided force and position input, an electric motor will control the flow of the fluid and achieve actuation. The actuation system is a highly crucial component as well. Initially, the aircraft under damage will violently roll towards the damaged side. While it is possible to use aileron control to slow down the rolling motion, if the morphing mechanism cannot deploy in time, the aircraft will still result in a crash.

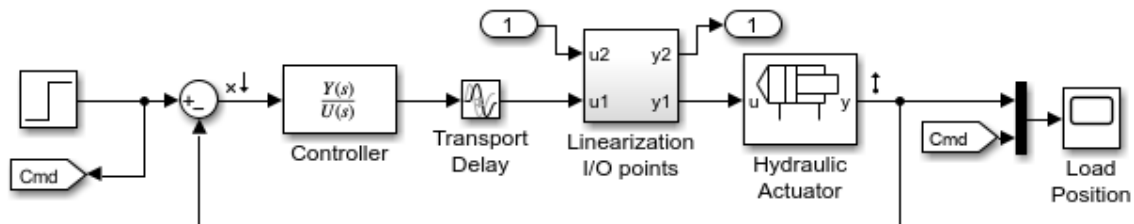


Figure 6.3 Linear hydraulic actuator control diagram [30]

### 6.3 Actuation simulation

The complete simulation would follow the flow chart presented in Figure 6.3. The damaged portion of the wing will determine the force and position command. Based on the damage percentage, the actuation will be fed into the linear hydraulic actuation, Figure 6.2. Using the linear hydraulic actuator, the actuation time and position will be used to calculate its effect in modifying the aerodynamic properties of the aircraft.

#### Actuation diagram

Input: Morph Requirement  
Output: Actuation Position

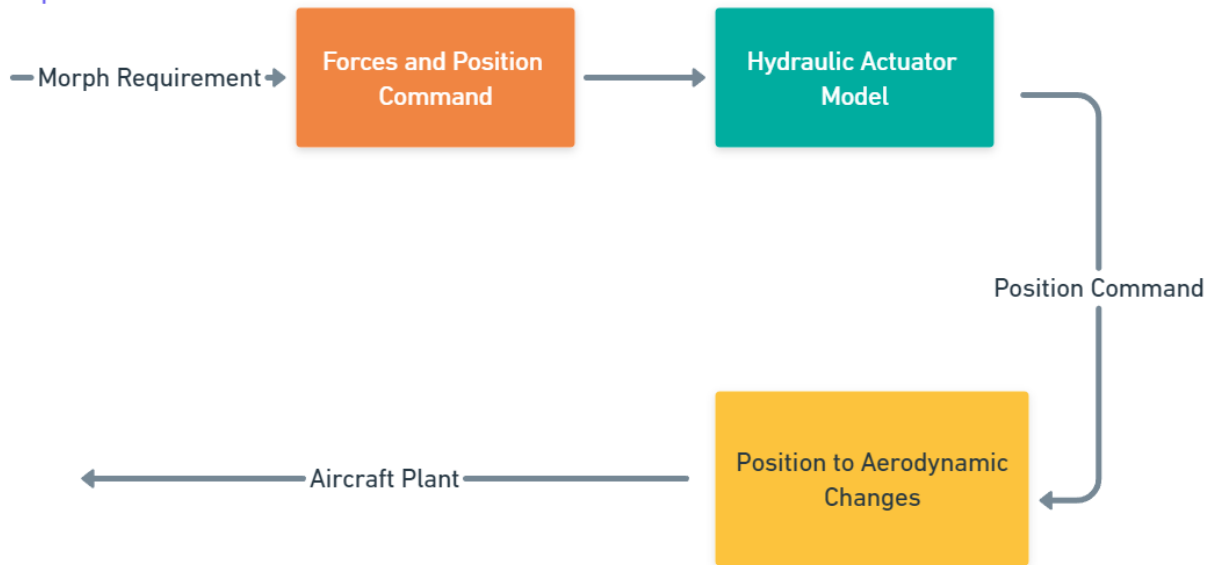


Figure 6.4 Actuation diagram flow chart

Figure 6.4 shows the actuation of the hydraulic system from its original position, 28.54 ft, to a fully extended/morphed position, 37.0680 ft. As seen in Figure 6.4, for the actuation to fully extend to 30 percent of its original position, it would take roughly 5 seconds to achieve the desired state. Although the 5-second response time suits the application of this scenario since the aircraft will lose control within a short time, a fast response time actuator can yield better results. The parameters of the linear hydraulic actuator are listed in Table 6.1.

**Table 6.1** - Hydraulic actuator parameters used in simulation [30]

Parameter	Value
Hydraulic fluid density	1.64927 slug/ft <sup>3</sup> (850 kg/m <sup>3</sup> )
Hydraulic fluid kinematic viscosity	1.937e-5 ft <sup>2</sup> /s (1.8e-5 m <sup>2</sup> /s)
Piston stroke	8.53 ft (2.6 m)
Constantly applied pressure	6900 psi (4.757e7 N/m <sup>2</sup> )

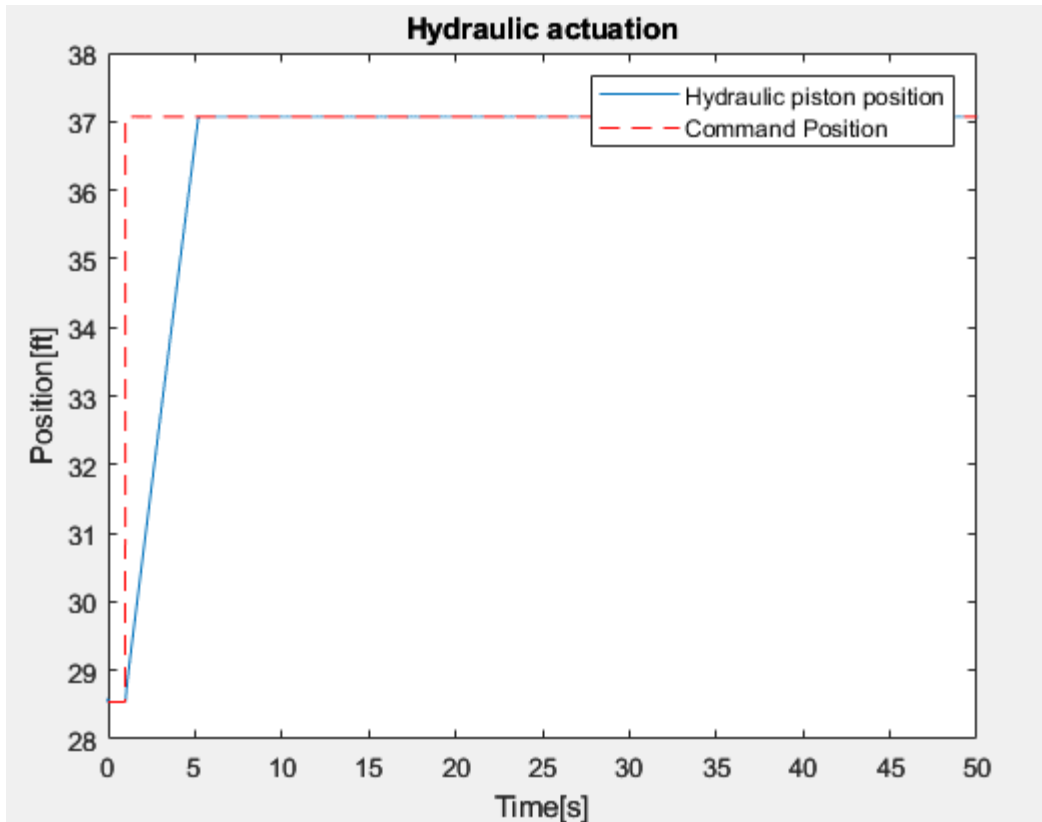


Figure 6.5 Hydraulic Actuation from zero percent morph to thirty percent morph

Using the hydraulic actuator discussed in this chapter, the fully damaged aircraft simulation can provide a much more realistic result with morphing actuation time. As seen in Figure 6.5, the actuation model used in this chapter can provide fast and accurate tracking of the command signal. In the following, a full-body damaged aircraft simulation will be provided along with control system tuning to achieve good results for damage recovery.

## 7. Morph Wing Controller Design and Full Simulation

Using the knowledge and design developed in previous chapters, this project section will combine all aspects of the morph wing design to provide a complete system simulation for the wing-damage aircraft, which includes:

- The damaged wing equation of motion for roll
- Linear hydraulic actuation model
- Morph wing implementation model
- PID controller design

Using the sub-system design listed above, the fully simulated response of the system will be presented in this chapter.

### 7.1 Setup

From Chapter 3, the damage wing roll rate equation of motion is reiterated in Equation 7.1. Although the roll rate equation depends on many system states, the rolling moment will be the dominant mode in this scenario during the initial motion post-damage. Utilizing this assumption, the equation of motion for roll rate can be simplified to Equation (7.2).

$$\dot{p} = \left[ \frac{m_a \Delta h Z_u}{I_{xx}} \right] u + \left[ -\frac{m_a \Delta h Z_\alpha}{I_{xx}} \right] \alpha + \left[ -\frac{m_a \Delta h h q}{I_{xx}} \right] q + \left[ L_p + \frac{m_a \Delta d Y_p}{I_{xx}} \right] p + \left[ L_\beta + \frac{m_a \Delta d Y_\beta}{I_{xx}} \right] \beta + \left[ L_r + \frac{m_a \Delta d Y_r}{I_{xx}} \right] r + \left[ L_{\delta_a} + \frac{m_a \Delta d Y_{\delta_a}}{I_{xx}} \right] \delta_a + \left[ L_{\delta_r} + \frac{m_a \Delta d Y_{\delta_r}}{I_{xx}} \right] \delta_r + \left[ -\frac{m_a \Delta h Z_{\delta_e}}{I_{xx}} \right] \delta_e \quad (7.1)$$

$$\dot{p} = \left[ L_p + \frac{m_a \Delta d Y_p}{I_{xx}} \right] p + \left[ L_{\delta_a} + \frac{m_a \Delta d Y_{\delta_a}}{I_{xx}} \right] \delta_a + \left[ L_{\delta_r} + \frac{m_a \Delta d Y_{\delta_r}}{I_{xx}} \right] \delta_r + \left[ -\frac{m_a \Delta h Z_{\delta_e}}{I_{xx}} \right] \delta_e \quad (7.2)$$

Like the baseline morph model, the effectiveness of the aileron is said to be only halved the original amount due to assuming only one aileron on the undamaged side is adequate. Figure 7.1 showcases the entire block diagram of the system. As shown in Figure 7.1, the system is broken down into multiple distinct sub-systems. For the input section, the system is simulated with a twenty degrees impulse signal to imitate the initial violent rolling motion. The reference signal is set to zero degrees for aircraft to track wing-level conditions. For the control surfaces section, elevator deflection is kept at zero degrees. Aileron and rudder are each controlled by their saturation, actuation, and PID block. Like previous chapters, the actuation for the aileron and rudder is shown in Equation (7.3).

$$A(s) = \frac{10}{s+10} \quad (7.3)$$

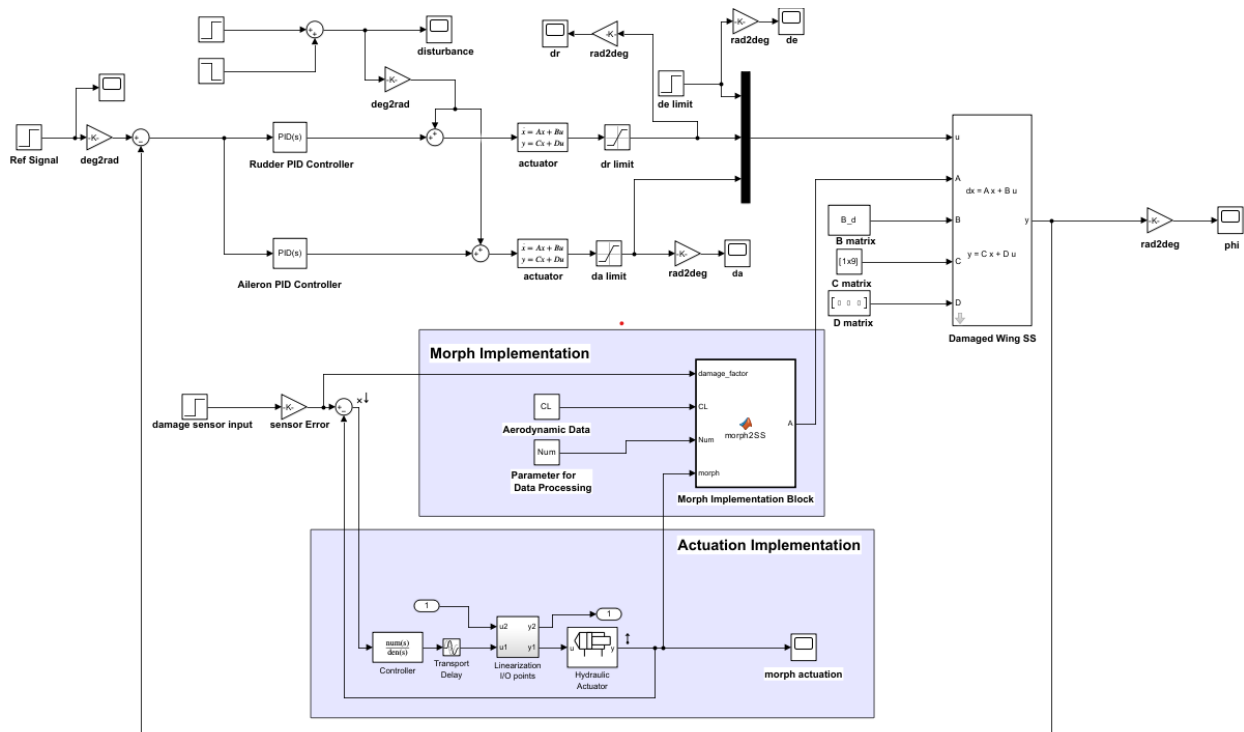


Figure 7.1 Full system morph design with damaged wing block diagram

Shaded in the area are the morph implementation and actuation block discussed separately in Chapters 5 and 6. The damage sensor readings are passed into the morph implementation, and actuation block with 90% accuracy. The morph implementation block will calculate the new aerodynamic and physical parameters based on damage and morph. And actuation implementation will start actuating the morphing mechanism.

## 7.2 Simulation Result and Analysis

The full implementation simulation results are displayed in this section using the setup presented above. First, the simulation data with no control tuning is presented under twenty degrees initial disturbance signal, Figure 7.2. Remember that from Chapter 4, when under a twenty degrees disturbance signal, the system cannot recover at all. Next, figure 7.3 and Figure 7.4 showcase the system response under the disturbance signal.

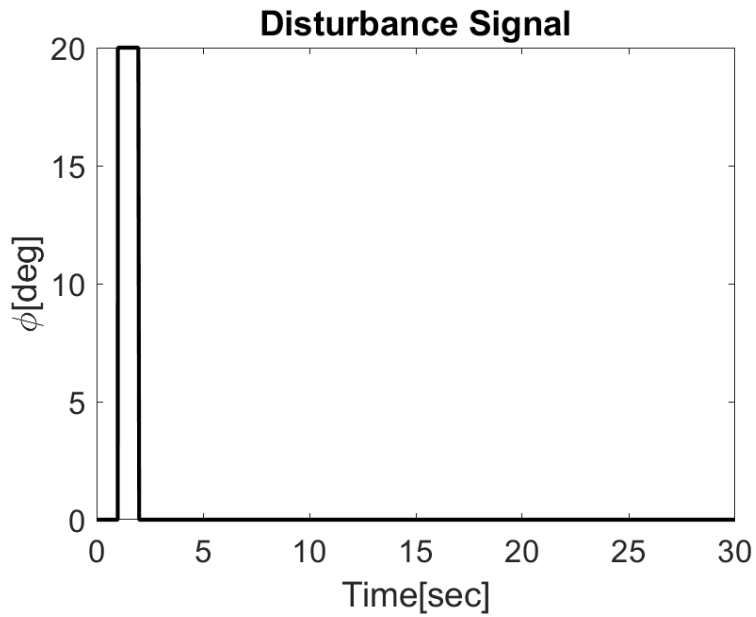


Figure 7.2 Disturbance signal

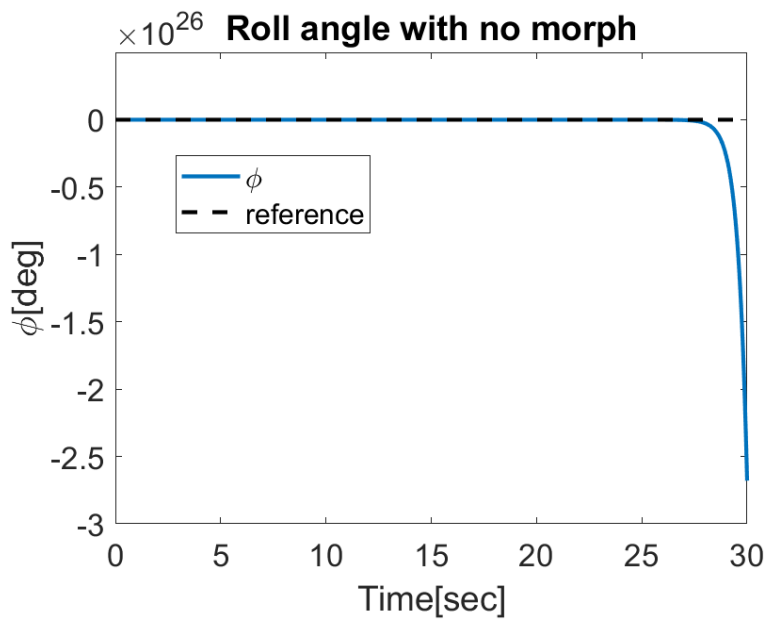


Figure 7.3 Roll response with no morph

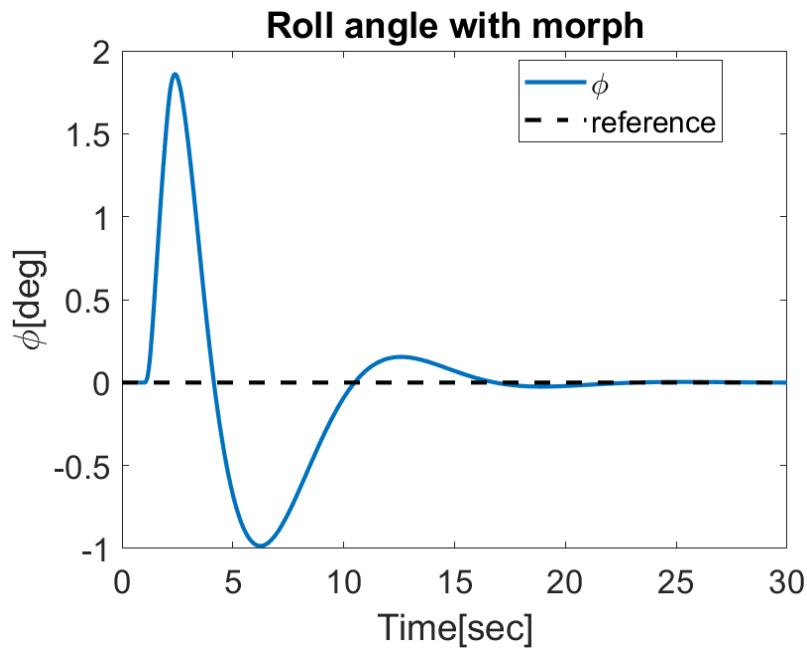


Figure 7.4 Roll response with morph

As seen in Figures 7.3 and 7.4, the no morph implementation model cannot recover from the damage wing scenario, while the morph wing model can successfully recover to its nominal state after 15 seconds. Paying closer attention to Figure 7.4 shows that initially, the system is highly unstable and increases extremely fast. However, once the morph actuation kicks in, around 5 seconds, it can slowly recover to its stable location. This can be confirmed by Figure 7.5-7.7.

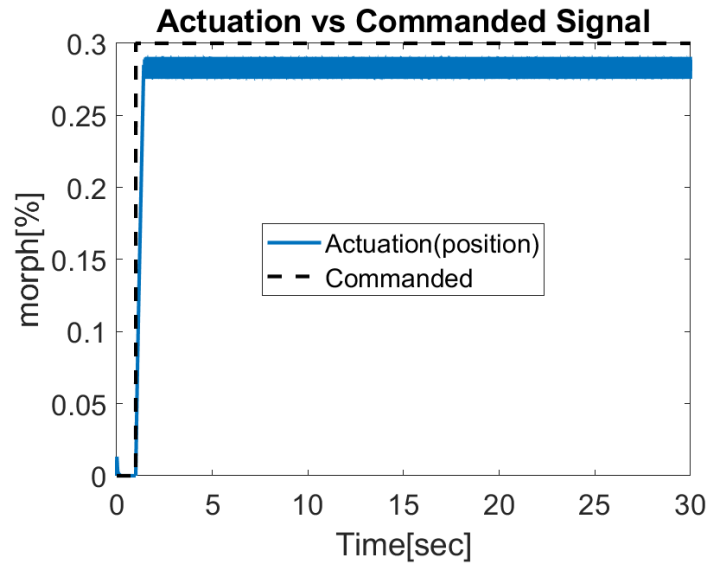


Figure 7.5 Actuation response commanded vs actual

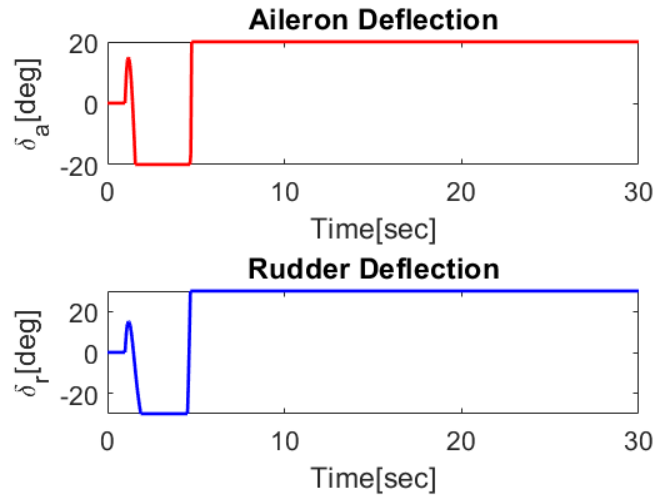


Figure 7.6 Aileron and rudder response with no morph

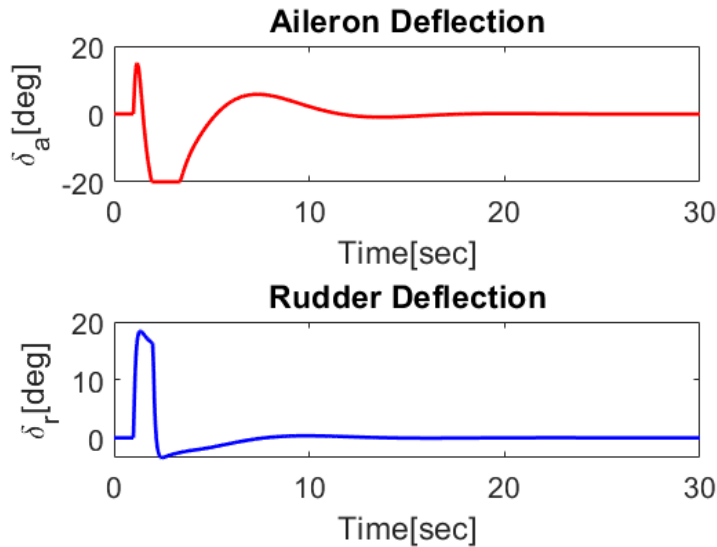


Figure 7.7 Aileron and rudder response with morph

With no morph implementation, the aircraft eventually becomes unstable after exhausting the onboard controls. However, with the morph implementation, the control surfaces deflection after the morph actuation is minimal. Therefore, the morphed model can provide sufficient restoring moments for the damaged aircraft even without controller tuning on the aileron and rudder. In addition, the actuation model oscillates due to poor tracking performance, and the intended sensor inaccuracy puts it at around 90% of the commanded position. However, with a 20-second recovery time, there is room for improvement. Figure 7.8 showcases the roll angle response under a tuned PID controller design for aileron and rudder control. The PID parameters are listed in Table 7.1, these values are obtained through iterative design in Simulink, and the equation utilized is listed as Equation (7.4).

$$P + I \frac{1}{s} + D \frac{N}{1+N\frac{1}{s}} \quad (7.4)$$

**Table 7.1** - PID controller parameters for aileron and rudder

Parameter	Aileron	Rudder
Proportional gain, Kp	20	10
Integral gain, Ki	9	5
Derivative gain, Kd	13	7
Filter coefficient, N	10	10

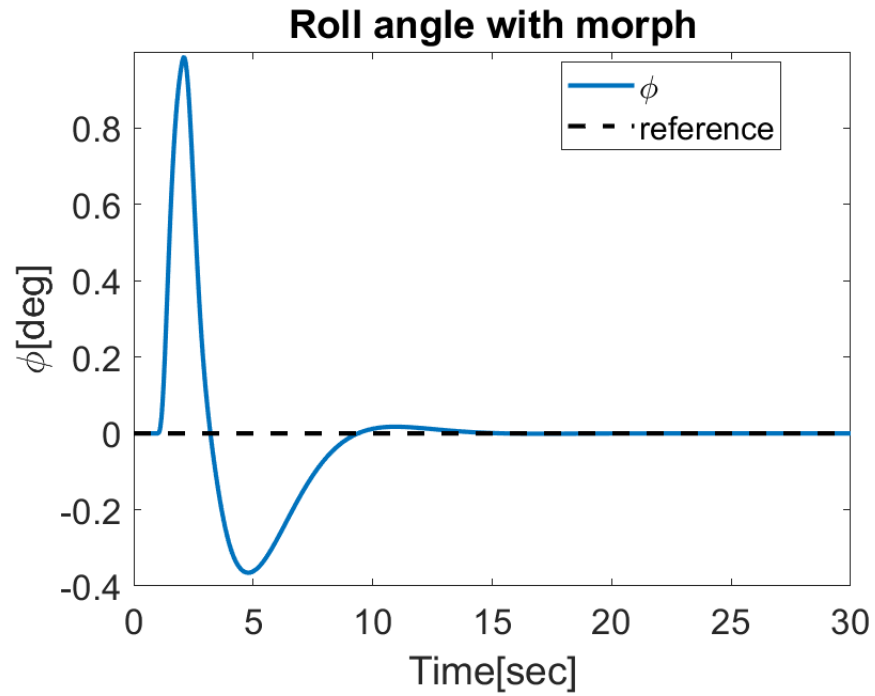


Figure 7.8 Roll angle response with morph and PID controller

The system can reach its reference position in 10 seconds, half the original amount, by utilizing a simple PID controller for aileron and rudder control. In addition, the magnitude of the system response is also dramatically minimized.

## 8. Conclusion and Future Work

### 8.1 Conclusion

This project studied the utilization of morph wings in damaged wing applications for general transport models like the Boeing-747. The motivation of this project is to provide additional/innovative methods to tackle the damaged wing issue and improve air travel safety. The proposed idea is to utilize morph wings to counter the differential lift and drag created by the loss of wing area.

Using Newton's equation, this project first discusses the damaged wing aircraft with full system dynamics and control modeling. From the entirely derived 6-degree-of-freedom equation of motion, the aerodynamic and stability parameters of the damaged aircraft were investigated and integrated into the damaged aircraft equation of motion. With a linearized equation of motion, using the perturbation model, the model was simulated with initial input conditions and compared with the undamaged aircraft dynamics. This showed the damaged aircraft's instability and inability to recover to its nominal state. Even with a controller design to maximize the effectiveness of aircraft control surfaces, the damaged wing aircraft still show significant unstable results. Using the knowledge of damaged aircraft models, a strategy of using morph wing implementation to stabilize the aircraft was presented. The full assumptions and characteristics of the morph wing implementation were laid out in this report, along with the motivation for using morph wing technologies. Next, the morph wing implementation feasibility was investigated and presented data to support its effectiveness. With the morph wing implementation, the morphing wing's aerodynamic properties and mechanical design were showcased. The details of morph wing actuation mechanisms and design structures were also listed in this project. The implementation flow chart and workings were also stated and explained in this project. With the end-to-end morph wing implementation, the simulation response of damaged aircraft with morph wing was presented. The strategy of using a morphing wing to recover damaged aircraft was found to be largely successful, with the morphing wing being able to deploy in time and restabilize the aircraft with a reasonable time, less than 20 seconds.

With the above analyses, this project acts as a framework/prototype of morph wing implementation in damaged aircraft use cases with promising results. This prototype also includes automatic control methodologies to recover from damaged wing aircraft and provide an elegant solution to the problem.

### 8.2 Future work

This project provided a feasible framework for morph wing implementation in damaged-wing aircraft use cases. Although it showed promising resultt, the highly complex and coupling aircraft dynamic for the morphing wing with damaged aircraft remains; here is a list of possible future areas to investigate to take it into production.

- Derivation of the entire damaged aircraft model with morph implementation as part of its variable
- Wind tunnel testing for damaged wing aircraft at various damaged locations and portions
- Morph wing mechanical design and structure with internal components considerations
- Small-scale model for prototype testing in a safe and controlled environment

- Controller design with multiple sensors, including damage, actuation, and morph sensors.
- Morph wing surface testing and material selection for large-scale aircraft
- Morph wing surface fatigue and reusability study

With the items mentioned above, soon the sky will be soaring with morph wing aircraft that provide stability and safety to its passengers.

## References

- [1] Obradovic, B., and Subbarao, K., “Modeling of Flight Dynamics of Morphing Wing Aircraft,” *Journal of Aircraft*, vol. 48, 2011, pp. 391–402.
- [2] Mardanpour, P., and Hodges, D. H., “Passive morphing of flying wing aircraft: Z-shaped configuration,” *Journal of Fluids and Structures*, vol. 44, 2014, pp. 17–30.
- [3] Rongqi, S., and Jianmei, S., “Dynamics and control for an in-plane morphing wing,” *Aircraft Engineering and Aerospace Technology*, vol. 85, 2013, pp. 24–31.
- [4] Seigler, T. M., Neal, D. A., Bae, J.-S., and Inman, D. J., “Modeling and flight control of large-scale morphing aircraft,” *Journal of Aircraft*, vol. 44, 2007, pp. 1077–1087.
- [5] Smith, D. D., Lowenberg, M. H., Jones, D. P., and Friswell, M. I., “Computational and experimental validation of the active morphing wing,” *Journal of Aircraft*, vol. 51, 2014, pp. 925–937.
- [6] Min, Z., Kien, V. K., and Richard, L. J. Y., “Aircraft morphing wing concepts with radical geometry change,” *The IES Journal Part A: Civil & Structural Engineering*, vol. 3, 2010, pp. 188–195.
- [7] Ajaj, R. M., Friswell, M. I., Bourchak, M., and Harasani, W., “Span morphing using the GNATSPAR wing,” *Aerospace Science and Technology*, vol. 53, 2016, pp. 38–46.
- [8] Cadogan, D., Graham, W., and Smith, T., “Inflatable and rigidizable wings for unmanned aerial vehicles,” *2nd AIAA "Unmanned Unlimited" Conf. and Workshop & Exhibit*, 2003.
- [9] Ajaj, R. M., Parancheerivilakkathil, M. S., Amoozgar, M., Friswell, M. I., and Cantwell, W. J., “Recent developments in the Aeroelasticity of morphing aircraft,” *Progress in Aerospace Sciences*, vol. 120, 2021, p. 100682.
- [10] Perkins, D., Reed, J., and Havens, E., “Morphing wing structures for Loitering Air Vehicles,” *45th AIAA/ASME/ASCE/AHS/ASC Structures, Structural Dynamics & Materials Conference*, 2004.
- [11] Yan, B., Li, Y., Dai, P., and Liu, S., “Aerodynamic analysis, dynamic modeling, and control of a morphing aircraft,” *Journal of Aerospace Engineering*, vol. 32, 2019.
- [12] Lentink, D., Müller, U. K., Stamhuis, E. J., de Kat, R., van Gestel, W., Veldhuis, L. L., Henningsson, P., Hedenström, A., Videler, J. J., and van Leeuwen, J. L., “How swifts control their glide performance with morphing wings,” *Nature*, vol. 446, 2007, pp. 1082–1085.

- [13] Zhang, X., and Li, Y., “Damage tolerance and fail-safety of welded aircraft wing panels,” *AIAA Journal*, vol. 43, 2005, pp. 1613–1623.
- [14] Nguyen, N., Krishnakumar, K., Kaneshige, J., and Nespeca, P., “Dynamics and adaptive control for stability recovery of damaged asymmetric aircraft,” *AIAA Guidance, Navigation, and Control Conference and Exhibit*, 2006.
- [15] Garcia, H., Abdulrahim, M., and Lind, R., “Roll control for a Micro Air Vehicle Using Active Wing Morphing,” *AIAA Guidance, Navigation, and Control Conference and Exhibit*, 2003.
- [16] Ajaj, R. M., and Friswell, M. I., “Aeroelasticity of compliant span morphing wings,” *Smart Materials and Structures*, vol. 27, 2018, p. 105052.
- [17] Ajaj, R. M., Omar, F. K., Darabseh, T. T., and Cooper, J., “Flutter of telescopic span morphing wings,” *International Journal of Structural Stability and Dynamics*, vol. 19, 2019, p. 1950061.
- [18] Huang, R., and Qiu, Z., “Transient aeroelastic responses and flutter analysis of a variable-span wing during the morphing process,” *Chinese Journal of Aeronautics*, vol. 26, 2013, pp. 1430–1438.
- [19] Cook, M. V., *Flight dynamics principles*, Amsterdam: Elsevier, 2008.
- [20] Hunter, J. Aerospace Vehicle Dynamics and Control Course Reader.
- [21] Kim, K.-joon, Ahn, J., Kim, S., Choi, J.-soo, Suk, J., Lim, H., and Hur, G.-bong, “Analysis of partial wing damage on flying-wing unmanned Air Vehicle,” *Proceedings of the Institution of Mechanical Engineers, Part G: Journal of Aerospace Engineering*, vol. 228, 2013, pp. 355–374.
- [22] Ogunwa, T. T., and Abdullah, E. J., “Flight Dynamics and control modelling of damaged asymmetric aircraft,” *IOP Conference Series: Materials Science and Engineering*, vol. 152, 2016, p. 012022.
- [23] Nelson, R. C., *Flight stability and automatic control*, Chennai: McGraw-Hill Education (India) Private Limited, 2010.
- [24] Sarigul-Klijn, N., Nespeca, P., Marchelli, T., and Sarigul-Klijn, M., “An approach to predict flight dynamics and stability derivatives of distressed aircraft,” *AIAA Atmospheric Flight Mechanics Conference and Exhibit*, 2008.
- [25] Wimmer, H. K., “Linear Matrix equations controllability and Observability, and the rank of solutions,” *SIAM Journal on Matrix Analysis and Applications*, vol. 9, 1988, pp. 570–578.

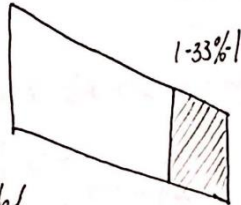
- [26] Ouellette, J. A., “Flight Dynamics and Maneuver Loads on a Commercial Aircraft with Discrete Source Damage,” *Virginia Polytechnic Institute and State University, department of Aerospace Engineering*, Apr. 2010.
- [27] La, S., Joe, W. Y., Akbar, M., and Alsaïdi, B., “Surveys on Skin Design for morphing wing aircraft: Status and challenges,” *2018 AIAA Aerospace Sciences Meeting*, 2018.
- [28] Barbarino, S., Gandhi, F., and Webster, S. D., “Design of extendable chord sections for morphing helicopter rotor blades,” *ASME 2010 Conference on Smart Materials, Adaptive Structures and Intelligent Systems, Volume 2*.
- [29] Majid, T., and Jo, B. W., “Status and challenges on design and implementation of camber morphing mechanisms,” *International Journal of Aerospace Engineering*, vol. 2021, pp. 1–14.
- [30] The MathWorks, Inc. (1994-2023). *MATLAB version: 9.1(R2022b)*. Hydraulic Actuator with Digital Position Controller. Available at:  
<https://www.mathworks.com/help/simscape/ug/hydraulic-actuator-with-digital-position-controller.html;jsessionid=eafd362affb88260ba8bbf8a2953>

## Appendices

### Appendix A – Damaged-Wing Dynamic Derivation

Assumptions:

1. Only one wing sustain damage
2. Range of damage from the wing tip



3. Flat Earth Model
4. Change in mass, where  $m_f = m_i - m_d$

E: earth, fixed  
ref. frame

B: body, rotating  
ref. frame

Let's the velocity of the aircraft express by:

Translational Velocity:  $U$

$$V^{B/E} = U b_x + V b_y + W b_z$$

Angular Velocity:

$$\omega^{B/E} = P b_x + Q b_y + R b_z$$

For the asymmetrical wing aircraft:

$$\sum F = m \frac{dV}{dt} + \frac{d}{dt} (\omega^{B/E} \times \int r dm)$$

\*  $\Delta r$  = shift in C.G. location

accounts for  
the extra wing  
from undamaged  
side

$$\int r dm = (r_2 - r_1) M = \Delta r M$$

$$\sum F = m \frac{dV}{dt} + m \frac{d\omega}{dt} \times \Delta r + m \omega \times \frac{d\Delta r}{dt}$$

$$\begin{aligned} m \frac{dV}{dt} &= m \frac{d}{dt} V^{B/E} + \omega^{B/E} \times V^{B/E} \\ &= m \begin{bmatrix} \dot{U} + QW - RV \\ \dot{V} + RU - PW \\ \dot{W} + PV - QU \end{bmatrix} \end{aligned}$$

$$m \frac{d\mathbf{w}}{dt} \times \Delta \mathbf{r} = m [\dot{p} l_{bx} + \dot{q} l_{by} + \dot{r} l_{bz}] \times [\Delta x, \Delta y, \Delta z]$$

$$= m [\dot{p} \Delta y l_{bz} - \dot{p} \Delta z l_{by} - \dot{q} \Delta x l_{bz} + \dot{q} \Delta z l_{bx} + \dot{r} \Delta x l_{by} - \dot{r} \Delta y l_{bx}]$$

~~m \frac{d\mathbf{w}}{dt}~~  $m \mathbf{w} \times \frac{d\Delta \mathbf{r}}{dt} = 0$ , since  $\frac{d\Delta \mathbf{r}}{dt}$  is neglect due to c.g. location shift is assumed to be small

The sum of the forces for the damaged aircraft:

$$\sum \mathbf{F} = \begin{bmatrix} X \\ Y \\ Z \end{bmatrix} = \begin{bmatrix} \dot{U} + QW - RV - \dot{R}\Delta y + \dot{Q}\Delta z \\ \dot{V} + RW - PV - \dot{P}\Delta z + \dot{R}\Delta x \\ \dot{W} + PV - QU + \dot{P}\Delta y - \dot{Q}\Delta x \end{bmatrix}$$

Sum of the moments of the system for the damaged aircraft:

$$\sum \mathbf{M} = \frac{Bd}{dt} (M \mathbf{H}^{\beta/\beta_0})$$

, where  $\mathbf{H}^{\beta/\beta_0}$  is the angular momentum of the symmetrical plane

For the extra wing portion on the undamaged side:

$$\int (r \times v) dm = M \Delta r \times v$$

$$\sum \mathbf{M} = \frac{Bd}{dt} \mathbf{H}^{\beta/\beta_0} + \omega^{\beta/\beta_0} \times \mathbf{H}^{\beta/\beta_0}$$

$$= I_{xx} \dot{p} l_{bx} + I_{xz} \dot{r} l_{by} + I_{yy} \dot{q} l_{by} + I_{xz} \dot{p} l_{bz} + I_{zz} \dot{r} l_{bz} + (I_{zz} - I_{yy}) \dot{Q} R l_{bx}$$

$$+ I_{xz} P Q l_{bx} + (I_{xx} - I_{zz}) P R l_{by} + I_{xz} (R^2 - P^2) l_{by} + (I_{yy} - I_{xx}) P Q l_{bz} + I_{xz} Q R l_{bz}$$

$$+ I_{yy} \dot{q} l_{bx}$$

$$\frac{Bd}{dt} [M \Delta r \times v] = \frac{Bd}{dt} [M \Delta r \times v] + \omega^{\beta/\beta_0} \times [M \Delta r \times v]$$

$$= m \frac{d\Delta \mathbf{r}}{dt} \times v + M \Delta \mathbf{r} \times \frac{dv}{dt} + \omega^{\beta/\beta_0} \times [M [\Delta x \Delta y \Delta z] \times [UVW]]$$

$$\begin{aligned}
\frac{E d}{dt} [m \dot{\alpha} r \times V] &= m \dot{\alpha} r \times \frac{dV}{dt} + \omega^B \times [m C \Delta x V b_z - \Delta x W b_y - \Delta y U b_z + \Delta y W b_x + \Delta z U b_y - \Delta z W b_x] \\
&= m \dot{\alpha} r \times [\dot{p} b_x + \dot{q} b_y + \dot{r} b_z] + \omega^B \times [m [(\Delta y W - \Delta z V) b_x + (\Delta z U - \Delta x W) b_y + (\Delta x V - \Delta y U) b_z]] \\
&= m [\Delta x \Delta y \Delta z] \times [\dot{p} b_x + \dot{q} b_y + \dot{r} b_z] + \omega^B \times m [(\Delta y W - \Delta z V) b_x + (\Delta z U - \Delta x W) b_y + (\Delta x V - \Delta y U) b_z] \\
&= m [\Delta x \dot{q} b_z - \Delta x \dot{r} b_y - \Delta y \dot{p} b_z + \Delta y \dot{r} b_x + \Delta z \dot{p} b_y - \Delta z \dot{q} b_x] + \\
&\quad [P b_x + Q b_y + R b_z] \times m [(\Delta y W - \Delta z V) b_x + (\Delta z U - \Delta x W) b_y + (\Delta x V - \Delta y U) b_z] \\
&= m [P(\Delta z U - \Delta x W) b_z - P(\Delta x V - \Delta y U) b_y - Q(\Delta y W - \Delta z V) b_z + Q(\Delta x V - \Delta y U) b_x + \\
&\quad R(\Delta y W - \Delta z V) b_y - R(\Delta z U - \Delta x W) b_x] \\
&= [(\Delta y \dot{r} - \Delta z \dot{q} + Q(\Delta x V - \Delta y U) - R(\Delta z U - \Delta x W)) b_x + (\Delta z \dot{p} - \Delta x \dot{r} + R(\Delta y W - \Delta z V) - P(\Delta x V - \Delta y U)) b_y \\
&\quad + (\Delta x \dot{q} - \Delta y \dot{p} + P(\Delta z U - \Delta x W) - Q(\Delta y W - \Delta z V)) b_z] m
\end{aligned}$$

$$\frac{E d}{dt} [m \dot{\alpha} r \times V] = m \begin{bmatrix} \Delta y \dot{r} - \Delta z \dot{q} + Q(\Delta x V - \Delta y U) - R(\Delta z U - \Delta x W) \\ \Delta z \dot{p} - \Delta x \dot{r} + R(\Delta y W - \Delta z V) - P(\Delta x V - \Delta y U) \\ \Delta x \dot{q} - \Delta y \dot{p} + P(\Delta z U - \Delta x W) - Q(\Delta y W - \Delta z V) \end{bmatrix}$$

note: to avoid confusion,  $m_a$  = mass of aircraft

Combining both parts:  $\dot{\alpha} \Sigma M =$

$$\begin{bmatrix} I_{xx} \dot{p} - I_{xy} \dot{q} - I_{xz} \dot{r} + I_{xy} P R - I_{xz} P Q + (I_{zz} - I_{yy}) Q R + (R^2 - Q^2) I_{yz} \\ -I_{xy} \dot{p} + I_{yy} \dot{q} - I_{yz} \dot{r} + I_{yz} P Q - I_{xy} Q R + (I_{xx} - I_{zz}) P R + (P^2 - R^2) I_{xz} \\ -I_{xz} \dot{p} - I_{yz} \dot{q} + I_{zz} \dot{r} + I_{yz} Q R - I_{yz} P R + (I_{yy} - I_{xx}) P Q + (Q^2 - P^2) I_{xy} \end{bmatrix}$$

+

$$\begin{bmatrix} m(PV - QU + \dot{w} - g \cos \Theta \cos \Phi) \Delta y + (PW - RU - \dot{v} + g \cos \Theta \sin \Phi) \Delta z \\ m(QU - PV - \dot{w} + g \cos \Theta \cos \Phi) \Delta x + (QW - RV + \dot{u} + g \sin \Theta) \Delta z \\ m(CRU - PW + \dot{v} - g \cos \Theta \sin \Phi) \Delta x + (RV - QW - \dot{u} - g \sin \Theta) \Delta y \end{bmatrix}$$

From  $\Sigma F$  and  $\Sigma M$  Equations, the small perturbation model is applied.

where:

$$\dot{U} = \dot{U}_1 + \dot{u}, \dot{R} = \dot{R}_1 + \dot{r}, \dot{Q} = \dot{Q}_1 + \dot{q}, Q_1 = Q_1 + q, U = U_1 + u, R = R_1 + r$$

$$W = W_1 + w, V = V_1 + v, \dot{V} = \dot{V}_1 + \dot{v}$$

due to small perturbation angle:

$$\sin(\text{small}) \rightarrow \text{angle}$$

$$\cos(\text{small}) \rightarrow 1$$

T subscript denotes  
thrust

X equation:

$$X = \dot{U} + QW - RV - \dot{R}\dot{y} + \dot{Q}\dot{z}$$

$$-mg\sin(\theta) + X + X_T = m[\dot{U}_1 + \dot{u} + Q_1W_1 + Q_1w + W_1q + qw - R_1V_1 - R_1v - V_1r - rv - \dot{R}_1\dot{y} - \dot{r}\dot{y} + \dot{Q}_1\dot{z} + \dot{q}\dot{z}]$$

applying small angle perturbation model to forces as well.

$$-g\sin(\theta)\cos\theta - g\cos(\theta)\sin\theta + \left(\frac{X_1 + f_x}{m}\right) + \left(\frac{X_{T1} + f_{Tx}}{m}\right) = [\dot{U}_1 + \dot{u} + Q_1W_1 + Q_1w + W_1q + qw - R_1V_1 - R_1v - V_1r - rv - \dot{R}_1\dot{y} - \dot{r}\dot{y} + \dot{Q}_1\dot{z} + \dot{q}\dot{z}]$$

Removing zero and high order terms yield:

$$\boxed{-g\theta\cos\theta_1 + \frac{f_x}{m} + \frac{f_{Tx}}{m} = \dot{u} - \dot{r}\dot{y} + \dot{q}\dot{z}} \quad X\text{-equation}$$

Y- Equation

$$Y = m_a [\dot{V} + RU - PW - \dot{p}\Delta z + \dot{r}\Delta x]$$

$$mg \sin \Phi \cos \theta + Y + Y_T = m_a [\dot{V} + RU - PW] - m [\dot{p}\Delta z - \dot{r}\Delta x]$$

$$mg (\sin \Phi_1 \cos \phi + \cos \Phi_1 \sin \phi) (\cos \theta_1 \cos \theta - \sin \theta_1 \sin \theta) + Y + Y_T = m_a [\dot{V}_1 + \dot{v} + (R_1 + r)(U_1 + u) - (P_1 + p)(W_1 + w)] - [\dot{p}_1 \Delta z - \dot{r}_1 \Delta x]$$

$$mg (\sin \Phi_1 + \phi \cos \Phi_1) (\cos \theta_1 - \theta \sin \theta_1) + Y + Y_T = m_a [\dot{V}_1 + \dot{v} + R_1 U_1 + R_1 u + U_1 r + r u - P_1 W_1 - P_1 w - p W_1 - p w - \dot{p}_1 \Delta z - \dot{p} \Delta z + \dot{r}_1 \Delta x + \dot{r} \Delta x]$$

Subtract with original Equation.

$$\boxed{mg \phi + f_y + f_{ey} = m_a [\dot{v} + U_1 r - \dot{p} \Delta z + \dot{r} \Delta x]}$$

Z - Equation:

$$Z = m_a [\dot{W} + PV - QU + \dot{p}\Delta y - \dot{q}\Delta x]$$

$$mg \cos \Phi \cos \theta + Z + Z_T = m_a [\dot{W} + PV - QU + \dot{p}\Delta y - \dot{q}\Delta x]$$

$$mg [\cos \Phi_1 \cos \phi - \sin \Phi_1 \sin \phi] (\cos \theta_1 \cos \theta - \sin \theta_1 \sin \theta) + Z_1 + Z_T + f_z + f_{ez} = m_a [\dot{W}_1 + \dot{w} + (P_1 + p)(U_1 + u) - (Q_1 + q)(V_1 + v) + \dot{p}_1 \Delta y + \dot{p} \Delta y - \dot{q}_1 \Delta x - \dot{q} \Delta x]$$

$$mg [\cos \Phi_1 \cos \theta_1 - \theta \sin \theta_1 \cos \Phi_1 - \phi \sin \Phi_1 \cos \theta_1 + \theta \phi \sin \Phi_1 \sin \theta_1] + Z_1 + f_z + f_{ez} + Z_T = m_a [\dot{W}_1 + \dot{w} + P_1 V_1 + p V_1 + P_1 v + p v + Q_1 U_1 + Q_1 u + U_1 q + u q + \dot{p}_1 \Delta y + \dot{p} \Delta y - \dot{q}_1 \Delta x - \dot{q} \Delta x]$$

Cancelling zero terms and high order terms:

$$\boxed{-mg \theta \sin \theta_1 + f_z + f_{ez} = m_a [\dot{w} + U_1 q + \dot{p} \Delta y - \dot{q} \Delta x]}$$

$M$  moment with respect to  $Y$ -axis:

$$M = (I_{xx} - I_{zz})PR + I_{xz}(R^2 - p^2) + m_a [\Delta z \dot{p} - \Delta x \dot{r} + R(\Delta y W - \Delta z V) - p(\Delta x V - \Delta y W) - I_{xy} \dot{p} + I_{yy} \dot{q} - I_{yz} \dot{r} + I_{yz} PQ - I_{xy} QR]$$

$$M + M_T = (I_{xx} - I_{zz})PR + I_{xz}(R^2 - p^2) + m_a [\Delta z \dot{p} - \Delta x \dot{r} + R(\Delta y W - \Delta z V) - p(\Delta x V - \Delta y W) - I_{xy} \dot{p} + I_{yy} \dot{q} - I_{yz} \dot{r} + I_{yz} PQ - I_{xy} QR]$$

$$M_1 + m_1 + M_{T_1} + m_{T_1} = (I_{xx} - I_{zz})(P_1 + p)(R_1 + r) + I_{xz}[(R_1 + r)^2 + (P_1 + p)^2] + m_a [\Delta z (\dot{P}_1 + \dot{p}) - \Delta x (\dot{R}_1 + \dot{r}) + (R_1 + r)(\Delta y (W_1 + w) - \Delta z (V_1 + v)) - (P_1 + p)(\Delta x (V_1 + v) - \Delta y (W_1 + w))] - I_{xy}(\dot{P}_1 + \dot{p}) + I_{yy}(\dot{Q}_1 + \dot{q}) - I_{yz}(\dot{R}_1 + \dot{r}) + I_{yz}(P_1 + p)(Q_1 + q) - I_{xy}(Q_1 + q)(R_1 + r)$$

$$M_1 + m_1 + M_{T_1} + m_{T_1} = (I_{xx} - I_{zz})(P_1 R_1 + P_1 r + R_1 p + rp) + I_{xz}(R_1^2 + 2R_1 r + r^2 + P_1^2 + 2P_1 p + p^2) + m_a [\Delta z (\dot{P}_1 + \dot{p}) - \Delta x (\dot{R}_1 + \dot{r}) + (R_1 + r)(\Delta y W_1 + \Delta y w - \Delta z V_1 - \Delta z v) - (P_1 + p)(\Delta x V_1 + \Delta x v - \Delta y W_1 - \Delta y w)] - I_{xy}(\dot{P}_1 + \dot{p}) + I_{yy}(\dot{Q}_1 + \dot{q}) - I_{yz}(\dot{R}_1 + \dot{r}) + I_{yz}(P_1 + p)(Q_1 + q) - I_{xy}(Q_1 + q)(R_1 + r)$$

Cancelling high order and zero terms:

$$M + M_T = -I_{xy} \dot{p} + I_{yy} \dot{q} - I_{yz} \dot{r} + m_a [(W_1 q - \dot{u} g \sin \theta) \Delta x + (\dot{u} r g \cos \theta) \Delta z]$$

Let  $\Sigma M$  of damaged aircraft be  $[L \ M \ N]$

$L$  moment with respect to  $x$ -axis

$$L = (I_{zz} - I_{yy})QR + I_{xz}PQ + m_a [\Delta y \dot{R} - \Delta z \dot{Q} + Q(\Delta x V - \Delta y U) - R(\Delta z U - \Delta x W)] \\ + I_{xx} \dot{p} + (I_{xy}) \dot{q} - I_{xz} \dot{r} + I_{xy} PR$$

Apply perturbation model

$$L = L_1 + \Delta L + L_T + \Delta L_T = (I_{zz} - I_{yy})(Q + \dot{q})(R_1 + r) + I_{xz}(P_1 + p)(Q_1 + q) + m_a [\Delta y(\dot{R}_1 + \dot{r}) \\ - \Delta z(\dot{Q}_1 + \dot{q}) + (Q_1 + q)(\Delta x(U_1 + u) - \Delta y(U_1 + u)) - (R_1 + r)(\Delta z(U_1 + u) - \Delta x(W_1 + w)) \\ + I_{xx}(\dot{p}_1 + \dot{p}) - I_{xy}(\dot{q}_1 + \dot{q}) - I_{xz}(\dot{r}_1 + \dot{r}) + I_{xy}(P_1 + p)(R_1 + r)]$$

$$L_1 + \Delta L + L_T + \Delta L_T = (I_{zz} - I_{yy})[Q_1 R_1 + Q_1 r + R_1 q + \dot{q} r] + I_{xz}[P_1 Q_1 + P_1 q + Q_1 p + \dot{q} p] + m_a [\Delta y(\dot{R}_1 + \dot{r}) \\ - \Delta z(\dot{Q}_1 + \dot{q}) + (Q_1 + q)(\Delta x U_1 + \Delta x u - \Delta y U_1 - \Delta y u) - (R_1 + r)(\Delta z U_1 - \Delta z u - \Delta x W_1 - \Delta x w)] \\ + I_{xx}(\dot{p}_1 + \dot{p}) - I_{xy}(\dot{q}_1 + \dot{q}) - I_{xz}(\dot{r}_1 + \dot{r}) + I_{xy}(R_1 P_1 + R_1 p + R_1 r + p r)$$

$$L_1 + \Delta L + L_T + \Delta L_T = (I_{zz} - I_{yy})[Q_1 R_1 + Q_1 r + R_1 q + \dot{q} r] + I_{xz}[P_1 Q_1 + P_1 q + Q_1 p + \dot{q} p] + m_a [\Delta y(\dot{R}_1 + \dot{r}) \\ - \Delta z(\dot{Q}_1 + \dot{q}) + Q_1 \Delta x U_1 + Q_1 \Delta x u - Q_1 \Delta y U_1 - Q_1 \Delta y u + \dot{q} \Delta x V_1 + \dot{q} \Delta x u - \Delta y U_1 \dot{q} - \Delta y U_1 \dot{q} \\ - R_1 \Delta z U_1 - R_1 \Delta z u + R_1 \Delta x W_1 + R_1 \Delta x w - r \Delta z U_1 - r \Delta z u + r \Delta x W_1 + r \Delta x w] \\ + I_{xx}(\dot{p}_1 + \dot{p}) - I_{xy}(\dot{q}_1 + \dot{q}) - I_{xz}(\dot{r}_1 + \dot{r}) + I_{xy}(R_1 P_1 + R_1 p + R_1 r + p r)$$

$$\boxed{L + \Delta L_T = I_{xx} \dot{p} - I_{xy} \dot{q} - I_{xz} \dot{r} + m_a [\dot{c} \dot{w} - U_1 \dot{q} + g \phi \sin \theta] \Delta y + (-U_1 r - \dot{u} + g \phi \cos \theta) \Delta z}$$

$\mathcal{N}$  moment with respect to z-axis

$$\mathcal{N} = m_a [\Delta x \dot{Q} - \Delta y \dot{p} + p(\Delta z U - \Delta x W) - Q(\Delta y W - \Delta z V)] + [I_{xz} \dot{p} - I_{yz} \dot{q} + I_{zz} \dot{r}]$$

$$\mathcal{N} + n + \mathcal{N}_T + n_T = m_a [\Delta x (\dot{Q}_1 + \dot{q}) - \Delta y (\dot{p}_1 + \dot{p}) + (p_1 + p)(\Delta z (U_1 + u) - \Delta x (W_1 + w)) - (Q_1 + q)(\Delta y (W_1 + w) - \Delta z (U_1 + u))] - [I_{xz} (\dot{p}_1 + \dot{p}) - I_{yz} (\dot{q}_1 + \dot{q}) + I_{zz} (\dot{r}_1 + \dot{r})]$$

$$\mathcal{N} + n + \mathcal{N}_T + n_T = m_a [\Delta x (\dot{Q}_1 + \dot{q}) - \Delta y (\dot{p}_1 + \dot{p}) + p_1 \Delta z U_1 + p_1 \Delta z u - \Delta x W_1 p_1 + \Delta x p_1 w + \Delta z U_1 p + \Delta z p u - \Delta x W_1 p + \Delta x w p - Q_1 \Delta y W_1 + \Delta y w Q_1 - \Delta z V_1 Q_1 - \Delta z v Q_1 - q \Delta y W_1 + \Delta y u q - \Delta z V_1 q - \Delta z v q] - [I_{xz} (\dot{p}_1 + \dot{p}) - I_{yz} (\dot{q}_1 + \dot{q}) + I_{zz} (\dot{r}_1 + \dot{r})]$$

Cancelling high order term, zero terms.

$$\mathcal{N} + \mathcal{N}_T = -I_{xz} \dot{p} - I_{yz} \dot{q} + I_{zz} \dot{r} + m_a [(U_1 r + v) - g \phi(\cos \theta) \Delta x + (u - \dot{u} - g \theta(\cos \theta) \Delta y)]$$

All of the equation:

$$-g \cos \theta + \frac{f_x}{m_a} = \ddot{u} - \dot{r} \Delta y + g \Delta z$$

$$g \phi \cos \theta + \frac{f_y}{m_a} = \ddot{v} - \dot{p} \Delta z + \dot{r} \Delta x + U_1 r$$

$$-g \theta \sin \theta + \frac{f_z}{m_a} = \ddot{w} - \dot{q} \Delta x + \dot{p} \Delta y - U_1 q$$

$$\frac{d}{I_{xx}} = \dot{p} - \frac{I_{xy}}{I_{xx}} \dot{q} - \frac{I_{xz}}{I_{xx}} \dot{r} + \frac{m_a}{I_{xx}} [(U_1 w - U_1 q + g \theta \sin \theta) \Delta y + (U_1 r - \dot{v} + g \phi \cos \theta) \Delta z]$$

$$\frac{m}{I_{yy}} = \frac{-I_{xy}}{I_{yy}} \dot{p} + \dot{q} - \frac{I_{yz}}{I_{yy}} \dot{r} + \frac{m_a}{I_{yy}} [(U_1 q - w - g \theta \sin \theta) \Delta y + (u + g \theta \cos \theta) \Delta z]$$

$$\frac{n}{I_{zz}} = \frac{-I_{xz}}{I_{zz}} \dot{p} - \frac{I_{yz}}{I_{zz}} \dot{q} + \dot{r} + \frac{m_a}{I_{zz}} [(U_1 r + v - g \phi(\cos \theta) \Delta x + (u - \dot{u} - g \theta \cos \theta) \Delta y)]$$

Aerodynamic and stability terms:

$$\frac{f_x}{m_a} = X_u u + X_\alpha \alpha + X_{\delta_e} \delta_e, \quad \frac{f_y}{m_a} = Y_p p + Y_{\delta_a} \delta_a + Y_{\delta_r} \delta_r + Y_r r + Y_\beta \beta$$

$$\frac{f_z}{m_a} = Z_u u + Z_\alpha \alpha + Z_{\dot{\alpha}} \dot{\alpha} + Z_q q + Z_{\delta_e} \delta_e, \quad \frac{\dot{\eta}}{I_{zz}} = N_{\delta_a} \delta_a + N_{\delta_r} \delta_r + N_\beta \beta + N_r r + N_p p$$

$$\frac{L}{I_{xx}} = L_{\delta_a} \delta_a + L_{\delta_r} \delta_r + L_p p + L_r r + L_p p, \quad \frac{M}{I_{yy}} = M_u u + M_\alpha \alpha + M_{\dot{\alpha}} \dot{\alpha} + M_q q + M_{\delta_e} \delta_e$$

$\dot{p}$  Equation:

$$\frac{L}{I_{xx}} = \dot{p} - \frac{I_{xy}}{I_{xx}} \dot{q} - \frac{I_{xz}}{I_{xx}} \dot{r} + \frac{m_a}{I_{xx}} [(w - U_0 + g \sin \theta) \Delta y + (U_1 r - \dot{v} + g \phi \cos \theta) \Delta z]$$

Sub for  $w, \dot{v}$

$$\dot{p} = \frac{L}{I_{xx}} + \frac{I_{xy}}{I_{xx}} \dot{q} + \frac{m_a}{I_{xx}} \Delta y g \sin \theta - \frac{m_a}{I_{xx}} \Delta y \frac{f_z}{m_a} - \frac{m_a}{I_{xx}} \Delta y U_1 r + \frac{m_a}{I_{xx}} U_1 g \phi \cos \theta - \frac{m_a}{I_{xx}} g \theta \sin \theta \Delta y$$

$$- \frac{m_a}{I_{xx}} U_1 r \Delta z + \frac{m_a}{I_{xx}} \Delta z g \phi \cos \theta + \frac{m_a}{I_{xx}} \Delta z \frac{f_y}{m_a} - \frac{m_a}{I_{xx}} \Delta z U_1 r - \frac{m_a}{I_{xx}} g \phi \cos \theta \Delta z$$

Canceling high order terms and small contributions

$$\boxed{\dot{p} = \frac{L}{I_{xx}} + \frac{I_{xy}}{I_{xx}} \dot{q} - \frac{m_a}{I_{xx}} \Delta y \frac{f_z}{m_a} + \frac{m_a}{I_{xx}} \Delta z \frac{f_y}{m_a}}$$

Solve for  $\dot{q}$

$$\frac{m}{I_{yy}} = -\frac{I_{xy}}{I_{yy}} \dot{p} + \dot{q} - \frac{I_{yz}}{I_{yy}} \dot{r} + \frac{m_a}{I_{yy}} [(U_1 q - \dot{w} - g \sin \theta) \Delta y + (U_1 q + g \cos \theta) \Delta z]$$

sub,  $w, z$

$$\dot{q} = \frac{m}{I_{yy}} + \frac{I_{xy}}{I_{yy}} \dot{p} - \frac{m_a}{I_{yy}} U_1 q \Delta y - \frac{m_a}{I_{yy}} \Delta y g \sin \theta + \frac{m_a}{I_{yy}} \Delta y \frac{f_z}{m_a} + \frac{m_a}{I_{yy}} \Delta y U_1 q + g \theta \sin \theta \Delta y \frac{m_a}{I_{yy}}$$

$$- g \theta \cos \theta \frac{m_a}{I_{yy}} \Delta z + \frac{m_a}{I_{yy}} \Delta z g \cos \theta - \frac{m_a}{I_{yy}} \Delta z \frac{f_x}{m_a}$$

Canceling high order terms and small contribution terms:

$$\boxed{\dot{q} = \frac{m}{I_{yy}} + \frac{I_{xy}}{I_{yy}} \dot{p} + \frac{m_a}{I_{yy}} \Delta y \frac{f_z}{m_a} - \frac{m_a}{I_{yy}} \Delta z \frac{f_x}{m_a}}$$

Sub  $\dot{p}$  into  $\dot{q}$

$$\dot{q} = \frac{m}{I_{yy}} + \frac{I_{xy}}{I_{yy}} \frac{1}{I_{xx}} + \frac{I_{xy}}{I_{yy}} \frac{I_{xy}}{I_{xx}} \dot{q} - \frac{I_{xy}}{I_{yy}} \frac{m_c}{I_{xx}} \Delta y \frac{f_z}{m_a} + \frac{I_{xy}}{I_{yy}} \frac{m_c}{I_{xx}} \Delta z \frac{f_y}{m_a} + \frac{m_c}{I_{yy}} \Delta x \frac{f_z}{m_a} - \frac{m_c}{I_{yy}} \Delta z \frac{f_x}{m_a}$$

$$\dot{q} = \left[ \frac{m}{I_{yy}} + \frac{I_{xy}}{I_{yy}} \frac{1}{I_{xx}} + \left( \frac{m_c}{I_{yy}} \Delta x - \frac{I_{xy}}{I_{yy}} \frac{m_c}{I_{xx}} \Delta y \right) \frac{f_z}{m_a} + \frac{I_{xy}}{I_{yy}} \frac{m_c}{I_{xx}} \Delta z \frac{f_x}{m_a} - \frac{m_c}{I_{yy}} \Delta z \frac{f_x}{m_a} \right] / \left( 1 - \frac{I_{xy}^2}{I_{yy} I_{xx}} \right)$$

assuming:  $I_{xy} \cdot I_{xz} \leq \frac{I_{xx}}{I_{yy}} I_{zz}$

$$\frac{I_{xy}}{I_{xx, y, z}} = 0, \quad \frac{I_{xz}}{I_{xx, y, z}} = 0$$

$$\dot{q} = \frac{m}{I_{yy}} + \frac{m_c}{I_{yy}} \Delta x \frac{f_z}{m_a} - \frac{m_c}{I_{yy}} \Delta z \frac{f_x}{m_a}$$

$$\dot{p} = \frac{1}{I_{xx}} + \frac{m_c}{I_{xx}} \Delta z \frac{f_y}{m_a} - \frac{m_c}{I_{xx}} \Delta y \frac{f_z}{m_a}$$

sub.  $\dot{p}$ ,  $\dot{q}$ ,  $\dot{v}$ ,  $\dot{u}$   
↓

$$\dot{r} = \frac{\eta}{I_{zz}} - \frac{m_c}{I_{zz}} U_1 r \Delta x + \frac{m_c}{I_{zz}} \Delta x U_1 r - \frac{m_c}{I_{zz}} \Delta x g \phi \cos \theta + \frac{m_c}{I_{zz}} g \phi \cos \theta \Delta x + \frac{m_c}{I_{zz}} g \theta \cos \theta \Delta y$$

$$+ \frac{m_c}{I_{zz}} \Delta y \frac{f_x}{m_a} - \theta g \cos \theta \frac{m_c}{I_{zz}} \Delta y - \frac{m_c}{I_{zz}} \Delta x \frac{f_y}{m_a}$$

$$\dot{r} = \frac{\eta}{I_{zz}} + \frac{m_c}{I_{zz}} \Delta y \frac{f_x}{m_a} - \frac{m_c}{I_{zz}} \Delta x \frac{f_y}{m_a}$$

finally:

$$\dot{u} = -\theta g \cos \theta + \frac{f_x}{m_a} + \frac{\eta}{I_{zz}} \Delta y - \Delta z \frac{m}{I_{yy}}$$

$$U_1 \dot{p} = \dot{v} = g \phi \cos \theta + \frac{f_y}{m_a} + \Delta z \frac{1}{I_{xx}} - \Delta x \frac{\eta}{I_{zz}} - U_1 r$$

$$\dot{\alpha} U_1 = -g \theta \sin \theta + \frac{f_z}{m_a} + \Delta x \frac{m}{I_{yy}} - \Delta y \frac{1}{I_{xx}} + U_1 q$$

$$\dot{q} = \frac{m}{I_{yy}} + \frac{m_c}{I_{yy}} \Delta x \frac{f_z}{m_a} - \frac{m_c}{I_{yy}} \Delta z \frac{f_x}{m_a}$$

$$\dot{p} = \frac{1}{I_{xx}} + \frac{m_c}{I_{xx}} \Delta z \frac{f_y}{m_a} - \frac{m_c}{I_{xx}} \Delta y \frac{f_z}{m_a}$$

$$\dot{r} = \frac{\eta}{I_{zz}} + \frac{m_c}{I_{zz}} \Delta y \frac{f_x}{m_a} - \frac{m_c}{I_{zz}} \Delta x \frac{f_y}{m_a}$$

Substituting Aerodynamic and stability derivative

$$\dot{\alpha} U_1 = -g\theta \sin\theta + Z_{\alpha} u + Z_{\alpha} \alpha + Z_{\dot{\alpha}} \dot{\alpha} + Z_{\dot{q}} \dot{q} + Z_{\dot{e}} \dot{e} + \Delta x M_{\dot{u}} u + \Delta x M_{\dot{\alpha}} \alpha + \Delta x M_{\dot{\alpha}} \dot{\alpha} \\ + M_{\dot{q}} \dot{q} \Delta x + M_{\dot{e}} \dot{e} \Delta x - \Delta y L_{\dot{\alpha}} \dot{\alpha} - \Delta y L_{\dot{r}} \dot{r} - \Delta y L_{\dot{r}} \dot{r} - \Delta y L_{\dot{\beta}} \dot{\beta} - \Delta y L_{\dot{p}} \dot{p} + U_1 \dot{q}$$

$$\dot{\alpha} = [-g\theta \sin\theta + Z_{\alpha} u + Z_{\alpha} \alpha + Z_{\dot{e}} \dot{e} + Z_{\dot{q}} \dot{q} + \Delta x M_{\dot{u}} u + \Delta x M_{\dot{\alpha}} \alpha + M_{\dot{q}} \dot{q} \Delta x + M_{\dot{e}} \dot{e} \Delta x \\ - \Delta y L_{\dot{\alpha}} \dot{\alpha} - \Delta y L_{\dot{r}} \dot{r} - \Delta y L_{\dot{r}} \dot{r} - \Delta y L_{\dot{\beta}} \dot{\beta} - \Delta y L_{\dot{p}} \dot{p} + U_1 \dot{q}] / (U_1 - \Delta x M_{\dot{\alpha}} - Z_{\dot{\alpha}})$$

$$(U_1 - \Delta x M_{\dot{\alpha}} - Z_{\dot{\alpha}}) = K$$

$$\dot{\alpha} = [Z_{\alpha} + \Delta x M_{\dot{\alpha}}] K^{-1} u + [Z_{\alpha} + \Delta x M_{\dot{\alpha}}] K^{-1} \alpha + [Z_{\dot{q}} + M_{\dot{q}} \Delta x + U_1] K^{-1} \dot{q} + [-g \sin\theta] K^{-1} \theta \\ + [-\Delta y L_{\dot{p}}] K^{-1} \dot{p} + [-\Delta y L_{\dot{\beta}}] K^{-1} \dot{\beta} + [-\Delta y L_{\dot{r}}] K^{-1} \dot{r} + [Z_{\dot{e}} + M_{\dot{e}} \Delta x] K^{-1} \dot{e} + [-\Delta y L_{\dot{\alpha}}] K^{-1} \dot{\alpha} \\ + [-\Delta y L_{\dot{r}}] K^{-1} \dot{r}$$

$$\dot{u} = -g\theta \cos\theta + X_{\dot{u}} u + X_{\dot{\alpha}} \alpha + X_{\dot{e}} \dot{e} + \Delta y N_{\dot{r}} \dot{r} + \Delta y N_{\dot{\alpha}} \dot{\alpha} + \Delta y N_{\dot{\beta}} \dot{\beta} + \Delta y N_{\dot{r}} \dot{r} + N_{\dot{p}} \dot{p} \Delta y \\ - \Delta z M_{\dot{u}} u - \Delta z M_{\dot{\alpha}} \alpha - \Delta z M_{\dot{\alpha}} \dot{\alpha} + \Delta z M_{\dot{q}} \dot{q} + M_{\dot{e}} \dot{e} \Delta z$$

$$\dot{u} = -g\theta \cos\theta + X_{\dot{u}} u + X_{\dot{\alpha}} \alpha + X_{\dot{e}} \dot{e} + \Delta y N_{\dot{\alpha}} \dot{\alpha} + \Delta y N_{\dot{r}} \dot{r} + \Delta y N_{\dot{\beta}} \dot{\beta} + \Delta y N_{\dot{r}} \dot{r} + N_{\dot{p}} \dot{p} \Delta y \\ - \Delta z M_{\dot{u}} u - \Delta z M_{\dot{\alpha}} \alpha - \Delta z M_{\dot{\alpha}} Z_{\dot{\alpha}} K^{-1} u - \Delta z M_{\dot{\alpha}} Z_{\dot{\alpha}} K^{-1} \alpha - \Delta z Z_{\dot{q}} K^{-1} \dot{q} M_{\dot{\alpha}} - \Delta z U_1 K^{-1} M_{\dot{\alpha}} \\ + g \sin\theta \Delta z M_{\dot{\alpha}} K^{-1} - \Delta z M_{\dot{\alpha}} Z_{\dot{e}} K^{-1} \dot{e}$$

$$\dot{u} = [X_{\dot{u}} - \Delta z M_{\dot{u}} - \Delta z M_{\dot{\alpha}} Z_{\dot{\alpha}} K^{-1}] u + [X_{\dot{\alpha}} - \Delta z M_{\dot{\alpha}} - \Delta z M_{\dot{\alpha}} Z_{\dot{\alpha}} K^{-1}] \alpha + [-\Delta z Z_{\dot{q}} M_{\dot{\alpha}} - \Delta z U_1 K^{-1} M_{\dot{\alpha}}] \dot{q} \\ + [g \sin\theta K^{-1} \Delta z M_{\dot{\alpha}} - g \cos\theta] \theta + [\Delta y N_{\dot{p}}] \dot{p} + [N_{\dot{p}} \Delta y] \dot{p} + [\Delta y N_{\dot{r}}] \dot{r} + [X_{\dot{e}} - \Delta z M_{\dot{\alpha}} Z_{\dot{e}} K^{-1}] \dot{e} \\ + [\Delta y N_{\dot{r}}] \dot{r} + [\Delta y N_{\dot{\alpha}}] \dot{\alpha}$$

$$\ddot{\mathbf{r}} = M_{\alpha} \ddot{u} + M_{\alpha} \ddot{\alpha} + M_{\alpha} \ddot{\alpha} + M_{\phi} \ddot{\phi} + M_{\delta} \ddot{\delta} + \frac{m_{\alpha}}{I_{yy}} \Delta x Z_{\alpha} \ddot{u} + \frac{m_{\alpha}}{I_{yy}} \Delta x Z_{\alpha} \ddot{\alpha}$$

$$+ \frac{m_{\alpha}}{I_{yy}} \Delta x Z_{\alpha} \ddot{\alpha} + \frac{m_{\phi}}{I_{yy}} \Delta x Z_{\phi} \ddot{\phi} + \frac{m_{\delta}}{I_{yy}} \Delta x Z_{\delta} \ddot{\delta} - \frac{m_{\alpha}}{I_{yy}} \Delta z X_{\alpha} \ddot{u} - \frac{m_{\alpha}}{I_{yy}} \Delta z X_{\alpha} \ddot{\alpha} - \frac{m_{\phi}}{I_{yy}} \Delta z X_{\phi} \ddot{\phi}$$

$$\dot{\mathbf{r}} = [M_{\alpha} - \frac{m_{\alpha}}{I_{yy}} \Delta z X_{\alpha} + \frac{m_{\alpha}}{I_{yy}} \Delta x Z_{\alpha} + Z_{\alpha} M_{\alpha} k^T + \Delta x M_{\alpha} M_{\alpha} k^T] \ddot{u} + [M_{\alpha} + \frac{m_{\alpha}}{I_{yy}} \Delta x Z_{\alpha} - \frac{m_{\alpha}}{I_{yy}} \Delta z X_{\alpha}$$

$$+ M_{\alpha} Z_{\alpha} k^T + M_{\alpha} \Delta x M_{\alpha} k^T + Z_{\alpha} \frac{m_{\alpha}}{I_{yy}} \Delta x Z_{\alpha} k^T] \ddot{\alpha} + [Z_{\alpha} \frac{m_{\alpha}}{I_{yy}} \Delta x Z_{\alpha} k^T] \ddot{u}$$

$$+ [M_{\phi} + \frac{m_{\phi}}{I_{yy}} \Delta x Z_{\phi} + M_{\phi} Z_{\phi} k^T + M_{\phi} M_{\phi} \Delta x k^T + M_{\phi} U_{\phi} k^T + Z_{\phi} \frac{m_{\phi}}{I_{yy}} \Delta x Z_{\phi} k^T + Z_{\phi} \frac{m_{\phi}}{I_{yy}} \Delta x U_{\phi} k^T] \ddot{\phi}$$

$$+ [-M_{\phi} g \sin \theta k^T - Z_{\phi} \frac{m_{\phi}}{I_{yy}} \Delta x g \sin \theta k^T] \ddot{\theta} + [-M_{\phi} \Delta y L_{\phi} k^T] \ddot{p} + [-M_{\phi} \Delta y L_{\phi} k^T] \ddot{\beta} + [-M_{\phi} \Delta y L_{\phi} k^T] \ddot{r}$$

$$+ [M_{\delta} + \frac{m_{\delta}}{I_{yy}} \Delta x Z_{\delta} - \frac{m_{\delta}}{I_{yy}} \Delta z X_{\delta} + M_{\delta} Z_{\delta} k^T + M_{\delta} M_{\delta} \Delta x k^T + Z_{\delta} Z_{\delta} k^T \frac{m_{\delta}}{I_{yy}} \Delta x] \ddot{\delta} +$$

$$[-M_{\delta} \Delta y L_{\delta} k^T] \ddot{\delta}_{\alpha} + [-M_{\delta} \Delta y L_{\delta} k^T] \ddot{\delta}_r$$

$$\ddot{\mathbf{p}} = \frac{g \cos \theta}{U_1} \ddot{\phi} + \frac{Y_P}{U_1} \ddot{p} + \frac{Y_{\delta} \delta_{\alpha}}{U_1} \ddot{\delta}_{\alpha} + \frac{Y_r}{U_1} \ddot{r} + \frac{Y_{\delta} \delta_r}{U_1} \ddot{\delta}_r + \frac{Y_{\beta} \beta}{U_1} \ddot{\beta} + \frac{\Delta z L_{\delta} \delta_{\alpha}}{U_1} \ddot{\delta}_{\alpha} + \frac{\Delta z L_{\delta} \delta_r}{U_1} \ddot{\delta}_r + \frac{\Delta z L_{\beta} \beta}{U_1} \ddot{\beta} + \frac{\Delta z L_r r}{U_1} \ddot{r}$$

$$+ \frac{\Delta z L_p p}{U_1} \ddot{p} - \frac{\Delta x N_{\delta_{\alpha}}}{U_1} \ddot{\delta}_{\alpha} - \frac{\Delta x N_{\delta_r}}{U_1} \ddot{\delta}_r - \frac{\Delta x N_{\beta}}{U_1} \ddot{\beta} - \frac{\Delta x N_r}{U_1} \ddot{r} - \frac{N_p \Delta x}{U_1} \ddot{p} - U_1 \ddot{r}$$

$$\ddot{\mathbf{p}} = [\frac{g \cos \theta}{U_1}] \ddot{\phi} + [\frac{Y_P}{U_1} + \frac{\Delta z L_p}{U_1} - \frac{\Delta x N_p}{U_1}] \ddot{p} + [\frac{Y_{\beta}}{U_1} + \frac{\Delta z L_{\beta}}{U_1} - \frac{\Delta x N_{\beta}}{U_1}] \ddot{\beta} +$$

$$[\frac{Y_r}{U_1} + \frac{\Delta z L_r}{U_1} - \frac{\Delta x N_r}{U_1} - U_1] \ddot{r} + [\frac{Y_{\delta_{\alpha}}}{U_1} + \frac{\Delta z L_{\delta_{\alpha}}}{U_1} - \frac{\Delta x N_{\delta_{\alpha}}}{U_1}] \ddot{\delta}_{\alpha} + [\frac{Y_{\delta_r}}{U_1} + \frac{\Delta z L_{\delta_r}}{U_1} - \frac{\Delta x N_{\delta_r}}{U_1}] \ddot{\delta}_r$$

$$\dot{r} = N_{\delta a} \delta a + N_{\delta r} \delta r + N_{\beta} \beta + N_r r + N_p p + \frac{m_a}{I_{zz}} \Delta y \chi_u u + \frac{m_a}{I_{zz}} \Delta y \chi_\alpha \alpha + \frac{m_a}{I_{zz}} \Delta y \chi_\delta \delta e$$

$$- \frac{m_a}{I_{zz}} \Delta x \chi_p p - \frac{m_a}{I_{zz}} \Delta x \chi_\delta e - \frac{m_a}{I_{zz}} \Delta x \chi_r r - \frac{m_a}{I_{zz}} \chi_{\delta r} \delta r \Delta x - \frac{m_a}{I_{zz}} \chi_{\beta} \beta \Delta x - \frac{m_a}{I_{zz}} \chi_{\delta a} \delta a$$

$$\dot{r} = \left[ \frac{m_a}{I_{zz}} \Delta y \right] u + \left[ \frac{m_a}{I_{zz}} \Delta y \chi_\alpha \right] \alpha + \left[ N_p - \frac{m_a}{I_{zz}} \Delta x \chi_p \right] p + \left[ N_\beta - \frac{m_a}{I_{zz}} \Delta x \chi_\beta \right] \beta + \left[ N_r - \frac{m_a}{I_{zz}} \Delta x \chi_r \right] r$$

$$+ \left[ \frac{m_a}{I_{zz}} \Delta y \chi_\delta \right] \delta e + \left[ N_{\delta r} - \frac{m_a}{I_{zz}} \Delta x \chi_{\delta r} \right] \delta r + \left[ N_{\delta a} - \frac{m_a}{I_{zz}} \Delta x \chi_{\delta a} \right] \delta a$$

$$\dot{p} = L_{\delta a} \delta a + L_{\delta r} \delta r + L_r r + L_\beta \beta + L_p p + \frac{m_a}{I_{xx}} \Delta z \chi_p p + \frac{m_a}{I_{xx}} \Delta z \chi_r r + \frac{m_a}{I_{xx}} \Delta z \chi_\beta \beta$$

$$+ \frac{m_a}{I_{xx}} \Delta z \chi_{\delta a} \delta a + \frac{m_a}{I_{xx}} \Delta z \chi_{\delta r} \delta r - \frac{m_a}{I_{xx}} \Delta y z_u u - \frac{m_a}{I_{xx}} \Delta y z_\alpha \alpha - \frac{m_a}{I_{xx}} \Delta y z_\delta \delta e - \frac{m_a}{I_{xx}} \Delta y z_\beta \beta$$

$$- \frac{m_a}{I_{xx}} \Delta y z_\delta \delta e$$

$$\dot{\theta} = \left[ -\frac{m_a}{I_{xx}} \Delta y z_u - \frac{m_a}{I_{xx}} \Delta y z_\alpha k^T z_u \right] u + \left[ -\frac{m_a}{I_{xx}} \Delta y z_\alpha - \frac{m_a}{I_{xx}} \Delta y z_\alpha k^T z_\alpha \right] \alpha + \left[ \frac{m_a}{I_{xx}} \Delta y z_\beta \sin \theta k^T \right] \theta$$

$$\left[ -\frac{m_a}{I_{xx}} \Delta y z_\beta - \frac{m_a}{I_{xx}} \Delta y z_\alpha z_\beta k^T - \frac{m_a}{I_{xx}} \Delta y z_\alpha v k^T \right] \beta + \left[ L_p + \frac{m_a}{I_{xx}} \Delta z \chi_p \right] p + \left[ L_\beta + \frac{m_a}{I_{xx}} \Delta z \chi_\beta \right] \beta$$

$$+ \left[ L_r + \frac{m_a}{I_{xx}} \Delta z \chi_r \right] r + \left[ -\frac{m_a}{I_{xx}} \Delta y z_\delta e - \frac{m_a}{I_{xx}} \Delta y z_\alpha z_\delta e k^T \right] \delta e + \left[ L_{\delta a} + \frac{m_a}{I_{xx}} \Delta z \chi_{\delta a} \right] \delta a$$

$$+ \left[ L_{\delta r} + \frac{m_a}{I_{xx}} \Delta z \chi_{\delta r} \right] \delta r$$

## Appendix B – Damage Wing Simulation Code

```
%% Setup
clc,clear,close all;
%% Givens_undamaged
Xu = -0.0218;
Xa = 1.2227;
Zu = -0.0569;
Za = -339.0036;
Mu = -0.0001;
Ma = -1.6165;
Madot = -0.1425;
Mq = -0.4038;
Xde = 0;
Zde = -18.3410;
Mde = -1.2124;
Yb = -55.7808;
Lb = -1.2555;
Lp = -0.4758;
Lr = 0.2974;
Nb = 1.0143;
Np = 0.0109;
Nr = -0.1793;
Ydr = 3.7187;
Ldr = 0.2974;
Ndr = -0.4589;
Yda = 0;
Lda = 0.185;
Yp = 0;
Yr = 0;
Nda = -0.0135;
U1 = 871;
Theta_1 = 2.4*(pi/180);
g = 32.174049;
S_u = 5500;
c_u = 27.3;
b_u = 196;
Ixx_u = 1.82e7;
Iyy_u = 3.31e7;
Izz_u = 4.97e7;
Ixz_u = -4.05e5;

%% Undamaged EoM
A_u_long = [
    Xu, Xa, 0, -g;
```

```

Zu/U1, Za/U1, 1, 0;
(Mu + (Madot*Zu)/U1), (Ma + (Madot*Za)/U1), (Mq+Madot), 0;
0, 0, 1, 0;
];

B_u_long = [
    Xde;
    Zde/U1;
    (Mde + (Madot*Zde)/U1);
    0;
];
C_u_long = eye(4);
D_u_long = zeros(4,1);

A_u_lat = [
    0,1,0,0,0;
    0,Lp,Lb,Lr,0;
    g*cos(Theta_1)/U1,Yp/U1,Yb/U1,Yr/U1-1,0;
    0,Np,Nb,Nr,0;
    0,0,0,1,0;
];
B_u_lat = [
    0,0;
    Ldr,Lda;
    Ydr/U1,Yda/U1;
    Ndr,Nda;
    0,0;
];
C_u_lat = eye(5);
D_u_lat = zeros(5,2);

undamaged_ss_long = ss(A_u_long,B_u_long,C_u_long,D_u_long);% nominal full state state
space system longitudinal
undamaged_ss_lat = ss(A_u_lat,B_u_lat,C_u_lat,D_u_lat);% nominal full state state space
system lateral/directional
%% Givens _ damaged aircraft
%aircraft params
damage_factor = 0.33; %Damaged 33%
m2ft = 3.28;
b = 161.06;
c = 28.54;
S = b*c;
S_fact = S/S_u;
b_fact = b/b_u;
c_fact = c/c_u;

```

```

del_x = -0.0048*m2ft;
del_y = 0.0145*m2ft;
del_z = -0.005/3*m2ft;
del_b = 0.0001;
Ixx = 15097500;
Iyy = 33090070;
Izz = 46598720;
m = 623903.08;
rho = 5.87e-4;
q = (1/2)*rho*U1^2;
U1 = 871;
Theta_1 = 2.4*(pi/180);
g = 32.174049;
m_a = m;

```

```

%stability and control derivatives

```

```

Yp = -272;
Xu = Xu*S_fact;
Xa = Xa*S_fact;
Zu = Zu*S_fact;
Za = Za*S_fact;
Mu = Mu*S_fact*c_fact;
Ma = Ma*S_fact*c_fact;
Madot = Madot*S_fact*c_fact^2;
Mq = Mq*S_fact*c_fact^2;
Xde = -0.0002;
Zde = Zde*S_fact;
Mde = Mde*S_fact*c_fact;
Yb = Yb*S_fact;
Lb = Lb*S_fact*c_fact;
Lp = Lp*S_fact*b_fact^2;
Lr = Lr*S_fact*b_fact^2;
Nb = Nb*S_fact*b_fact;
Np = Np*S_fact*b_fact^2;
Nr = Nr*S_fact*b_fact^2;
Ydr = Ydr*S_fact;
Ldr = Ldr*S_fact*b_fact;
Ndr = Ndr*S_fact*b_fact;
Yde = 0;
Lde = -0.001;
Nda = Nda*S_fact;
Yp = Yp*q*S*b/(2*U1*m_a);
Yr = 0.8274*q*S*b/(2*U1*m_a);
Lda = Lda*S_fact*b_fact;
Yda = Yda*S_fact;

```

```

Zadot = 0;
Zq = 0;

%% Damaged EoM
% order: x = [u alpha q theta phi p beta r psi]
K = 1/(U1-del_x*Madot-Zadot);
A_d = [
    Xu-del_z*Mu-del_z*Madot*Zu*K,Xa-del_z*Ma-del_z*Madot*Za*K,-del_z*Zq*Madot-
del_z*U1*K*Madot-del_z*Mq,g*sin(Theta_1)*K*del_z*Madot-
g*cos(Theta_1),0,del_y*Np,del_y*Nb,del_y*Nr,0;
    (Zu+del_x*Mu)*K,(Za+del_x*Ma)*K,(Zq+Mq*del_x+U1)*K,-g*sin(Theta_1)*K,0,-
del_y*Lp*K,-del_y*Lb*K,-del_y*Lr*K,0;
    Mu-
(m_a/Iyy)*del_z*Xu+(m_a/Iyy)*del_x*Zu+Zu*Madot*K+del_x*Mu*Madot*K+Zadot*(m_a/Iy
y)*del_x*Zu*K,Ma+(m_a/Iyy)*del_x*Za-
(m_a/Iyy)*del_z*Xa+Madot*Za*K+Madot*del_x*Ma*K+Zadot*(m_a/Iyy)*del_x*Za*K,Mq+(
m_a/Iyy)*del_x*Zq+Madot*Zq*K+K*Madot*Mq*del_x+Madot*U1*K+Zadot*(m_a/Iyy)*del_
x*Zq*K+Zadot*(m_a/Iyy)*del_x*U1*K,-Madot*g*sin(Theta_1)-
Zadot*(m_a/Iyy)*del_x*g*sin(Theta_1)*K,0,-Madot*del_y*Lp*K,-Madot*del_y*Lb*K,-
Madot*del_y*Lr*K,0;
    0,0,1,0,0,0,0,0,0;
    0,0,0,0,0,1,0,0,0;
    -(m_a/Ixx)*del_y*Zu,-(m_a/Ixx)*del_y*Za,-(m_a/Ixx)*del_y*Zq-
(m_a/Ixx)*del_y*Zadot*Zq*K-
(m_a/Ixx)*del_y*Zadot*U1*K,(m_a/Ixx)*del_y*Zadot*g*sin(Theta_1)*K,0,Lp*del_b+(m_a/Ix
x)*del_z*Yp,Lb+(m_a/Ixx)*del_z*Yb,Lr+(m_a/Ixx)*del_z*Yr,0;
    0,0,0,0,g*cos(Theta_1)/U1,(Yp+del_z*Lp-del_x*Np)/U1,(Yb+del_z*Lb-
del_x*Nb)/U1,(Yr+del_z*Lr-del_x*Nr)/U1-1,0;
    (m_a/Izz)*del_y*Xu,(m_a/Izz)*del_y*Xa,0,0,0,Np-(m_a/Izz)*del_x*Yp,Nb-
(m_a/Izz)*del_x*Yb,Nr-(m_a/Izz)*del_x*Nr,0;
    0,0,0,0,0,0,0,1,0;

];
% order: u = [de, dr, da]
B_d = [
    Xde-del_z*Madot*Zde*K-del_z*Mde,del_y*Ndr,del_y*Nda;
    Zde*K+Mde*del_x*K,-del_y*Lda*K,-del_y*Ldr*K;
    Mde+(m_a/Iyy)*del_x*Zde-
(m_a/Iyy)*del_z*Xde+Madot*Zde*K+Madot*Mde*del_x*K+Zadot*Zde*K*(m_a/Iyy)*del_x,-
Madot*del_y*Ldr*K,-Madot*del_y*Lda*K;
    0,0,0;
    0,0,0;
    -(m_a/Ixx)*del_y*Zde-
(m_a/Ixx)*del_y*Zadot*Zde*K,Ldr+(m_a/Ixx)*del_z*Ydr,Lda+(m_a/Ixx)*del_z*Yda;
    0,(Ydr+del_z*Ldr-del_x*Ndr)/U1,(Yda+del_z*Lda-del_x*Nda)/U1;

```

```

(m_a/Izz)*del_y*Xde,Ndr-(m_a/Izz)*del_x*Ydr,Nda-(m_a/Izz)*del_x*Yda;
0,0,0;
];
C_d = eye(9);

D_d = zeros(9,3);
damaged_ss = ss(A_d,B_d,C_d,D_d); % damaged full state state space system
%% Controllability and observability
rank(observ(damaged_ss))
rank(ctrb(damaged_ss))
%% Plot
open("damage_wing_model.slx");
sim("damage_wing_model.slx");

% u
figure;
plot(u_output_d(:,1),u_output_d(:,2),'r',"LineWidth",2);
hold on;
plot(u_output_u(:,1),u_output_u(:,2),'--b',"LineWidth",2);
hold off;
xlabel("Time[s]"),ylabel("Velocity[ft/s]");
title("Velocity Damaged vs Undamaged");
legend("damaged","undamaged",'Location',"Best");
set(gca,'FontSize',16)

% alpha
figure;
plot(alpha_output_d(:,1),alpha_output_d(:,2),'r');
hold on;
plot(alpha_output_u(:,1),alpha_output_u(:,2),'--b');
hold off;
xlabel("Time[s]"),ylabel("\alpha [deg]");
title("AoA Damaged vs Undamaged");
legend("damaged","undamaged");

% q
figure;
plot(q_output_d(:,1),q_output_d(:,2),'r');
hold on;
plot(q_output_u(:,1),q_output_u(:,2),'--b');
hold off;
xlabel("Time[s]"),ylabel("q[deg/s]");
title("Pitch rate Damaged vs Undamaged");
legend("damaged","undamaged");

```

```

%theta
figure;
plot(theta_output_d(:,1),theta_output_d(:,2),'r');
hold on;
plot(theta_output_u(:,1),theta_output_u(:,2),'--b');
hold off;
xlabel('Time[s]'),ylabel("\theta[deg]");
title("Pitch Angle Damaged vs Undamaged");
legend("damaged","undamaged");

```

```

%phi
figure;
plot(phi_output_d(:,1),phi_output_d(:,2),'r');
hold on;
plot(phi_output_u(:,1),phi_output_u(:,2),'--b');
hold off;
xlabel('Time[s]'),ylabel("\phi[deg]");
title("Roll Angle Damaged vs Undamaged");
legend("damaged","undamaged");

```

```

%p
figure;
plot(p_output_d(:,1),p_output_d(:,2),'r');
hold on;
plot(p_output_u(:,1),p_output_u(:,2),'--b');
hold off;
xlabel('Time[s]'),ylabel("p[deg/s]");
title("Roll rate Damaged vs Undamaged");
legend("damaged","undamaged");
%ylim([-30,30])

```

```

%beta
figure;
plot(beta_output_d(:,1),beta_output_d(:,2),'r');
hold on;
plot(beta_output_u(:,1),beta_output_u(:,2),'--b');
hold off;
xlabel('Time[s]'),ylabel("\beta[deg]");
title("Side-slip angle Damaged vs Undamaged");
legend("damaged","undamaged");

```

```

%r
figure;
plot(r_output_d(:,1),r_output_d(:,2),'r');
hold on;

```

```

plot(r_output_u(:,1),r_output_u(:,2),'--b');
hold off;
xlabel("Time[s]"),ylabel("r[deg/s]");
title("Yaw Rate Damaged vs Undamaged");
legend("damaged","undamaged");
%ylim([-30,30])

%psi
figure;
plot(psi_output_d(:,1),psi_output_d(:,2),'r');
hold on;
plot(psi_output_u(:,1),psi_output_u(:,2),'--b');
hold off;
xlabel("Time[s]"),ylabel("\psi[deg/s]");
title("Yaw Angle Damaged vs Undamaged");
legend("damaged","undamaged");

%% Lateral/Directional Analysis
% Angle plots
figure;
plot(alpha_output_d(:,1),alpha_output_d(:,2),'r','LineWidth',2);
hold on;
plot(phi_output_d(:,1),phi_output_d(:,2),'--g','LineWidth',2);
plot(psi_output_d(:,1),psi_output_d(:,2),'--b','LineWidth',2);
hold off;
title("Rotational Angle for 33% damaged aircraft")
xlabel("Time[s]"),ylabel("Angles[deg]");
legend("\alpha", "\phi", "\psi", "Location", "Best");
set(gca,'FontSize',16)
%ylim([-10 1])

% angular rate plots
figure;
plot(q_output_d(:,1),q_output_d(:,2),'r','LineWidth',2);
hold on;
plot(p_output_d(:,1),p_output_d(:,2),'--g','LineWidth',2);
plot(r_output_d(:,1),r_output_d(:,2),'--b','LineWidth',2);
hold off;
title("Angular Rates for 33% damaged aircraft")
xlabel("Time[s]"),ylabel("Angular rate[deg/s]");
legend("q", "p", "r", 'Location', "Best");
set(gca,'FontSize',16)

```

```

%input plot
figure;
plot(input_signal(:,1),input_signal(:,2),'r','LineWidth',2);
title("Unit Impulse Input Signal");
xlabel("Time[s]"),ylabel("Magnitude");
ylim([0 1.5])
xlim([0 10])
set(gca,'FontSize',16)

%% Analysis
%short-period
%damage
fprintf("Damaged SP pole location:")
pole(ss([A_d(2,2),A_d(2,3);A_d(3,2),A_d(3,3)], [B_d(2,:);B_d(3,:)],eye(2),0))

%no damage
fprintf("Undamaged SP pole location: ")
pole(ss([A_u_long(2,2),A_u_long(2,3);A_u_long(3,2),A_u_long(3,3)], [B_u_long(2,1);B_u_long(3,1)],eye(2),0))

%Phugoid
%damaged
fprintf("Damaged Phugoid pole location: ")
pole(ss([A_d(1,1),A_d(1,4);A_d(4,1),A_d(4,4)], [B_d(1,:);B_d(4,:)],eye(2),0))

%no damaged
fprintf("Undamaged Phugoid pole location: ")
pole(ss([A_u_long(1,1),A_u_long(1,4);A_u_long(4,1),A_u_long(4,4)], [B_u_long(1,1);B_u_long(4,1)],eye(2),0))

%Roll
%damage
fprintf("Damaged Roll, Pole Location: ")
pole(tf(B_d(6,3),[1 -A_d(6,6)]))

%no damage
fprintf("Undamaged Roll pole location: ")
pole(tf(0.185,[1 -(-0.4758)]))

```

## Appendix C – Wing-level Controller Design for Damaged Wing

```
%% Setup
clc,clear,close all;
%% Parameters
%% Undamaged case
Xu = -0.0218;
Xa = 1.2227;
Zu = -0.0569;
Za = -339.0036;
Mu = -0.0001;
Ma = -1.6165;
Madot = -0.1425;
Mq = -0.4038;
Zde = -18.3410;
Mde = -1.2124;
Yb = -55.7808;
Lb = -1.2555;
Lp = -0.4758;
Lr = 0.2974;
Nb = 1.0143;
Np = 0.0109;
Nr = -0.1793;
Ydr = 3.7187;
Ldr = 0.2974;
Ndr = -0.4589;
Yda = 0;
Lda = 0.185;
Yp = 0;
Yr = 0;
Nda = -0.0135;
g = 32.174049;

% aircraft params
S_u = 5500;
c_u = 27.3;
b_u = 196;
damage_factor = 0.33;
m2ft = 3.28;
b = 161.06;
c = 28.54;
S = b*c;
S_fact = S/S_u;
b_fact = b/b_u;
c_fact = c/c_u;
```

```

del_x = -0.0048*m2ft;
del_y = 0.0145*m2ft;
del_z = -0.005/10*m2ft;
Ixx = 15097500;
Iyy = 33090070;
Izz = 46598720;
m = 623903.08;
rho = 5.87e-4;
U1 = 871;
q = (1/2)*rho*U1^2;
Theta_1 = 2.4*(pi/180);
g = 32.174049;
m_a = m;

%stability and control derivatives
Xu = Xu*S_fact;
Xa = Xa*S_fact;
Zu = Zu*S_fact;
Za = Za*S_fact;
Mu = Mu*S_fact*c_fact;
Ma = Ma*S_fact*c_fact;
Madot = Madot*S_fact*c_fact^2;
Mq = Mq*S_fact*c_fact^2;
Xde = 0;
Zde = Zde*S_fact;
Mde = Mde*S_fact*c_fact;
Yb = Yb*S_fact;
Lb = Lb*S_fact*c_fact;
Lp = Lp*S_fact*b_fact^2;
Lr = Lr*S_fact*b_fact^2;
Nb = Nb*S_fact*b_fact;
Np = Np*S_fact*b_fact^2;
Nr = Nr*S_fact*b_fact^2;
Ydr = Ydr;
Ldr = Ldr;
Ndr = Ndr;
Yde = 0;
Lde = -0.001;
Nda = Nda*S_fact;
Yp = Yp*S_fact*b_fact;
Yr = Yr*S_fact*b_fact;
Lda = Lda*S_fact*b_fact;
Yda = Yda*S_fact;
Zadot = 0;
Zq = 0;

```

```

%% Damaged EoM
% order: x = [u alpha q theta phi p beta r psi]
K = 1/(U1-del_x*Madot-Zadot);
A_d = [
    Xu-del_z*Mu-del_z*Madot*Zu*K,Xa-del_z*Ma-del_z*Madot*Za*K,-del_z*Zq*Madot-
del_z*U1*K*Madot,g*sin(Theta_1)*K*del_z*Madot-
g*cos(Theta_1),0,del_y*Np,del_y*Nb,del_y*Nr,0;
    (Zu+del_x*Mu)*K,(Za+del_x*Ma)*K,(Zq+Mq*del_x+U1)*K,-g*sin(Theta_1)*K,0,-
del_y*Lp*K,-del_y*Lb*K,-del_y*Lr*K,0;
    Mu-
(m_a/Iyy)*del_z*Xu+(m_a/Iyy)*del_x*Zu+Zu*Madot*K+del_x*Mu*Madot*K+Zadot*(m_a/Iy
y)*del_x*Zu*K,Ma+(m_a/Iyy)*del_x*Za-
(m_a/Iyy)*del_z*Xa+Madot*Za*K+Madot*del_x*Ma*K+Zadot*(m_a/Iyy)*del_x*Za*K,Mq+(
m_a/Iyy)*del_x*Zq+Madot*Zq*K+K*Madot*Mq*del_x+Madot*U1*K+Zadot*(m_a/Iyy)*del_
x*Zq*K+Zadot*(m_a/Iyy)*del_x*U1*K,-Madot*g*sin(Theta_1)-
Zadot*(m_a/Iyy)*del_x*g*sin(Theta_1)*K,0,-Madot*del_y*Lp*K,-Madot*del_y*Lb*K,-
Madot*del_y*Lr*K,0;
    0,0,1,0,0,0,0,0,0;
    0,0,0,0,0,1,0,0,0;
    -(m_a/Ixx)*del_y*Zu,-(m_a/Ixx)*del_y*Za,-(m_a/Ixx)*del_y*Zq-
(m_a/Ixx)*del_y*Zadot*Zq*K-
(m_a/Ixx)*del_y*Zadot*U1*K,(m_a/Ixx)*del_y*Zadot*g*sin(Theta_1)*K,0,Lp+(m_a/Ixx)*del
_z*Yp,Lb+(m_a/Ixx)*del_z*Yb,Lr+(m_a/Ixx)*del_z*Yr,0;
    0,0,0,0,g*cos(Theta_1)/U1,(Yp+del_z*Lp-del_x*Np)/U1,(Yb+del_z*Lb-
del_x*Nb)/U1,(Yr+del_z*Lr-del_x*Nr)/U1-1,0;
    (m_a/Izz)*del_y*Xu,(m_a/Izz)*del_y*Xa,0,0,0,Np-(m_a/Izz)*del_x*Yp,Nb-
(m_a/Izz)*del_x*Yb,Nr-(m_a/Izz)*del_x*Nr,0;
    0,0,0,0,0,0,0,1,0;
];
% order: u = [de, dr, da]
B_d = [
    Xde-del_z*Madot*Zde*K,del_y*Ndr,del_y*Nda;
    Zde*K+Mde*del_x*K,-del_y*Lda*K,-del_y*Ldr*K;
    Mde+(m_a/Iyy)*del_x*Zde-
(m_a/Iyy)*del_z*Xde+Madot*Zde*K+Madot*Mde*del_x*K+Zadot*Zde*K*(m_a/Iyy)*del_x,-
Madot*del_y*Ldr*K,-Madot*del_y*Lda*K;
    0,0,0;
    0,0,0;
    -(m_a/Ixx)*del_y*Zde-
(m_a/Ixx)*del_y*Zadot*Zde*K,Ldr+(m_a/Ixx)*del_z*Ydr,Lda+(m_a/Ixx)*del_z*Yda;
    0,(Ydr+del_z*Ldr-del_x*Ndr)/U1,(Yda+del_z*Lda-del_x*Nda)/U1;
    (m_a/Izz)*del_y*Xde,Ndr-(m_a/Izz)*del_x*Ydr,Nda-(m_a/Izz)*del_x*Yda;
    0,0,0;
];

```

```

];

C_d = eye(9);

D_d = zeros(9,3);

Cphi = [
    0 0 0 0 1 0 0 0 0
]; % phi output matrix
Bda = B_d;
Dphi = zeros(1,3);
phi_ss = ss(A_d,B_d,Cphi,Dphi);

%% PID Variables
Kp_a = 15;
Ki_a = 6;
Kd_a = 10;

Kp_r = 1;
Ki_r = 1;
Kd_r = 1;

%% Plot
open("wingLevelModel.slx");
sim("wingLevelModel.slx");
% figure;
% subplot(3,1,1);
% plot(de_output(:,1),de_output(:,2),'r','LineWidth',2);
% title("Elevator deflection");
% xlabel("Time[s]"),ylabel("de[deg]");
% set(gca,'FontSize',16)

subplot(2,1,2);
plot(dr_output(:,1),dr_output(:,2),'b','LineWidth',2);
title("Rudder deflection");
xlabel("Time[s]"),ylabel("dr[deg]");
set(gca,'FontSize',16)

subplot(2,1,1);
plot(da_output(:,1),da_output(:,2),'g','LineWidth',2);
title("Aileron deflection");
xlabel("Time[s]"),ylabel("da[deg]");
set(gca,'FontSize',16)

```

```
figure;
plot(phi_output(:,1),phi_output(:,2),'r','LineWidth',2);
hold on;
plot(ref_output(:,1),ref_output(:,2),'--k','LineWidth',2);
hold off;
title("Roll angle output");
xlabel("Time[s]"),ylabel("\phi[deg]")
legend("\phi signal", "Ref Signal", "Disturbance Signal")
set(gca,'FontSize',16)
```

```
figure;
plot(disturb_output(:,1),disturb_output(:,2),'b','LineWidth',2);
title("Disturbance Signal")
xlabel("time[s]");
ylabel("Magnitude")
set(gca,'FontSize',16)
```

### Appendix D – Aerodynamic Data for Airfoil

Percentage morph	Cl	Chord (ft)	Cd	Cl/Cd
0	18.8071	28.54	0.11549	162.8461339
1	18.8872	28.8254	0.11611	162.666437
2	18.9674	29.1108	0.11672	162.503427
3	19.0472	29.3962	0.11748	162.1314266
4	19.127	29.6816	0.1182	161.8189509
5	19.207	29.967	0.11886	161.5934713
6	19.287	30.2524	0.1195	161.3974895
7	19.367	30.5378	0.12014	161.2035958
8	19.4469	30.8232	0.1208	160.9842715
9	19.5267	31.1086	0.12149	160.7268088
10	19.6066	31.394	0.12214	160.5256263
11	19.6864	31.6794	0.12278	160.3388174
12	19.7663	31.9648	0.12341	160.1677336
13	19.8462	32.2502	0.12404	159.9983876
14	19.926	32.5356	0.12465	159.8555957
15	20.0059	32.821	0.12527	159.7022432
16	20.0857	33.1064	0.12588	159.5622815
17	20.1656	33.3918	0.12649	159.4244604
18	20.2453	33.6772	0.12713	159.2488004
19	20.325	33.9626	0.12778	159.0624511
20	20.4048	34.248	0.12843	158.8787666
21	20.4846	34.5334	0.12904	158.7461252
22	20.5633	34.8188	0.13015	157.9969266
23	20.6428	35.1042	0.1309	157.6990069
24	20.7225	35.3896	0.13155	157.5256556
25	20.8019	35.675	0.13224	157.304144
26	20.8788	35.9604	0.13342	156.489282
27	20.9576	36.2458	0.13424	156.1203814
28	21.0369	36.5312	0.13495	155.8866247

29	21.1166	36.8166	0.1356	155.7271386
30	21.1963	37.102	0.13625	155.5691743

## Appendix E – Instantaneous Morph Simulation Code

```
%% Setup
clc,clear,close all

%% Givens
morph = 0;
damage_factor = 0.3;
U1 = 871;
rho = 5.87e-4;
q = 0.5*rho*U1^2;

%% Helper fuctions and data loader (All of these functions are part of the matlab block)
mass_property = mass_properties(0.3);
data = readtable("airfoil_data.csv");
CL = table2array(data(:,2));
Morph = table2array(data(:,3));
CD = table2array(data(:,4));
CL_CD = table2array(data(:,5));
Num = table2array(data(:,1));

%% Morph Implementation
% L_right = aero_extra(data,0,0)*moment_arm(0);
% L_left = aero_extra(data,0.3,0.3)*moment_arm(damage_factor);
% Lp = ((L_right - L_left)*2*q)/(mass_property(1)*U1); %
% open("base_line_wing_level_model.slx")
% sim("base_line_wing_level_model.slx")
% figure;
% plot(phi_a(:,1),phi_a(:,2));
% title("phi");
% figure;
% plot(da(:,1),da(:,2));
% title("da");

open('instantaneousMorphModel.slx')
sim('instantaneousMorphModel.slx')

figure;
plot(phi(:,1),phi(:,2),'r','LineWidth',2);
title("Instantaneous morph roll angle response");
xlabel("Time[sec]");
ylabel("\phi [deg]");
set(gca,"FontSize",16)

figure;
plot(da(:,1),da(:,2),'b','LineWidth',2);
```

```
title("Instantaneous morph aileron response");  
xlabel("Time[sec]");  
ylabel("\delta_{a} [deg]");  
set(gca,"FontSize",16)
```

```
figure;  
plot(disturbance(:,1),disturbance(:,2),'k','LineWidth',2);  
title("Instantaneous morph disturbance signal");  
xlabel("Time[sec]");  
ylabel("Disturbance Signal[deg]");  
set(gca,"FontSize",16)
```

## Appendix F – Actuation Code

```
%% Givens Achieve from [30]
ClosedLoop = 1;
data = [0, 0, 0.1950, 0.1950, 0.1462, 0.1450, 0, 0];
den = [0.00, 1];
num = -0.5;
time = [0, 0.38, 1.8, 2, 3, 4.6, 8, 10];
ts = 1e-3;
%% Simulation and plot
open("actuator.slx");
sim("actuator.slx");
figure;
plot(position(:,1),position(:,2).*3.28084+28.54,'LineWidth',2)
hold on;
plot(command(:,1),command(:,2).*3.28084+28.54,'--r','LineWidth',2)
xlabel("Time[s]")
ylabel("Position[ft]")
title("Hydraulic actuation")
legend("Hydraulic piston position", "Command Position")
set(gca,"FontSize",16)
```

## Appendix G – Full Simulation Code

```
%% Setup
clc,clear,close all;
warning('off','all');
%% Parameters
%%Undamaged case
Xu = -0.0218;
Xa = 1.2227;
Zu = -0.0569;
Za = -339.0036;
Mu = -0.0001;
Ma = -1.6165;
Madot = -0.1425;
Mq = -0.4038;
Zde = -18.3410;
Mde = -1.2124;
Yb = -55.7808;
Lb = -1.2555;
Lp = -0.4758;
Lr = 0.2974;
Nb = 1.0143;
Np = 0.0109;
Nr = -0.1793;
Ydr = 3.7187;
Ldr = 0.2974;
Ndr = -0.4589;
Yda = 0;
Lda = 0.185;
Yp = 0;
Yr = 0;
Nda = -0.0135;
g = 32.174049;
```

```
%aircraft params
S_u = 5500;
c_u = 27.3;
b_u = 196;
damage_factor = 0.33;
m2ft = 3.28;
b = 161.06;
c = 28.54;
S = b*c;
S_fact = S/S_u;
```

```

b_fact = b/b_u;
c_fact = c/c_u;
del_x = -0.0048*m2ft;
del_y = 0.0145*m2ft;
del_z = -0.005/10*m2ft;
Ixx = 15097500;
Iyy = 33090070;
Izz = 46598720;
m = 623903.08;
rho = 5.87e-4;
U1 = 871;
q = (1/2)*rho*U1^2;
Theta_1 = 2.4*(pi/180);
g = 32.174049;
m_a = m;

%stability and control derivatives
Xu = Xu*S_fact;
Xa = Xa*S_fact;
Zu = Zu*S_fact;
Za = Za*S_fact;
Mu = Mu*S_fact*c_fact;
Ma = Ma*S_fact*c_fact;
Madot = Madot*S_fact*c_fact^2;
Mq = Mq*S_fact*c_fact^2;
Xde = 0;
Zde = Zde*S_fact;
Mde = Mde*S_fact*c_fact;
Yb = Yb*S_fact;
Lb = Lb*S_fact*c_fact;
Lp = Lp*S_fact*b_fact^2;
Lr = Lr*S_fact*b_fact^2;
Nb = Nb*S_fact*b_fact;
Np = Np*S_fact*b_fact^2;
Nr = Nr*S_fact*b_fact^2;
Yde = 0;
Lde = -0.001;
Nda = Nda*S_fact;
Yp = Yp*S_fact*b_fact;
Yr = Yr*S_fact*b_fact;
Lda = Lda*S_fact*b_fact;
Yda = Yda*S_fact;
Zadot = 0;
Zq = 0;

```

```

%% Damaged EoM
% order: x = [u alpha q theta phi p beta r psi]
K = 1/(U1-del_x*Madot-Zadot);
A_d = [
    Xu-del_z*Mu-del_z*Madot*Zu*K,Xa-del_z*Ma-del_z*Madot*Za*K,-del_z*Zq*Madot-
del_z*U1*K*Madot,g*sin(Theta_1)*K*del_z*Madot-
g*cos(Theta_1),0,del_y*Np,del_y*Nb,del_y*Nr,0;
    (Zu+del_x*Mu)*K,(Za+del_x*Ma)*K,(Zq+Mq*del_x+U1)*K,-g*sin(Theta_1)*K,0,-
del_y*Lp*K,-del_y*Lb*K,-del_y*Lr*K,0;
    Mu-
(m_a/Iyy)*del_z*Xu+(m_a/Iyy)*del_x*Zu+Zu*Madot*K+del_x*Mu*Madot*K+Zadot*(m_a/Iy
y)*del_x*Zu*K,Ma+(m_a/Iyy)*del_x*Za-
(m_a/Iyy)*del_z*Xa+Madot*Za*K+Madot*del_x*Ma*K+Zadot*(m_a/Iyy)*del_x*Za*K,Mq+(
m_a/Iyy)*del_x*Zq+Madot*Zq*K+K*Madot*Mq*del_x+Madot*U1*K+Zadot*(m_a/Iyy)*del_
x*Zq*K+Zadot*(m_a/Iyy)*del_x*U1*K,-Madot*g*sin(Theta_1)-
Zadot*(m_a/Iyy)*del_x*g*sin(Theta_1)*K,0,-Madot*del_y*Lp*K,-Madot*del_y*Lb*K,-
Madot*del_y*Lr*K,0;
    0,0,1,0,0,0,0,0;
    0,0,0,0,0,1,0,0,0;
    -(m_a/Ixx)*del_y*Zu,-(m_a/Ixx)*del_y*Za,-(m_a/Ixx)*del_y*Zq-
(m_a/Ixx)*del_y*Zadot*Zq*K-
(m_a/Ixx)*del_y*Zadot*U1*K,(m_a/Ixx)*del_y*Zadot*g*sin(Theta_1)*K,0,Lp+(m_a/Ixx)*del
_z*Yp,Lb+(m_a/Ixx)*del_z*Yb,Lr+(m_a/Ixx)*del_z*Yr,0;
    0,0,0,0,g*cos(Theta_1)/U1,(Yp+del_z*Lp-del_x*Np)/U1,(Yb+del_z*Lb-
del_x*Nb)/U1,(Yr+del_z*Lr-del_x*Nr)/U1-1,0;
    (m_a/Izz)*del_y*Xu,(m_a/Izz)*del_y*Xa,0,0,0,Np-(m_a/Izz)*del_x*Yp,Nb-
(m_a/Izz)*del_x*Yb,Nr-(m_a/Izz)*del_x*Nr,0;
    0,0,0,0,0,0,0,1,0;

];
%[de, dr, da]
B_d = [
    Xde-del_z*Madot*Zde*K,del_y*Ndr,del_y*Nda;
    Zde*K+Mde*del_x*K,-del_y*Lda*K,-del_y*Ldr*K;
    Mde+(m_a/Iyy)*del_x*Zde-
(m_a/Iyy)*del_z*Xde+Madot*Zde*K+Madot*Mde*del_x*K+Zadot*Zde*K*(m_a/Iyy)*del_x,-
Madot*del_y*Ldr*K,-Madot*del_y*Lda*K;
    0,0,0;
    0,0,0;
    -(m_a/Ixx)*del_y*Zde-
(m_a/Ixx)*del_y*Zadot*Zde*K,Ldr+(m_a/Ixx)*del_z*Ydr,Lda+(m_a/Ixx)*del_z*Yda;
    0,(Ydr+del_z*Ldr-del_x*Ndr)/U1,(Yda+del_z*Lda-del_x*Nda)/U1;
    (m_a/Izz)*del_y*Xde,Ndr-(m_a/Izz)*del_x*Ydr,Nda-(m_a/Izz)*del_x*Yda;
    0,0,0;

];

```

```

C_d = eye(9);

D_d = zeros(9,3);

Cphi = [
    0 0 0 0 1 0 0 0 0
];
Bda = B_d;
Dphi = zeros(1,3);
phi_ss = ss(A_d,B_d,Cphi,Dphi);

%% PID Variables
Kp_a = 20;
Ki_a = 9;
Kd_a = 13;

Kp_r = 10;
Ki_r = 5;
Kd_r = 7;

%Morph data table
data = readtable("airfoil_data.csv");
CL = table2array(data(:,2));
Morph = table2array(data(:,3));
CD = table2array(data(:,4));
CL_CD = table2array(data(:,5));
Num = table2array(data(:,1));

%% Sim
open("morphWingLevel.slx")
sim("morphWingLevel.slx")

%% Plot
figure;
plot(disturbance(:,1),disturbance(:,2),'k','LineWidth',2);
xlabel("Time[sec]")
ylabel("\phi[deg]")
title("Disturbance Signal")
set(gca,'FontSize',16)

figure;

```

```

subplot(2,1,1)
plot(da1(:,1),da1(:,2),'r','LineWidth',2);
xlabel("Time[sec]")
ylabel("\delta_{a}[deg]")
title("Aileron Deflection")
set(gca,'FontSize',16)
subplot(2,1,2)
plot(dr1(:,1),dr1(:,2),'b','LineWidth',2);
xlabel("Time[sec]")
ylabel("\delta_{r}[deg]")
title("Rudder Deflection")
set(gca,'FontSize',16)

```

```

figure;
subplot(2,1,1)
plot(da2(:,1),da2(:,2),'r','LineWidth',2);
xlabel("Time[sec]")
ylabel("\delta_{a}[deg]")
title("Aileron Deflection")
set(gca,'FontSize',16)
subplot(2,1,2)
plot(dr2(:,1),dr2(:,2),'b','LineWidth',2);
xlabel("Time[sec]")
ylabel("\delta_{r}[deg]")
title("Rudder Deflection")
set(gca,'FontSize',16)

```

```

figure;
plot(actuation(:,1),actuation(:,2),'LineWidth',2);
hold on;
plot(commandPosition(:,1),commandPosition(:,2),'--k','LineWidth',2);
hold off;
xlabel("Time[sec]")
ylabel("morph[%]")
title("Actuation vs Commanded Signal")
legend("Actuation(position)","Commanded","Location','Best')
set(gca,'FontSize',16)

```

```

figure;
plot(phi1(:,1),phi1(:,2),'LineWidth',2);
hold on;
plot(ref1(:,1),ref1(:,2),'--k','LineWidth',2);
hold off;
xlabel("Time[sec]")
ylabel("\phi[deg]")

```

```
title("Roll angle with morph")
legend("\phi", 'reference', "Location", 'Best')
set(gca, 'FontSize', 16)
```

```
figure;
plot(phi2(:,1), phi2(:,2), 'LineWidth', 2);
hold on;
plot(ref1(:,1), ref1(:,2), '--k', 'LineWidth', 2);
hold off;
xlabel("Time[sec]")
ylabel("\phi[deg]")
title("Roll angle with no morph")
legend("\phi", 'reference', "Location", 'Best')
set(gca, 'FontSize', 16)
```